2017

Design and structural testing of tall Hexcrete wind turbine towers

Robert Peggar
Iowa State University

Design and structural testing of tall Hexcrete wind turbine towers

by

Robert Peggar

A dissertation submitted to the graduate faculty

in partial fulfillment of the requirements for the degree of

DOCTOR OF PHILOSOPHY

Co-majors: Civil Engineering (Structural Engineering);
Wind Energy Science Engineering & Policy

Program of Study Committee:
Sri Sritharan, Major Professor
Partha Sarkar
Jon Matthew Rouse
H. David Jeong
Frank Peters

Iowa State University

Ames, Iowa

2017

TABLE OF CONTENTS

LIST OF TABLES

LIST OF FIGURES

ACKNOWLEDGEMENTS

I am grateful for the opportunity to complete a doctoral dissertation and know that without the work of Christ Jesus in my life it would not be possible. I would like to recognize and thank my wife, Elyse Peggar, who has supported me each step along this journey. I would also like to specifically acknowledge my major professor, Dr. Sri Sritharan, who presented the opportunity to work on this topic, has provided much guidance and advice, and has helped prepare me for engineering after graduation. Thank you also to the many others who contributed to this research: my doctoral committee, Bin Cai, Shibin Lin, Phil Barutha, Ali Nahvi, Hartanto Wibowo, Owen Steffens, Doug Wood, Zhao Cheng, Liang Zhong, Chris Levandowski, Nate Scharenbrock, Carol Shield, Paul Bergson, and Chris Bruhn. Finally, I would also like to acknowledge the many industry partners who contributed to the outcomes described in this writing.

ABSTRACT

Wind energy continues to be an important renewable energy resource across the United States (U.S.) with the goal of the U.S. Department of Energy (DOE) to install wind capacity in all 50 states. In order to increase the amount of installed wind energy, technology innovation such as taller wind towers is needed. At taller hub heights, wind speed increases, there is often less turbulence, and power production significantly increases from a moderate increase in height. These benefits can allow wind energy in new regions, such as the southeast U.S., and also increase energy production in current wind rich regions such as Iowa and Texas. Current wind towers are 262 ft (80 m) tall and constructed of circular steel shells. As hub heights increase, the shells must become wider and are difficult to transport. Concrete shells can also be used but these towers require specialized curved formwork which can be expensive. In order to effectively increase tower hub heights, the Hexcrete tower system was developed at Iowa State University (ISU). The Hexcrete tower is a hexagon shaped, precast concrete tower system constructed out of six hexagon shaped columns, and six flat wall panels. All the tower members are precast from high strength concrete materials and are designed to fit on a standard flatbed semi-trailer. The members are assembled at the wind farm site and connected by unbonded steel post-tensioning tendons. As part of a DOE funded project, three full concrete Hexcrete towers and three hybrid Hexcrete towers (steel shells compose top third of tower) were designed for hub heights of 394 ft (120 m) and 459 ft (140 m) for Siemens SWT 2.3-108 and SWT 3.2-113 turbines. A strength and design validation experimental test was performed on a full scale section of one of the 120 m towers in a laboratory setting and it was found that the Hexcrete tower design adequately met the required operating and extreme load requirements and also had significant reserve capacity. Finite element and numerical models were created to aid in the design process and were verified with experimental test data. A numerical surface pressure analysis was conducted according to the American Society of Civil Engineers (ASCE) 7-10 guidelines and compared to Computational Fluid Dynamic (CFD) analysis to compare the Hexcrete wind interaction with that of a circular tower section. It was found that the Hexcrete section created larger drag forces and surface pressures than a circular tower but that the Hexcrete hybrid towers had the potential to reduce the Hexcrete tower drag and corresponding pressures. Based on test and analysis results, the Hexcrete wind turbine tower provides a cost-effective opportunity to employ precast concrete for hub heights above 262 ft (80 m) and enable economical wind power in all 50 states.

CHAPTER 1 - INTRODUCTION

1.1 Historical background

As the population in the United States (U.S.) continues to increase, the renewable energy market continues to expand in an effort to reduce reliance on the traditional energy sources of petroleum and coal. Wind energy is one of the leading renewable energy sources in the U.S. with 73.9 gigawatts (GW) of installed power in 2015 compared to 7.5 GW of solar and 3.5 GW of geothermal (AWEA, 2015; SEIA, 2015; GEA, 2015). Since 2008 the U.S. has continued to expand with new investments in wind plants averaging $13 billion per year between 2008 and 2013. In fact, the installed capacity in 2015 is more than four times the 2008 installed capacity of 16,702 MW (AWEA, 2015) and accounts for almost 5% of the U.S. electricity demand. American companies are also increasing national production of the large wind equipment components with the percentage of imported equipment decreasing from 80% in 2006-2007 to 30% in 2012-2013 (U.S. Department of Energy, 2015). In response to growing wind energy market, the DOE released the 2015 Wind Vision Report, which outlines the current state of wind energy in the U.S. The report explores new opportunities and directions for growth of the national wind energy market; summarizes the economic, social, and environmental impacts of increased wind production; and identifies future goals and technology advances that could directly impact future wind development. One of the future goals of the Wind Vision Report is for 35% of U.S. electric power to be generated by wind power by 2050 which calls for even larger increases in installed wind capacity (U.S. Department of Energy, 2015).

The amount of new wind installation has closely followed the federal production tax credit (PTC) which has expired and been extended multiple times over the past 20 years (Figure 1.1). The intent of the PTC was to increase the installment of new wind projects by providing a rebate for every kilowatt-hour (kWh) of energy produced over the first ten years of wind turbine operation and subsequently making wind energy competitive with coal and natural gas. The PTC started at 1.5 cents per kWh (1993 dollars) and is adjusted for inflation according to rates set by the Internal Revenue Service. The most recent extension of the PTC was in 2016 and provided a 2.3 cents per kWh (2015 dollars) rebate for 2016 but also created a phase-out of the PTC through the end of 2019. The phase-out of the PTC reduces the tax credit by 20% in 2017, 40% in 2018, and 60% in 2019 before final expiration at the end of 2019 (U.S. Department of Energy, 2015).

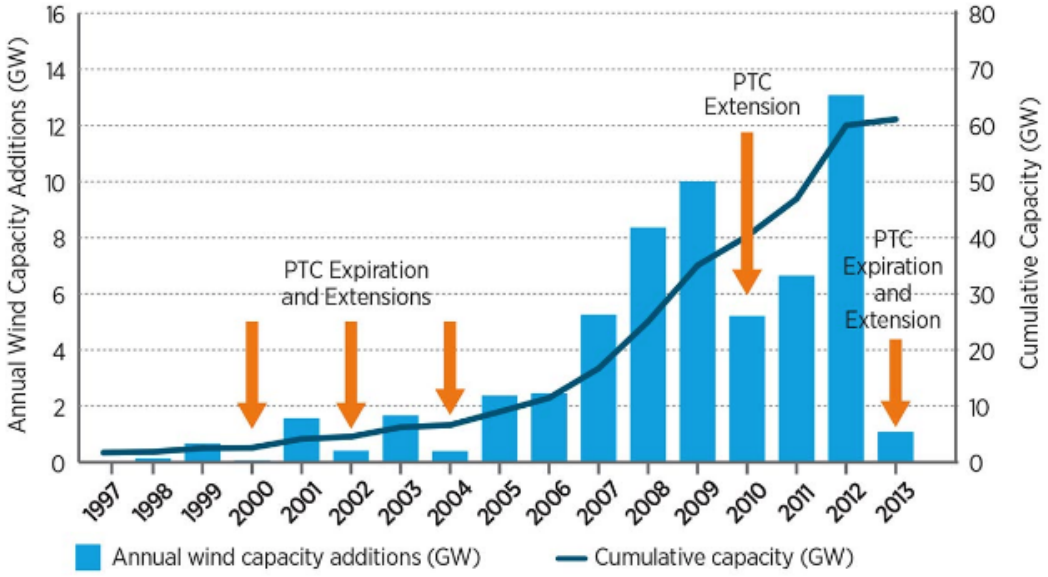

Figure 1.1. Installation of new wind capacity compared with PTC extensions (U.S. Department of Energy, 2015)

As the PTC reduces over the next few years, technological advancement is needed in multiple areas of wind turbine design, manufacturing, and deployment to produce 35% of the U.S. electricity demand by 2050. One such advancement is designing taller wind towers with hub heights above 328 ft (100 m). There are currently over 48,800 utility scale wind turbines in the U.S. and only approximately 1,100 (2.5%) towers are at or above 328 ft with an average tower hub height of 262 ft (80 m) (U.S. Department of Energy, 2015; AWEA, 2015). The majority of wind towers installed at 328 ft were built in 2012 (Figure 1.2) which was the largest year for growth of new installed wind capacity. Taller hub heights can substantially increase energy production due to the wind resource at heights above 328 ft. Wind speed increases with height and often wind is less turbulent at higher elevations due to reduced interaction with geographical and manmade obstructions. Wind speeds are related to power production by a cubic relationship which allows a significant increase in power production capacity from a moderate increase in height as shown in Figure 1.3 where the black line represents a typical 262 ft (80 m) hub height, the red line is a 361 ft (110 m) hub height and the blue line is a 459 ft (140 m) hub height.

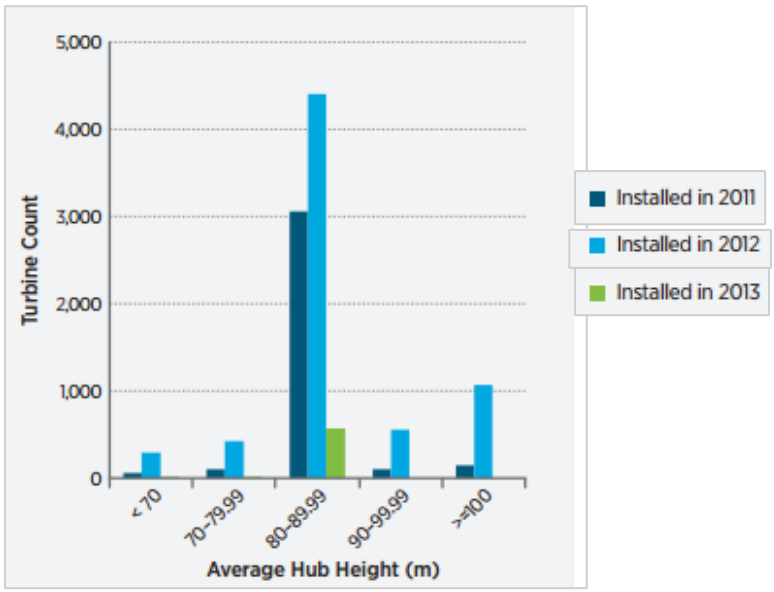

Figure 1.2. Hub Heights for installed wind turbines 2011-2013 (U.S. Department of Energy, 2015)

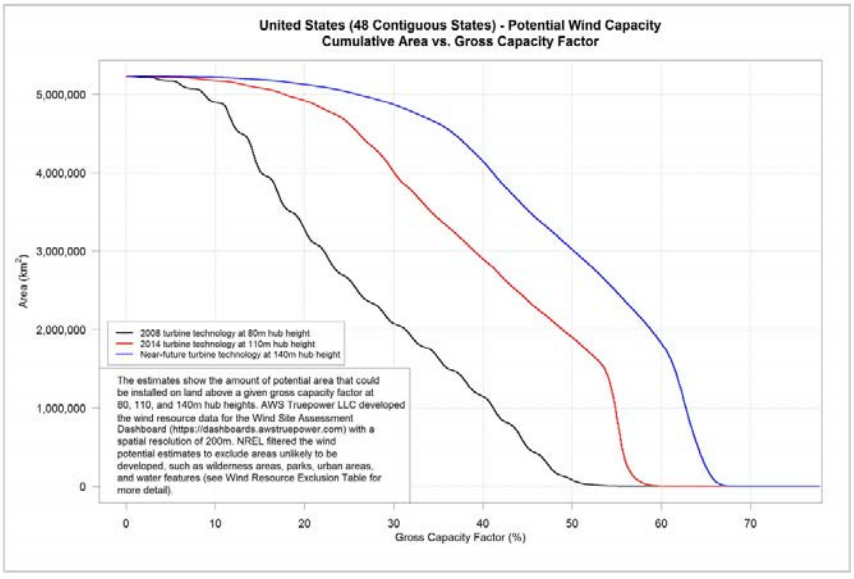

Figure 1.3. Potential wind capacity by height (National Renewable Energy Laboratory, 2016)

Taller hub heights also allow larger capacity machines and longer rotors to be implemented which increases the swept area of a wind turbine and results in higher energy production. Hub heights at higher elevations coupled with an increase in rotor diameter can result in a reduction in the Levelized Cost of Energy (LCOE) of the wind turbine system as shown in Figure 1.4. In 2000, the average rotor diameter was around 180 ft (55 m) with an

average turbine capacity of 0.9 MW on a 164 ft (50 m) tower. The average rotor diameter in 2013 was 318 ft (97 m) with and average turbine capacity of 1.87 MW on an 262 ft (80 m) to 328 ft (100 m) tower.

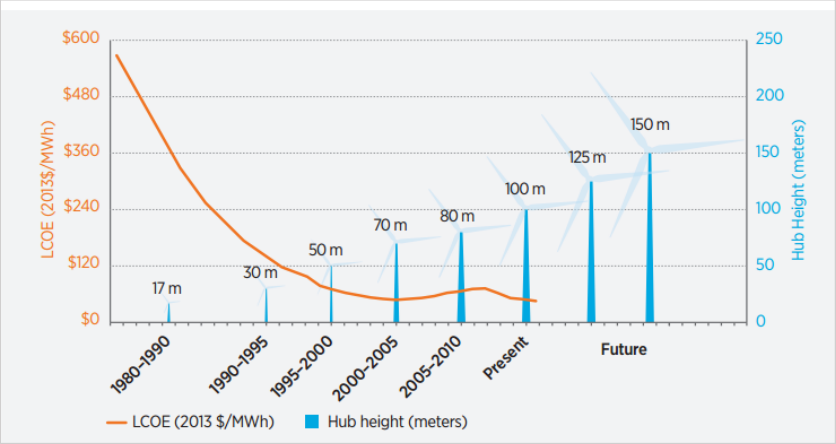

Figure 1.4. Decrease in LCOE of wind turbines corresponding with increases in tower height (U.S. Department of Energy, 2015)

Towers at higher elevations also open new opportunities for the implementation of wind energy in new regions throughout the United States. Figure 1.5 shows the current amount of wind energy produced in the U.S. by each state. It is worth noting that all of the states with no wind energy production are located in the southeast part of the U.S. Low wind speeds at current hub heights of 262 ft to 328 ft make the installation of wind uneconomical. However, if hub heights are increased to 459 ft, the southeast becomes a viable option for cost-effective wind energy as shown in Figure 1.6.

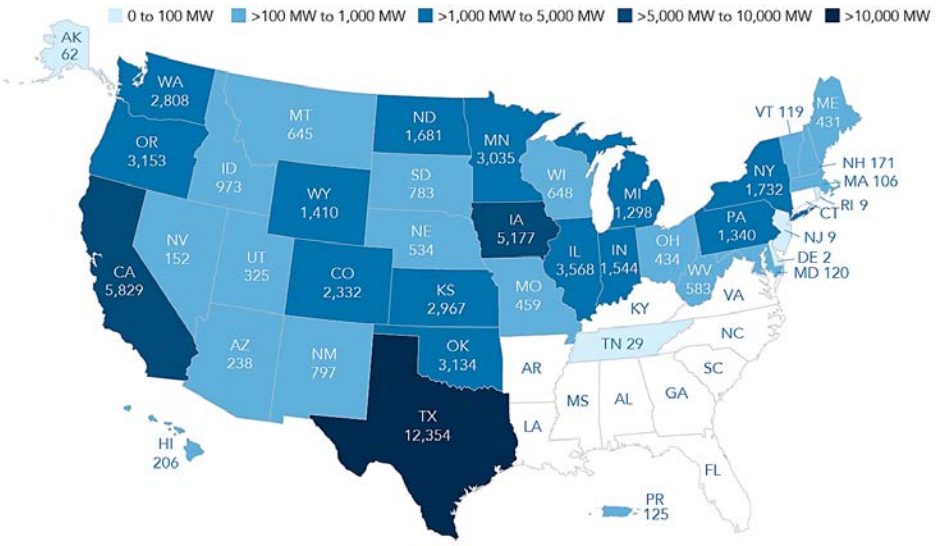

Figure 1.5. U.S. wind capacity divided by state (AWEA, 2015)

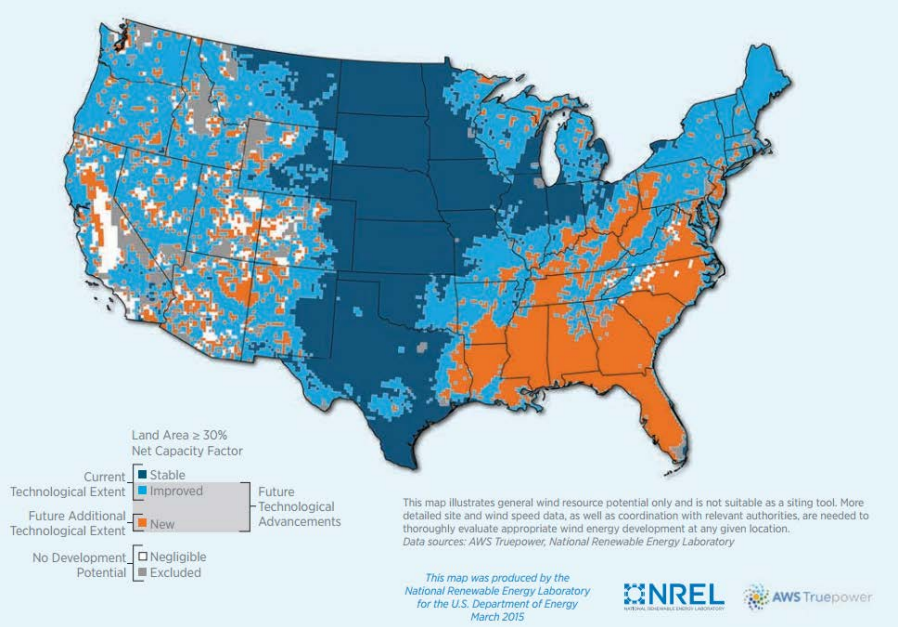

Figure 1.6. Areas of U.S. open to wind deployment with larger rotors and 459 ft tower hub heights (U.S. Department of Energy, 2015)

1.2 Current tower technology

The most common type of wind tower currently in use is the tubular steel shell tower with a standard height of 262 ft The 262 ft steel tower base is typically around 13-14 ft (4-4.25 m) in diameter with long sections that require special transportation equipment and road permits (Figure 1.7). Extending the tubular steel tower to heights at or above 328 ft requires widening the base diameter to 18 ft (5.49 m) which severely limits transportation due to the height of highway overpasses and lane widths (Lewin & Sritharan, 2010). Instead of expanding the base diameter of the a steel tower, the thickness of the shell can be increased, but this results in almost doubling the volume of steel and significantly increasing material costs (Lewin & Sritharan, 2010). For these reasons it is clear that an alternative tower design is needed to extend wind towers to taller hub heights, and companies on the leading edge of innovative wind technology from around the world have produced multiple design solutions to solve this problem. The following sections summarizes current tall wind tower designs and limits the included concepts to include only tower designs for which a prototype tower already exists or is currently in production. The included tower designs are also limited to steel, concrete, and hybrid towers since these three tower types dominate the current utility scale wind tower market.

Figure 1.7. 80-m wind tower barely fits under bridge (top) (Sun Journal, n.d.); 80-m standard wind tower transportation (bottom) (National Renewable Energy Labs (NREL), 2009)

1.2.1 Steel towers:

Vestas Wind Systems designs and constructs Large Diameter Steel Towers (LDSTs) with hub heights up to 545 ft (166 m). The two bottom sections of the tower are divided into three curved sections which are transported to the wind site separately and then bolted together along vertical flanges. The two bottom sections are then topped with traditional steel circular sections as shown in Figure 1.8. The typical base diameter of the LDST is 20.7 ft (6.3 m) for a 449 ft (137 m) hub height tower (Vestas Wind Systems A/S, 2016). A prototype was built in Germany in 2013, and over 80 LDSTs have been installed in Finland (de Vries, 2015). Figure 1.9 shows the base of a constructed LDST.

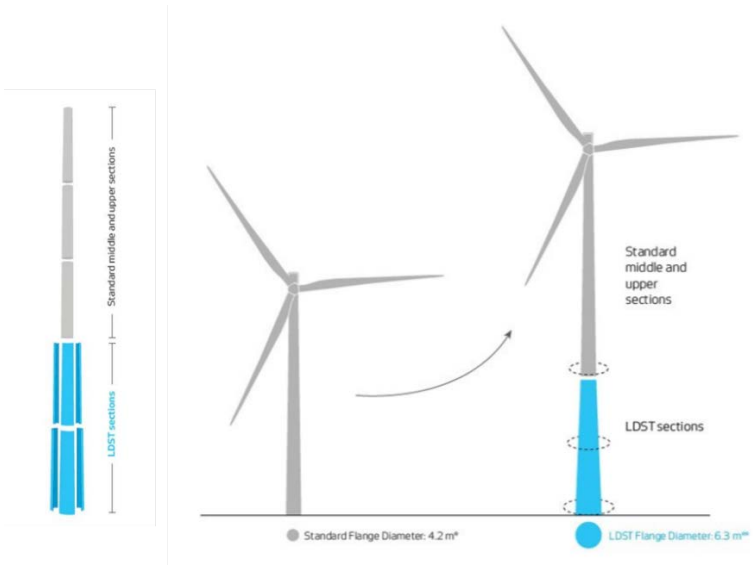

Figure 1.8. Vestas LDST section stacking (left); tower base diameter details (right) (Vestas Wind Systems A/S, 2016)

Figure 1.9. Base of Vestas LDST (de Vries, 2015)

Andresen Towers, which is based in Denmark, developed the Bolted Steel Shell (BSS) Tower and signed a sole distribution agreement with Siemens Wind Power in 2012 (Andresen Towers, 2015). The BSS tower is formed by steel shells (bent steel plates) that are bolted together as shown in Figure 1.10. The bolts do not require re-tensioning for the life of the tower and the bent steel plate design allows for hub heights above 459 ft (140 m) (Siemens, 2011). Depending on the height of the tower, nine or more shell sections are connected to form a minimum base diameter of 26.2 ft (8 m). All of the steel shells are precision manufactured, painted for corrosion resistance, and able to be shipped with standard truck loads. The BSS tower also has no restriction on maximum hub height and uses less steel than traditional steel tubular towers (Siemens, 2011). Siemens built two prototype towers in 2012: a 295 ft (90 m) tower in

Hovsore, Denmark (de Vries, 2012) and a 377 ft (115 m) tower in Lelystad in the Netherlands which required 15,000 bolts (Eneco, 2012). Two hundred towers with hub heights up to 466 ft (142 m) were produced by Andresen for locations across Europe from 2013-2014 before the sole distribution agreement with Siemens was mutually ended; Andresen filed for bankruptcy in 2015.

Figure 1.10. Andresen tower assembly (Andresen Towers, 2015)

1.2.2 Concrete towers:

Concrete towers are beginning to be utilized more often in the wind industry due to high accessibility of materials, long durability, use of precast members, and the ability to use prestressing for structural stability and member connections. In Europe, South America, and Mexico Acciona WindPower has built over 200 precast concrete shell towers with hub heights of 262 ft to 394 ft. A 328 ft tower is made up of 5 circular sections and each section requires a separate form or mold (Figure 1.11) (Gouws, 2015). Each circular section of the tower is made up of two to four concrete curved shells depending on the diameter of the tower; the vertical joints between each precast member are grouted for continuity (Gouws, 2015). The five circular sections are preassembled on the ground using the curved shell pieces and then lifted into place. The sections are then connected using steel dowel bars embedded in the concrete (Figure 1.12) and the tower is completed by attachment of the nacelle and rotor.

Figure 1.11. Acciona Curved shell formwork (left); shell assembly (right) (Acciona WindPower, 2016)

Figure 1.12. Stacking of Acciona concrete tower sections (Acciona WindPower, 2016)

Inneo Torres produces concrete shell towers in a manner similar to Acciona. Inneo has designed concrete wind towers with up to 394 ft hub heights. Currently Inneo is engaged in a lawsuit claiming that Accionia violated Inneo patents in developing the Acciona concrete tower (Orihuela & Parkin, 2015). Many characteristics of the Acciona and Inneo towers are similar including connection details, curved shell members, and transportation logistics (Figure 1.13).

Figure 1.13. Inneo Torres tower transportation and erection (Inneo Torres, 2008)

Currently in the U.S. there are only two concrete towers and both are prototypes. Acciona built a 328 ft version of its concrete tower in West Branch, Iowa in 2012 (NAW Staff, 2012) in order to test the U.S. market for circular concrete towers. Postensa Wind Structures also built a 328 ft concrete prototype tower in Sublette, Illinois in 2012 (Del Franco, 2015). The Postensa tower design is exclusively licensed to Blattner Energy and is able to reach heights of 459 ft (Blattner Energy, 2015). The base of the tower is a rounded square which is made up of two curved section and two flat wall panels as shown in Figure 1.14. The tower then transitions to a circular section at higher elevations as the tower tapers and the flat panels are no longer needed. All of the tower components are able to be shipped on a flatbed trailer, however, no information was available regarding how the members of the tower are connected (Blattner Energy, 2016). The tower does contain vertical post-tensioning which provides structural continuity between vertically stacked members.


Figure 1.14. Rounded square base of Potensa Wind Tower (left) (Potensa Wind Structures, 2016); taper from square to circular section in completed tower (right) (Ericksen Roed & Associates, 2015)

1.2.3 Hybrid towers:

Hybrid towers are defined for the purposes of this discussion as part concrete and part steel. An example of this type of hybrid tower system is the Tindall Atlas Concrete Tower Base (CTB) (Figure 1.15). The flared concrete base is typically 98-131 ft (30-40 m) in height and is made up of precast concrete components with a base diameter of 49-59 ft (15-18 m). The precast components are rectangular staves which can be combined in various numbers to construct bases for different tower heights and larger turbine loads (Figure 1.16). The dimension of each stave is identical as shown in Figure 1.17 and the staves are designed to be transferred on standard railroad cars. The staves are temporarily bolted together and then connected with cast-in-place concrete at the joints. Post-tensioning cables are also run bi-axially around the base to protect the stave sections from fatigue. The staves are then vertically post-tensioned to a transition concrete ring which provides a connection point for a traditional steel tubular 262 ft steel tower sections (Zavitz & Kirkley, 2016). The Atlas CTB also utilizes a simple ring foundation (Figure 1.18) with a maximum thickness of 3.28 ft (1 m) which uses significantly less concrete than a conventional tower foundation (Table 1.1) (Zavitz & Kirkley, 2016). A prototype of the CTB base was built in Georgia at one of Tindall's manufacturing facilities in 2012 but the CTB base has not yet been implemented in existing wind farms.

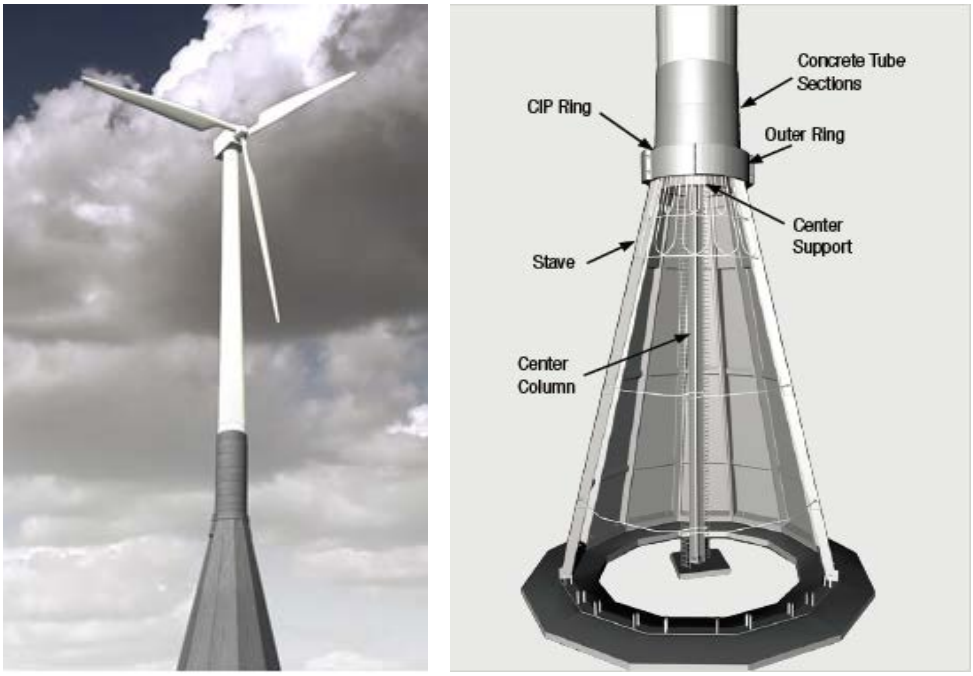

Figure 1.15. Tyndall Atlas CTB tower concept (left) and tower details (right) (Zavitz & Kirkley, 2016)

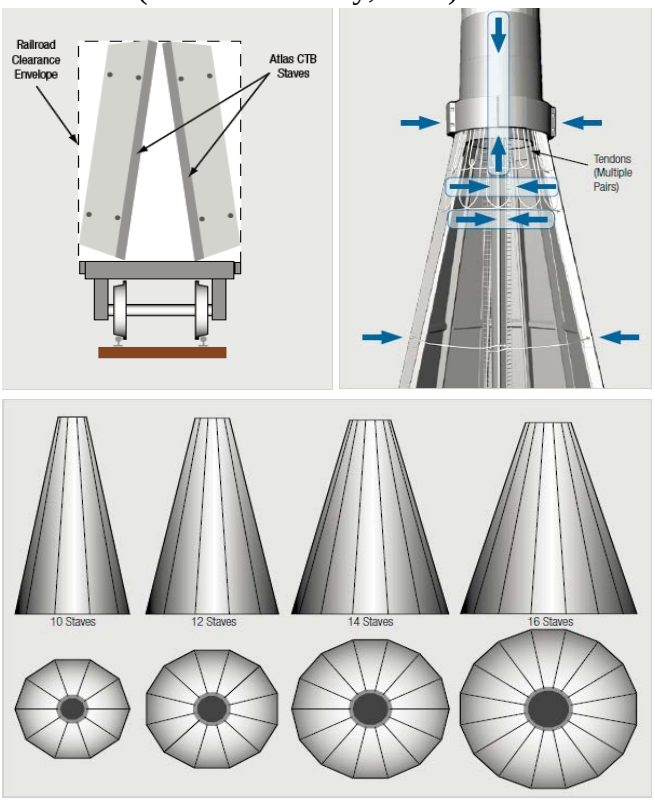

Figure 1.16. Variation in number of staves (Zavitz & Kirkley, 2016)

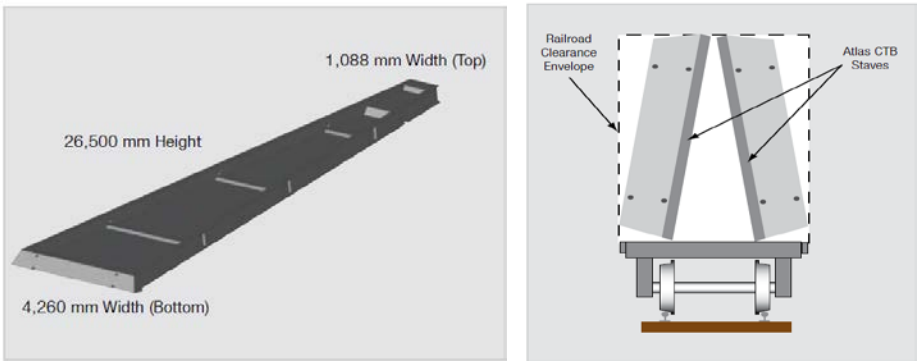

Figure 1.17. Standard stave dimensions (left); railroad transportation (right) (Zavitz & Kirkley, 2016)

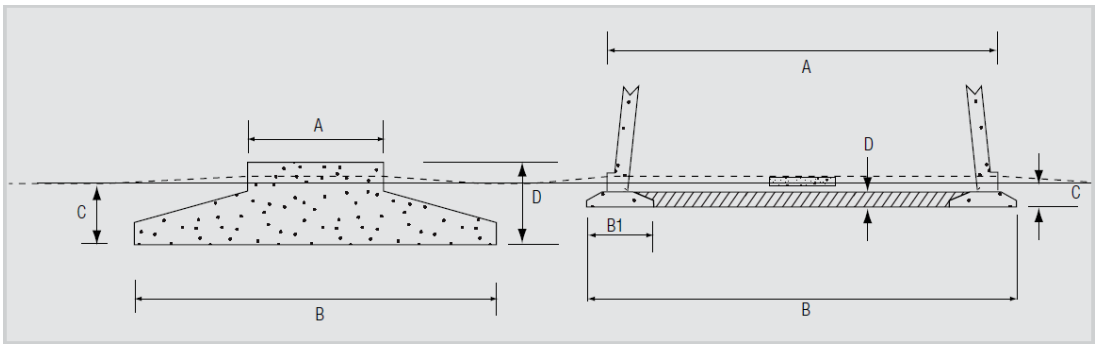

Figure 1.18. Comparison of conventional tower foundation (left) and Tindall ring foundation (right) (Zavitz & Kirkley, 2016)

Table 1.1. Dimensions and details of conventional and Atlas CTB foundations (Zavitz & Kirkley, 2016)

Significant Cost Factors	*80 m Hub Height*		*100 m Hub Height*	
	Atlas CTB	*Conventional*	*Atlas CTB*	*Conventional*
Tower footprint at foundation, m (A)	15	5	15	5
Foundation footprint, m (B)	17	15	18	16
Ring width, m (B1)	3	NA	4	NA
Footing depth, m (C)	1	2	1	3
Overall pour depth, m (D)	0.6	3	0.7	3
Concrete volume, m^3	70% less	287	67% less	344

Advanced Tower System (ATS) developed a hybrid tower which combines an 262 ft precast concrete base with a 131 ft (40 m) steel tower section (Figure 1.19). The square shaped concrete base of the ATS tower consists of precast corner elements joined with flat precast wall panels. The corner portions of the concrete base are identical along the height of the ATS tower and the connecting flat panels taper as the tower increases in height. A wet concrete joint connects the corner pieces and flat wall panels and vertical post-tensioning provides structural

stability and connects the vertically stacked sections to a circular transition piece (Figure 1.20). The 131 ft steel tower section is then attached above the transition piece and connected to the rotor and nacelle (Advanced Tower Systems, 2016). Only three sets of forms are needed to cast the concrete sections of the ATS tower which makes the design relatively simplistic. All of the precast pieces can also be shipped via standard trucks according to European shipping methods and regulations. Twenty-five of the ATS towers have been constructed across Germany with hub heights ranging from 433-476 ft (132-145 m).

Figure 1.19. ATS hybrid tower (Advanced Tower Systems, 2016)

Figure 1.20. Stacking of ATS square concrete base sections (Advanced Tower Systems, 2016)

Max Bogl, a German based company, is one of the largest producers of hybrid towers in Europe (Figure 1.21). The Max Bogl hybrid tower is customizable and the amount of concrete and steel varies according to the needs of the client. Typical hub heights for Max Bogl towers range between 403 ft (123 m) and 469 ft (143 m) (Max Bogl, 2016). Concrete rings made out of high performance concrete (14.5 ksi (100 MPa) (BFT International, 2014)) form the base of the tower and each ring has a height of 12.5 ft (3.8 m) and a thickness of 1 ft (30 cm). The rings are either a full circular shell or a half shell depending on the diameter and weight of the section. Max Bogl specializes in precision precasting and the top and bottom of each ring are finished using a grinding CNC machine to allow for a precise fit when the tower sections are stacked. The precise fit results in a "dry joint" where no grout or cementitious material are placed between the two sections. A concrete ring transition piece, similar to other hybrid towers, is used to connect the concrete to a regular steel shells in order to reach the desired hub height. Before the steel shell tower sections are placed, vertical post-tensioning is installed to provide stability for the stacked concrete sections. The steel shells are bolted in place and the nacelle rotor are then attached (Max Bogl, 2016). Due to the large volume of towers produced, multiple tower pieces are prefabricated and stored at the production facility which ensure that the tower components are readily available to begin construction (Figure 1.22). Transportation of the different wind tower components occurs by trucks but can also be done by ship depending on the wind tower location (Figure 1.23). Max Bogl has installed over 200 hybrid towers for multiple types of turbines across Europe (General Electric, 2013).

Figure 1.21. Max Bogl hybrid tower

Figure 1.22. Storage of precast concrete components at production facility (Max Bogl, 2016)

Figure 1.23. Transportation of wind tower components: concrete sections (upper left); steel section (upper right); concrete sections via ship (lower)

A self-erection hybrid tower has been designed by Esteyco Energia. The self-erecting tower uses heavy lift strand jacks and interlocking tower shells to erect the tower system off a platform located at a height of 131 ft (Esteyco Energia, 2014). The top steel tube of the tower is set in place at the final tower location and the concrete shells are assembled directly around the steel tube starting from the top of the tower so that the bottom shell of the tower is constructed last on the outside of the rest of the tower segments. The top steel shell is slightly taller than the surrounding concrete pieces allowing attachment of the nacelle and rotor while all the shells are on the ground (Figure 1.24). Post-tensioning strands are then attached to the two top pieces as

shown in Figure 1.25 and the top of the tower is lifted into place by the strand jacks and secured with post-tensioning anchors. This process is repeated so that pieces of the tower are incrementally added to the base of the top tower section which increases the overall height of the nacelle and blades. The process is continued until the entire tower is joined together in a fashion that resembles a telescope. A prototype of the tower was built in 2014 without a nacelle and rotor (Figure 1.26).

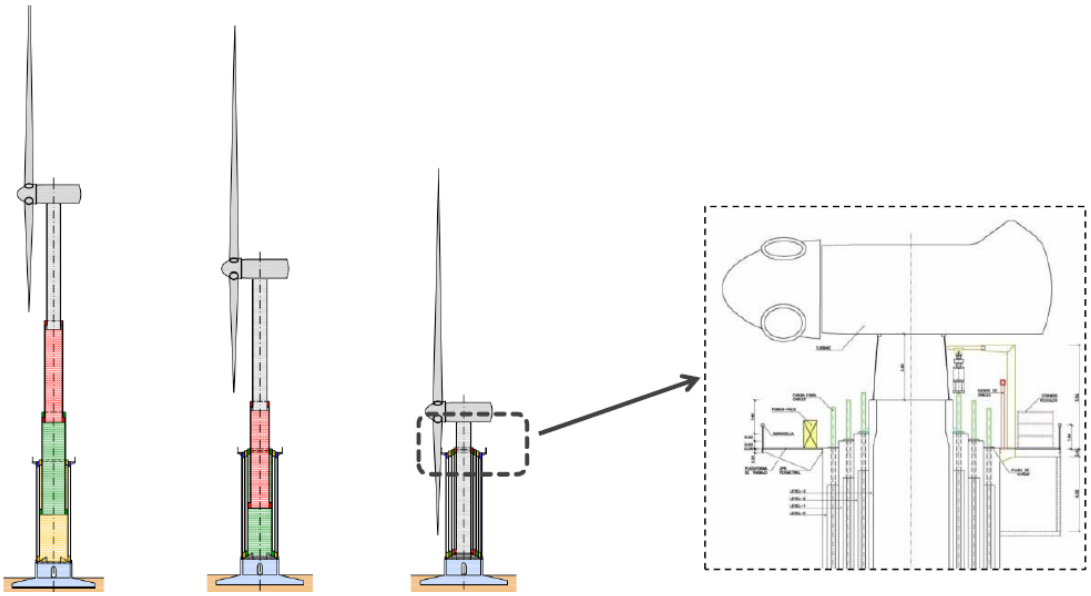

Figure 1.24. Esteyco self-lift tower concept (Esteyco Energia, 2014)

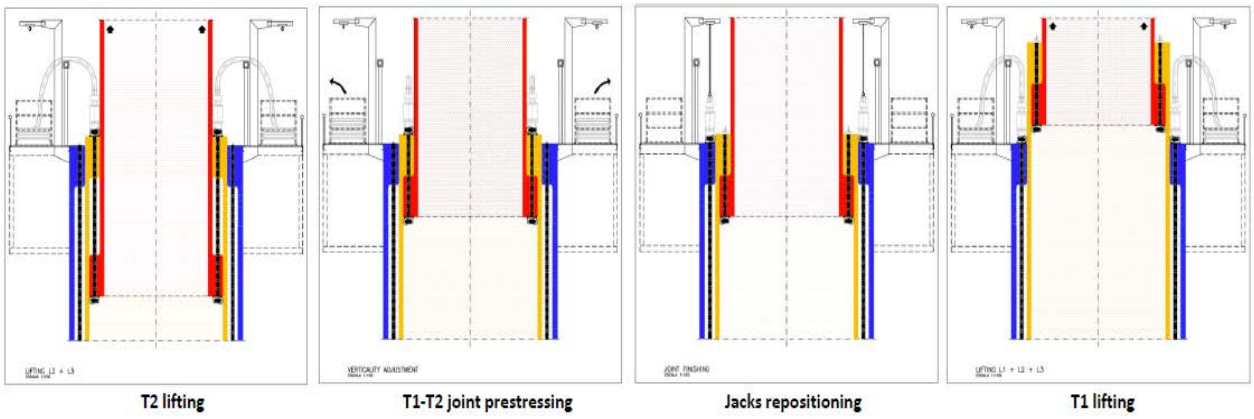

Figure 1.25. Strand jack lifting of tower sections (Esteyco Energia, 2014)

Figure 1.26. Prototype of self-lift Esteyco tower (Esteyco Energia, 2014)

In the U.S., hybrid towers are just starting to be utilized. MidAmerican Energy recently built a 377 ft (115 m) hybrid tower in Adams County, Iowa (Figure 1.27). Twenty-four circular concrete sections were poured onsite with 12 sets of forms supplied by EFCO Corporation (Figure 1.28). The sections were then allowed to cure and subsequently stacked to construct the tower (Figure 1.29). The top and bottom surfaces of each section were cast with matching indentations to allow alignment of the sections during construction. Once all of the concrete pieces were stacked to a height of 308 ft (94 m), a transition piece was then installed to connect the concrete tower to a 49 ft (15 m) steel shell. Vertical post-tensioning tendons were run to provide the tower with stability followed by installation of the nacelle and rotor. Transportation of the tower components was not needed due to onsite casting after the forms were shipped to the site. Total tower weight was 1,200 tons (1089 metric tons) with a final blade tip height of 558 ft (170 m) (MidAmerican Energy, 2016).

Figure 1.27. MidAmerican hybrid tower (MidAmerican Energy, 2016)

Figure 1.28. Formwork and onsite casting (MidAmerican Energy, 2016)

Figure 1.29. Stacked concrete tower sections (MidAmerican Energy, 2016)

1.3 Research objectives

The majority of the towers previously listed are manufactured and erected in Europe. Taller towers have not yet made a significant move into the United States and only a small number of towers utilizing concrete have been erected in the U.S. In an effort to advance tall tower design, manufacturing, and construction in the U.S., Dr. Sritharan and Iowa State Univerisity began working on the Hexcrete tower concept in 2010. The current research is a continuation of the original tower design project and is currently the third phase of research for the Hexcrete tower technology. Phase I of the study conducted by Dr. Sritharan and Thomas

Lewin in 2010 investigated the use of precast Ultra High Performance Concrete (UHPC) in wind turbine tower design and completed detailed 328 ft designs of a UHPC circular shell tower and a UHPC lattice tower (Lewin & Sritharan, 2010). The non-circular tower was defined as a lattice tower because of columns and bracing options as shown in Figure 1.30.

Figure 1.30. Lattice tower with horizontal bracing (left); horizontal tower with panel bracing (right) (Lewin & Sritharan, 2010)

Phase II of the research conducted by Dr. Sritharan and Grant Schmitz in 2013 focused on the UHPC lattice tower with panel bracing in partnership with Clipper Windpower. The goal of the Phase II research was to further investigate the magnitude of loads on the tower, reduce the tower cost, develop structurally sufficient connections between precast tower components, experimentally verify the developed connections, and produce an improved 328 ft UHPC tower design (Schmitz, 2013). The resulting Hexcrete tower concept from Phase II (Figure 1.31) was patented by Iowa State University.

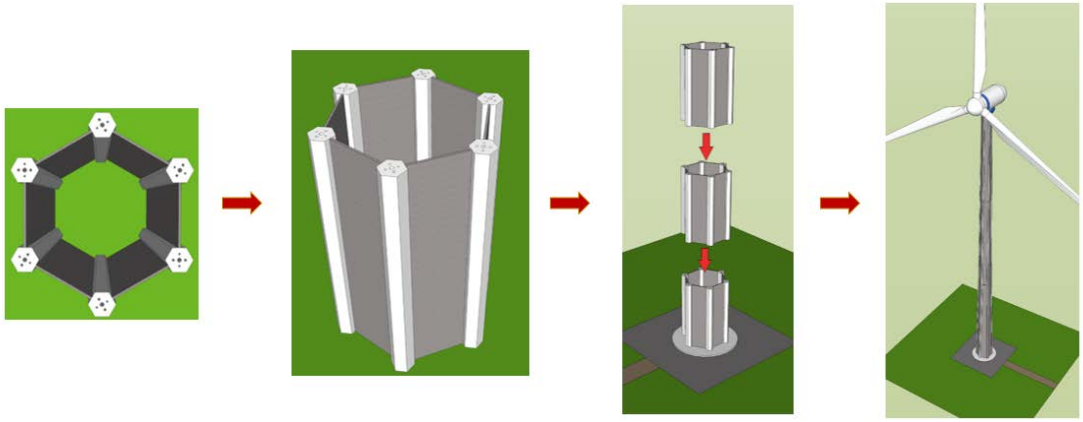

Figure 1.31. Hexcrete tower concept upon completion of Phase II of research (Schmitz, 2013)

The current Phase III research work began in the fall of 2014 and was made possible with sponsorship from the DOE, Iowa Department of Energy, and LaFarge North America. The primary goal of the Phase III research was to further develop the Hexcrete tower technology for hub heights up to 459 ft (140 m) with the goal of commercialing the tower technology and constructing a prototype tower. Industry partners for the project included Siemens, BergerABAM, Coreslab Structures of Omaha, and the National Renewable Energy Labs (NREL). The following sections summarize the tasks outlined for completion in Phase III. Some of the tasks are already completed while others require further investigation.

1.3.1 Design of Hexcrete towers above 100 m (328 ft):

The Hexcrete tower system provides an innovative solution to the transportation and logistical limitations of traditional steel towers when reaching higher hub heights. The design of the Hexcrete tower system was specifically adapted to meet emerging challenges faced for tall tower construction. The hexagon shape of the Hexcrete tower is unconventional but provides multiple benefits for segmenting the large diameter necessary for taller tower construction. First, the Hexcrete tower members are cast on a flat surface which eliminates curved sections therefore reducing the cost of formwork and simplifying transportation. Members are also easily replicable with all the columns and panels utilizing the same set of forms. The length of the Hexcrete members is customizable based on weight and length in order to best optimize the transportation and erection costs. Finally, the dimensions of the overall tower system can be adjusted to meet a site specific requirement such as a specific base diameter size. The towers are also designed to meet current certification standards, such as IEC 61400-01 part 1 and the GL guidelines, which ensure reliable tower designs.

By utilizing these advantages and partnering with Siemens, six Hexcrete wind turbine towers with hub heights above 328 ft were designed. Three towers were full Hexcrete towers and three were hybrid Hexcrete towers that combined Hexcrete with traditional steel at the tower top. The three tower design combinations included a 394 ft 2.3 MW turbine, a 459 ft 2.3 MW turbine, and a 459 ft 3.2 MW turbine. A full concrete and hybrid tower were designed for each combination. The towers utilized a combination of Ultra-High Performance Concrete (UHPC) with a compressive strength of 26 ksi (179.3 MPa) and High Strength Concrete (HSC) with a compressive strength of 13 ksi (89.6 MPa). All of the connections between precast members were design as post-tensioned connections using seven wire 270 ksi (1862 MPa) low relaxation

unbonded tendons. The dimensions of each tower will be discussed and along with specific design equations and methodology in later sections.

1.3.2 Experimental full-scale testing of Hexcrete tower section:

To validate the Hexcrete design methodology and further evaluate tower performance, a proof test of a full-scale tower segment was designed and tested at the Multi-Axial Subassemblage Testing (MAST) Laboratory in Minneapolis, Minnesota in 2015 (Figure 1.32). The dimensions of the tower section were taken directly from the 394 ft 2.3 MW turbine tower design and the test was designed to ensure that the precast tower segments acted as a single unit to resist both operational and extreme loads. The Hexcrete test unit performed well during testing and reserve capacity was observed beyond the design load limits. Test results, along with of the test unit design and construction details, will be reported in a subsequent chapter.

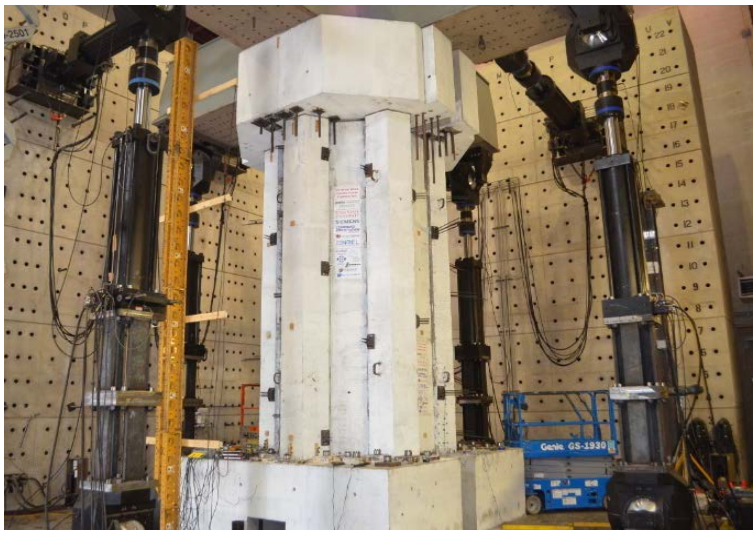

Figure 1.32. Completed Hexcrete full-scale test unit at MAST laboratory

1.3.3 Finite element and numerical analysis:

The finite element analysis program SAP2000 was used to model the dynamic response of the the six designed towers as well as the MAST test unit. Frequency and deflection limitations for each tower were based on the height of the tower as well as the size of the wind turbine. The MAST test unit was modeled in order to verify the test design and were verified based on test unit data.

Finite element modeling is a useful tool but is typically too involved and time-consuming for preliminary analysis as compared to numerical methods. In order to simplify the preliminary

tower design process, a simplified numerical method for identifying the capacity of the Hexcrete tower section is in the process of development. This process, defined as a modified section analysis method, will use a displacement based approach to calculate the strain in the vertical unbonded post-tensioning tendons. Accurate calculation of tendon strain will enable the behavior of the preliminary tower design to be more accurate and eliminate overdesign of the column components.

1.3.4 Hexcrete design guide formulation:

Development of a Hexcrete design guide will provide a useful set of data verified equations for design and optimization of the Hexcrete tower system. The design methodology of the six designed tall towers, along with design loads and limitations including MAST test unit observations, will be presented along with the design assumptions. Optimization of the Hexcrete tower system will then be outlined and will include guidelines and observations obtained from collaboration with Siemens and the ISU Construction Engineering department. Hybrid towers, which consisted of placing a steel top on the tower to replace the last 131- 164 ft (40-50 m) of Hexcrete, will also be discussed as a possible outcome of the optimization process. The streamlined design guide will enable rapid development and certification of the Hexcrete tower in the commercial wind tower market.

1.3.5 Surface pressure coefficients of Hexcrete towers

Due to the unique shape of the Hexcrete tower system, a study was performed according to current American Society of Civil Engineer (ASCE) 7-10 guidelines for chimneys, tanks, and other structures in order to better understand the surface pressures on the Hexcrete tower systems. A previously conducted Computational Fluid Dynamic (CFD) analysis was used as a baseline for comparison. The findings of the study will be presented with regard to surface pressures and base overturning moments. A comparison will also be made to an equivalent diameter circular tower for reference to current industry practice. Recommendation will be made according to the findings of the study.

1.4 Dissertation organization

After the introductory chapter, Chapter 2 presents a literature review of Phase I and Phase II research for the Hexcrete tower as well as a review of wind tower loads, dynamic factors affecting tower design, and the effect of post-tensioning on the natural frequency of structures.

The remainder of the material presented in this document is formatted as journal articles written for submission to structural engineering and wind energy journals. Chapter 3 outlines the Hexcrete tower design methodology, presents the six designed wind towers, and provides documentation and discussion for tower certification. The experimental test of a full scale Hexcrete tower section for design validation and strength evaluation is presented in Chapter 4 including the test design, setup, construction, and results. Chapter 5 details finite element and numerical modeling of the Hexcrete tower system. Chapter 6 presents an investigation of the surface pressure coefficients of the Hexcrete tower with comparison to the ASCE 7-10 code, Chapter 7 concludes the dissertation and provides a detail summary of the research results along with the long-term research impact.

1.5 References

Acciona WindPower. (2016, July). *Concrete Towers*. Retrieved from Acciona WindPower: http://www.acciona-windpower.com/technology/concrete-towers/

Advanced Tower Systems. (2016, July). *Advanced Tower Systems (ATS) higher hub heights for more economical wind projects*. Retrieved from ATS: http://www.hybridturm.de/en/home.html

Andresen Towers. (2015, June). *Andresen Towers News*. Retrieved from Andresen Towers: http://andresen-towers.com/news

AWEA. (2015, December). *U.S. wind industry leaders praise multi-year extension of tax credits*. Retrieved from American Wind Energy Association: http://www.awea.org/MediaCenter/pressrelease.aspx?ItemNumber=8254

AWEA. (2015). *Wind Energy Facts at a Glance*. Retrieved from American Wind Energy Association: http://www.awea.org/Resources/Content.aspx?ItemNumber=5059

BFT International. (2014, December). *Mixing Tower produces UHPC Concrete for Wind Turbines*. Retrieved from BFT International News: http://www.bft-international.com/en/artikel/bft_Mixing_Tower_produces_UHPC_Concrete_for_Wind_Turbines_2235978.html

Blattner Energy. (2015, May). *Balttner Energy Announces Post-Tension Concrete Tower Offering*. Retrieved from Blattner Energy: http://blattnerenergy.com/news/blattner-energy-announces-post-tension-concrete-tower-offering/

Blattner Energy. (2016, July). *Blattner Energy is the Premier EPC Wind Contractor in North America*. Retrieved from Blattner Energy: http://blattnerenergy.com/power-generation-construction/wind-energy-contractor/

de Vries, E. (2012). *Close up - Siemens' prototype steel shell tower.* Retrieved from Wind Power Monthly: http://www.windpowermonthly.com/article/1129016/close---siemens-prototype-steel-shell-tower

de Vries, E. (2015). *Close up: Vestas pushes on to meet the demands of low wind sites*. Retrieved from Wind Power Monthly: http://www.windpowermonthly.com/article/1363771/close-up-vestas-pushes-meet-demands-low-wind-sites

Del Franco, M. (2015, June). *Small Project in Illinois Could Make Big Headlines in Wind Farm Construction*. Retrieved from North American WindPower: http://nawindpower.com/small-project-in-illinois-could-make-big-headlines-in-wind-farm-construction

Eneco. (2012). *Siemens and Eneco test wind turbine with high 'construction set' tower*. Retrieved from Eneco: http://news.eneco.com/siemens-and-eneco-test-wind-turbine-with-high-construction-set-tower

Ericksen Roed & Associates. (2015). *Energy: Wind*. Retrieved from Ericksen Roed & Associates (ERA): http://eraeng.com/projects/unique-projects/energy-wind

Esteyco Energia. (2014). *Auto Lift Precast Concrete Towers: Double High with Half the Cranes.*

Esteyco Energia. (2014, October 10). *Esteyco Present at the Windaba 2014 Exhibition in South Africa*. Retrieved from Esteyco Energia : http://www.esteycoenergia.es/en/not.php?tipo=N&tip=&pag=4

GEA. (2015). *2015 Annual U.S. & Global Geothermal Power Production Report.* Geothermal Energy Association.

General Electric. (2013, September). *Max Bogl Wiesner GmbH Installs GE 2.5-120, World's Most Efficient High Output Wind Turbine*. Retrieved from GE News Room: http://www.genewsroom.com/Press-Releases/Max-B%C3%B6gl-Wiesner-GmbH-Installs-GE-25-120-Worlds-Most-Efficient-High-Output-Wind-Turbine-215422

Gouws, S. (2015, February). *Quality Management of Precast Concrete Segments for Wind Turbine Towers*. Retrieved from Slideshare: http://www.slideshare.net/SantieGouws/quality-management-of-precast-concrete-segments-for-wind-turbine-towers

Inneo Torres. (2008). *Precast Concrete Wind Towers*. Retrieved from Inneo Torres: http://www.inneotorres.es/web/index.php/en/tower-assembly.html

Lewin, T., & Sritharan, S. (2010). *Design of 328-ft (100-m) Tall Wind Turbine Towers Using UHPC.* Ames, IA: Department of Civil, Construction, and Enviromental Engineering Report ERI-ERI-10336.

Max Bogl. (2016). Max Bogl Hybrid Tower System. Neumarkt, Germany.

MidAmerican Energy. (2016, July). *Wind Energy*. Retrieved from MidAmerican Energy: https://www.midamericanenergy.com/wind-energy.aspx

National Renewable Energy Laboratory. (2016). *Potential Wind Capacity*. Retrieved from WINDExchange : http://apps2.eere.energy.gov/wind/windexchange/windmaps/resource_potential.asp

National Renewable Energy Labs (NREL). (2009, January). *Bigger and Better: Lab Aims to Improve Giant Wind Tubines*. Retrieved from NREL: http://www.nrel.gov/news/features/2009/1927

NAW Staff. (2012, July). *Construction Begins on Iowa Project Featureing 100-Meter Concrete Tower*. Retrieved from Norht American WindPower: http://nawindpower.com/construction-begins-on-iowa-project-featuring-100-meter-concrete-tower

Orihuela, R., & Parkin, B. (2015, November). *Nordex Told Assets It's to Buy From Acciona Targeted in Lawsuit*. Retrieved from Bloomberg: http://www.bloomberg.com/news/articles/2015-11-17/nordex-told-assets-it-s-to-buy-from-acciona-targeted-in-lawsuit

Potensa Wind Structures. (2016). *Cutting Edge Technology*. Retrieved from Potensa Wind Structures: http://www.postensaws.com/#

Schmitz, G. (2013). *Design and experimental validation of 328 ft (100 m) tall wind turbine towers utilizing high strength and ultra-high performance concrete.* Ames, IA: MS Thesis, Iowa State University.

SEIA. (2015). *Solar Industry Data: Solar Industry Growing at a Record Pace*. Retrieved from Solar Energy Industries Association: http://www.seia.org/research-resources/solar-industry-data

Siemens. (2011). *An Innovative Solution for High Hub Heights: Bolted Steel Shell Tower.* Retrieved from Siemens Energy: http://www.energy.siemens.com/us/pool/hq/power-generation/renewables/wind-power/Bolted_Steel_Shell_Tower_brochure_EN.pdf

Sun Journal. (n.d.). *Wind-turbine sections squeeze through 1935 Rumford Bridge*. Retrieved from Sun Journal: http://www.sunjournal.com/files/imagecache/story_large/2010/08/18/RUMwindtower3P081910.jpg

U.S. Department of Energy. (2015). *Renewable Electricity Production Tax Credit (PTC).* Retrieved from Energy.gov: http://energy.gov/savings/renewable-electricity-production-tax-credit-ptc

U.S. Department of Energy. (2015). *Wind Vision: A New Era for Wind Power in the United States.*

Vestas Wind Systems A/S. (2016). *Large Diameter Steel Tower (LDST).* Retrieved from Vestas Wind Systems A/S: http://nozebra.ipapercms.dk/Vestas/Communication/Productbrochure/LargeDiameterSteelTowerLDST/

Zavitz, B., & Kirkley, K. (2016, July). *Tindall White Paper Series No. WT-102.* Retrieved from Tindall Corporation - Anatomy of a Titan: http://www.tindallcorp.com/anatomy-concrete-tower-base/

CHAPTER 2 – LITERATURE REVIEW

2.1 Introduction:

The following sections provide a literature review of topics that directly relate to the design and testing of tall, concrete wind turbine towers. Wind turbine tower loads and design standards are examined, existing concrete tower designs above 262 ft (80 m) are reviewed, the effect of prestressing tendons on the natural frequency of structures is outlined, and dynamic factors considered in wind tower design are addressed.

2.2 Wind turbine tower loads and design standards:

2.2.1 International Electrotechnical Commission:

The International Electrotechnical Commission (IEC) document 64100-00, part 1, is the primary standard for classifying turbine types and specifying design load cases (DLCs) for wind turbine tower design. Each wind turbine is classified according to the intended installation site (Table 1) with numerical values given for *Vref*, which corresponds to the average 10 minute wind speed at the tower hub height. Turbulence characteristics are classified using letter designations with *Iref* corresponding to turbulence intensity values. These designations are for land based turbines with turbine classification *S* corresponding to offshore turbines, or turbines subject to tropical storms, hurricanes, or typhoons (IEC, 2008).

Table 2.1. IEC wind turbine classification

Wind turbine class	I	II	III	S
Vref, mph (m/s)	111.8 (50)	95.1 (42.5)	83.9 (37.5)	Values specified by the designer
A, *Iref*	0.16			
B, *Iref*	0.14			
C, *Iref*	0.12			

After a turbine is classified, wind profiles are created using the *Vref* wind speed and *Iref* turbulence values. The wind profiles correspond to specific wind events such as extreme operating gust (EOG) or extreme direction change (EDC) and the IEC code prescribes equations for each wind profile. Complete discussion of each profile will not be discussed, but prescriptive equations can be found in the IEC standards. Table 2.2 provides an outline of all the DLCs that must be considered in design of wind turbine towers, along with the corresponding wind condition (abbreviations provided in Figure 2.1). The type of analysis to be checked for each DLC is also indicated where “U” refers to ultimate strength and “F” to fatigue strength. Partial safety factors for each DLC are then listed with an explanation of safety factors provided in

Table 2.3. Further details regarding how to properly assess complex topographic conditions, wake effects from neighboring turbines, earthquake effects, soil conditions, assembly, installation, and erection are also included in the IEC guidelines (IEC, 2008).

Table 2.2. IEC design load cases (IEC, 2008)

Design situation	DLC	Wind condition	Other conditions	Type of analysis	Partial safety factors
1) Power production	1.1	NTM $V_{in} < V_{hub} < V_{out}$	For extrapolation of extreme events	U	N
	1.2	NTM $V_{in} < V_{hub} < V_{out}$		F	*
	1.3	ETM $V_{in} < V_{hub} < V_{out}$		U	N
	1.4	ECD $V_{hub} = V_r - 2$ m/s, V_r, $V_r + 2$ m/s		U	N
	1.5	EWS $V_{in} < V_{hub} < V_{out}$		U	N
2) Power production plus occurrence of fault	2.1	NTM $V_{in} < V_{hub} < V_{out}$	Control system fault or loss of electrical network	U	N
	2.2	NTM $V_{in} < V_{hub} < V_{out}$	Protection system or preceding internal electrical fault	U	A
	2.3	EOG $V_{hub} = V_r \pm 2$ m/s and V_{out}	External or internal electrical fault including loss of electrical network	U	A
	2.4	NTM $V_{in} < V_{hub} < V_{out}$	Control, protection, or electrical system faults including loss of electrical network	F	*
3) Start up	3.1	NWP $V_{in} < V_{hub} < V_{out}$		F	*
	3.2	EOG $V_{hub} = V_{in}$, $V_r \pm 2$ m/s and V_{out}		U	N
	3.3	EDC $V_{hub} = V_{in}$, $V_r \pm 2$ m/s and V_{out}		U	N
4) Normal shut down	4.1	NWP $V_{in} < V_{hub} < V_{out}$		F	*
	4.2	EOG $V_{hub} = V_r \pm 2$ m/s and V_{out}		U	N
5) Emergency shut down	5.1	NTM $V_{hub} = V_r \pm 2$ m/s and V_{out}		U	N
6) Parked (standing still or idling)	6.1	EWM 50-year recurrence period		U	N
	6.2	EWM 50-year recurrence period	Loss of electrical network connection	U	A
	6.3	EWM 1-year recurrence period	Extreme yaw misalignment	U	N
	6.4	NTM $V_{hub} < 0{,}7\ V_{ref}$		F	*
7) Parked and fault conditions	7.1	EWM 1-year recurrence period		U	A
8) Transport, assembly, maintenance and repair	8.1	NTM V_{maint} to be stated by the manufacturer		U	T
	8.2	EWM 1-year recurrence period		U	A

The following abbreviations are used in Table 2:	
DLC	Design load case
ECD	Extreme coherent gust with direction change (see 6.3.2.5)
EDC	Extreme direction change (see 6.3.2.4)
EOG	Extreme operating gust (see 6.3.2.2)
EWM	Extreme wind speed model (see 6.3.2.1)
EWS	Extreme wind shear (see 6.3.2.6)
NTM	Normal turbulence model (see 6.3.1.3)
ETM	Extreme turbulence model (see 6.3.2.3)
NWP	Normal wind profile model (see 6.3.1.2)
$V_r \pm 2$ m/s	Sensitivity to all wind speeds in the range shall be analysed
F	Fatigue (see 7.6.3)
U	Ultimate strength (see 7.6.2)
N	Normal
A	Abnormal
T	Transport and erection
*	Partial safety for fatigue (see 7.6.3)

Figure 2.1. IEC abbreviation definitions used in Table 2.2 (IEC, 2008)

Table 2.3. Partial safety factors

Unfavourable loads			Favourable[9] loads
Type of design situation (see Table 2)			All design situations
Normal (N)	Abnormal (A)	Transport and erection (T)	
1,35*	1,1	1,5	0,9

2.2.2 Germanischer Lloyd:

Germanischer Lloyd (GL) is a classification company that has provided a set of guidelines that have become standard for wind turbine tower design. The guidelines are similar to IEC standards with the addition of material specific recommendations. For concrete towers these additions provide service level limits including stress limitations and crack control. The stress limitation provision provides a combination of load cases (DLCs 1.5, 1.6, plus temperature effects) that must be considered and result in material stress less than 0.6f'c. It is also specified that for prestressed concrete towers the compressive stress of the concrete due to the tower weight and prestressing must be limited to 0.45f'c (GL, 2010). Theoretical crack width limits of 0.2 mm are required under the load combination of DLC 1.5 and temperature effects, and decompression of prestressed concrete towers must also be checked under the DLC combination of DLC 1.1 and DLC 6.4 with a probability of exceedance of pf $=10^{-2}$ (GL, 2010).

Decompression and tower cracking are related in that decompression of a prestressed interface often leads to cracking; the GL guidelines are verifying that large cracks do not appear in concrete towers under service loads which would subsequently cause a reduction in tower stiffness and eventual tower failure.

2.2.3 American Society of Civil Engineers:

In 2011, the American Society of Civil Engineers (ASCE) and the American Wind Energy Association (AWEA) released a recommended practice document for wind tower designers in the United States (U.S.). Currently, a standardized code for wind turbine towers does not exist in the U.S and the purpose of the ASCE/AWEA document was to clarify appropriate standards and institute a minimum level of safety to ensure long term success of wind turbine structures (ASCE/AWEA, 2011). The document recommends following IEC wind load standards and specifications provided by turbine manufacturers above ASCE 7-10 wind load guidelines. It is noted that ASCE 7-10 guidelines and the IEC extreme wind model (EWM) produce similar results for calculating extreme 3 second gust wind loads on the tower for a fifty year return period with exposure classification C (open terrain with little to no obstructions) (Figure 2.2) (ASCE/AWEA, 2011). This finding can be useful in checking direct wind loads on wind turbine towers as hub heights increase since at lower hub heights tower loads are considered to be almost negligible.

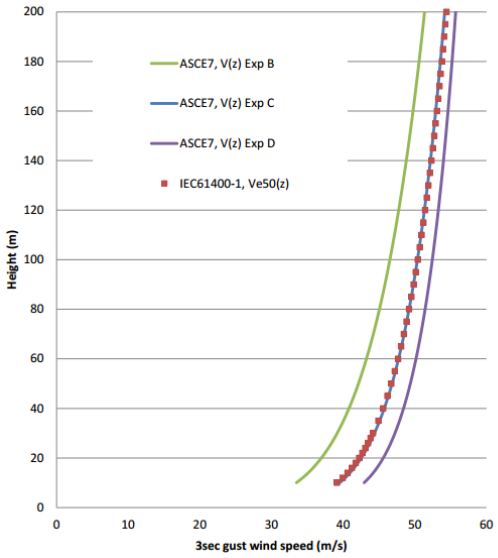

Figure 2.2. IEC extreme wind model (EWM) and ASCE 7-10 extreme 3-sec gust wind profiles with 50 year return period

2.3 Concrete tower design above 262 ft (80 m):

2.3.1 Introduction:

As summarized previously, multiple precast concrete wind towers have been constructed with various designs and details. The following section provides information regarding precast concrete tower designs for which load magnitudes and resulting tower dimensions were publicly available since specific turbine load information is often proprietary. Specific design calculations are not outlined; instead load information and tower design outcomes are summarized in order to provide a baseline reference for future precast concrete tower design. Detailed tower equations are available from the specified tower design sources.

2.3.2 National Renewable Energy Laboratory and BergerAbam:

The National Renewable Energy Laboratory (NREL) partnered with BergerAbam in 2004 to examine the cost benefits of all concrete and concrete/steel hybrid wind turbine towers for 100 m (328 ft) hub heights (Lanier, 2005). One of the goals of the study was to reduce the tower installation and construction costs and well as targeting the southeast region of the United States for Low Speed Wind Turbine (LSWT) projects with a target Levelized Cost of Energy (LCOE) of $0.03/kWh (Lanier, 2005). The project examined wind farms with a minimum of 50 turbines and designed both concrete and hybrid 100 m towers for 1.5 MW, 3.6 MW, and 5.0 MW machines (Lanier, 2005). Both the concrete and hybrid towers utilized precast, prestressed circular concrete sections. Construction procedures and cost estimates were also developed and subsequently compared to the cost of 100 m steel towers. Significant work was done regarding evaluation of tower loads, applying appropriate load factors, and investigation of construction costs. The tower top design loads resulting from turbine operation are listed in Table 2.4. Direct wind loads were evaluated according to ASCE 7-05 guidelines for chimneys, tanks, and other structures and added to the listed loads. Fatigue design of the towers was also performed following the 1990 Model Code (MC90) from the International Federation for Prestressing (CEB-FIP). The complete tower design process, outlined in Figure 2.3, was then applied with the resulting concrete tower designs listed in Table 2.5. The hybrid tower design results included earthquake loading and can be found in NREL report (Lanier, 2005).

Table 2.4. Tower top design loads

		Axial (kN)	Axial (kips)	Shear (kN)	Shear (kips)	Moment (kNm)	Moment (k-ft)
1.5 MW	Factored EWM50	999	225	519	117	53730	39630
	Unfactored EWM50	832	187	384	86	39800	29360
	Unfactored EOG50	832	187	402	90	33060	24380
3.6 MW	Factored EWM50	3796	853	1467	330	165900	122400
	Unfactored EWM50	3155	709	1087	244	122900	90640
	Unfactored EOG50	3129	703	1199	270	100700	74280
5.0 MW	Factored EWM50	6041	1358	781	176	189500	139800
	Unfactored EWM50	4998	1124	578	130	140400	103500
	Unfactored EOG50	4879	1097	1065	239	145500	107300

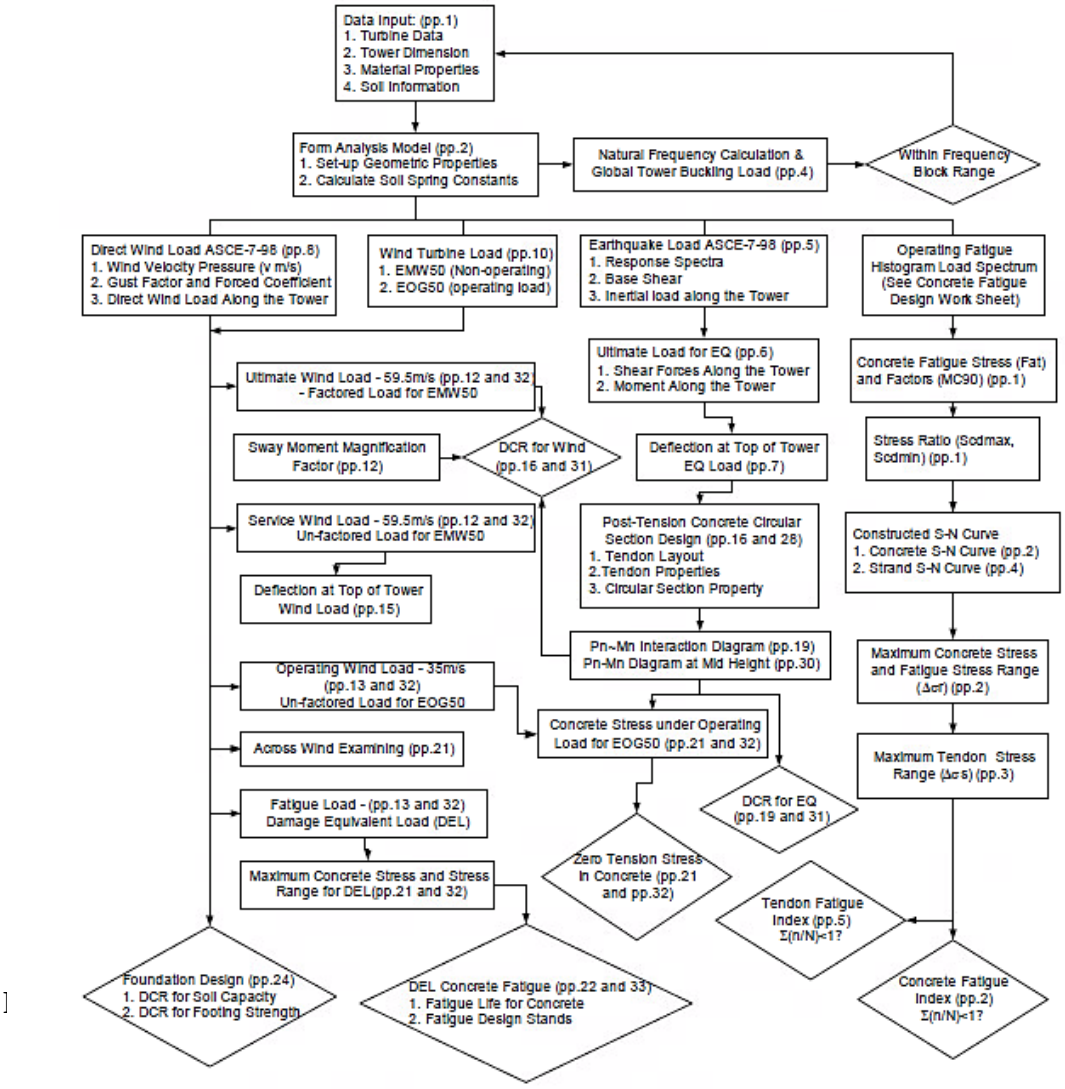

Figure 2.3. Tower design process

Table 2.5. Concrete tower design details

	1.5 MW		3.6 MW		5.0 MW	
Rotor Diameter	70.5 m	231.2 ft	108.4 m	29.63 ft	128 m	419.8 ft
Weight of nacelle, hub, and rotor	832 kN	187 kips	3087.2 kN	694 kips	4706.4 kN	1058 kips
Outside diameter of tower base	5.79 m	19 ft	6.706 m	22 ft	7.62 m	25 ft
Wall thickness at tower base	0.61 m	2 ft	0.6858 m	2.25 ft	0.762 m	2.5 ft
Outside diameter at tower top	2.90 m	9.5 ft	3.658 m	12 ft	3.658 m	12 ft
Wall thickness at tower top	0.46 m	1.5 ft	0.46 m	1.5 ft	0.46 m	1.5 ft
Tower Weight	14470 kN	3254 kips	20370 kN	4579 kips	24470 kN	5502 kips
Tower Frequency	0.377 Hz		0.377 Hz		0.384 Hz	
Number of prestress tendons at tower base	30		40		56	
Controlling Load Case	Tower frequency		Concrete fatigue		Concrete fatigue and tendon strength	

A cost estimate was also performed for the precast concrete towers assuming installation of 50 towers. The cost estimate was for the entire construction cost including, materials, labor, fabrication, transportation, installation, and erection (Lanier, 2005). The total cost, shown in Table 2.6, also included the foundation for each tower where the overall cost of energy ($/KW) decreased with nacelle size. These precast tower costs were compared with current cast-in-place concrete technology and it was found that the precast concrete did not provide enough cost advantage to be recommended over cast-in-place solutions. The study concludes with the recommendation that cast-in-place concrete towers be pursued over precast options (Lanier, 2005).

Table 2.6. Precast concrete tower costs

	Installed Cost	$/KW
1.5 MW	$ 1,581,707	$ 1,054
3.6 MW	$ 2,026,608	$ 563
5.0 MW	$ 2,402,928	$ 481

2.3.3 Iowa State University - Lewin and Sritharan:

In 2010, Thomas Lewin and Sri Sritharan designed multiple wind turbine towers with hub heights of 328 ft (100 m). Tower design materials included steel, concrete, and Ultra High Performance Concrete (UHPC) (Lewin & Sritharan, 2010). UHPC is a high performance concrete mix that contains steel fibers and has a compressive strength of 26 ksi (179.3 MPa) (Lewin & Sritharan, 2010). The towers were designed for a 3 MW Acciona AW-109/3000 turbine. The tower top loads resulting from the operation of the turbine; the nacelle and blade weights, including an additional axial compression force from turbine rotation; and the tower damage equivalent loads (DEL) for fatigue are listed in Table 2.7 through Table 2.9. Direct wind loads were also calculated based on ASCE 7-05 guidelines utilizing IEC wind profiles. The fifty year extreme wind model (EWM50) and fifty year extreme operating gust (EOG50) were determined to be the controlling profiles for each tower design and the resultant tower forces (Table 2.10) were calculated for each tower material based on the tower shape and geometry (Lewin & Sritharan, 2010) (IEC, 2008).

Table 2.7. Lewin tower top loads

	Vx kips (kN)	Vy kips (kN)	Mx kip-ft (kN-m)	My kip-ft (kN-m)	Mz kip-ft (kN-m)
EWM50	144.6 (643)	191.9 (854)	8120 (11,020)	4440 (6030)	3930 (5330)
EOG50	245 (1092)	15.00 (65.5)	2530 (3420)	4380 (6820)	727 (985)

Table 2.8. Nacelle, blade, and operating weights

Weight per blade - kips (kN)	25.4 (113.2)
Nacelle + hub - kips (kN)	340 (1510)
Additional axial compression - kips (kN)	70.0 (311)
Total axial turbine load - kips (kN)	486 (2160)

Table 2.9. Damage equivalent loads (DEL)

DEL Vx - kips (kN)	26.8 (119.2)
DEL My - kip-ft (Kn-m)	1210 (1640)

Table 2.10. Direct wind loads for each type of tower

Tower Material	IEC Load Case	Mid Vx kips (kN)	Mid My kip-ft (kN-m)	Base Vx kips (kN)	Base My kip-ft (kN-m)
Steel	EWM50	126.6 (563)	9930 (13330)	252 (1121)	40,780 (55300)
	EOG50	20.9 (93.0)	1623 (2200)	41.5 (184.6)	6730 (9120)
Concrete	EWM50	137.6 (612)	10260 (13910)	300 (1334)	46000 (62400)
	EOG50	24.3 (108.1)	1805 (2450)	53.2 (237)	8120 (11010)
UHPC Shell	EWM50	126.3 (562)	9890 (13410)	261 (1161)	41300 (56000)
	EOG50	21.1 (93.9)	1650 (2240)	43.6 (193.9)	6900 (9360)
UHPC Lattice	EWM50	198.0 (881)	15730 (21300)	389 (1730)	64000 (86800)
	EOG50	34.3 (152.6)	2720 (3690)	67.6 (239)	11090 (15040)

As noted in Table 2.10, a total of four towers were designed. The steel, concrete, and UHPC shell tower were traditional hollow circular towers, while the UHPC lattice tower was hexagon in shape with six circular columns and corresponding column bracing that consisted of horizontal bracing members or full wall braces (Figure 2.4). The resulting tower designs and geometry are shown in Table 2.11. The UHPC Lattice tower was further investigated due to its innovative design and the lower amount of tower top deflection when compared to the steel and UHPC shell tower (Lewin & Sritharan, 2010). The concrete shell tower also had significantly less top deflection, however, the large amount of required concrete material resulted in a significantly heavier tower and larger material costs which made the UHPC lattice tower more favorable.

Figure 2.5. UHPC lattice towers, horizontal braces (left); wall braces (right) (Lewin & Sritharan, 2010)

Table 2.11. Tower design details

	Steel tower	Concrete tower	UHPC Shell	UHPC Lattice
Material Strength, ksi (Mpa)	fy = 50 (345)	f'c = 7 (48)	f'c = 26 (179.3)	f'c = 26 (179.3)
Diameter at base, in. (m)	216 (5.49)	360 (9.15)	270 (6.86)	354 (8.99)
Shell thickness at base, in. (mm)	1.5 (38.1)	8.375 (213)	4.25 (108.0)	-
Diameter at 110 ft (33.5 m), in. (m)	198 (5.03)	312 (7.93)	213 (5.41)	294 (7.47)
Shell thickness at 110 ft (33.5 m), in. (mm)	1.25 (31.8)	7.875 (200)	3.865 (98.2)	-
Diameter at 220 ft (67.1 m), in. (m)	168 (4.27)	222 (5.64)	166.5 (4.23)	246 (6.25)
Shell thickness at 220 ft (67.1 m), in. (mm)	1.25 (31.8)	9.4 (239)	3.25 (82.6)	-
Diameter at 322 ft (98.2 m), in. (m)	120 (3.05)	130.5 (3.31)	132 (3.35)	120 (3.05)
Shell thickness at 322 ft (98.2 m), in. (mm)	1.1 (27.9)	9.4 (239)	3.25 (82.6)	-
Material Volume, yd^3 (m^3)	55.81 (42.7)	574 (439)	183 (139.9)	173 (132.4)
Tower Weight, kips (kN)	739 (3290)	2300	866 (139.9)	1120 (4980)
Fundamental Natural Frequency of Tower, Hz	0.338	0.568	0.372	0.495
Top Deflection, in. (m)	63.6 (1.617 m)	15.98 (0.406)	55.18 (1.402)	27.2 (0.691)
Controlling Limit State	Tower base strength, steel fatigue	Service level strength, concrete fatigue	Shear and torsion interaction	Service level moment

In order to further investigate the UHPC lattice tower, a specific bracing system utilizing both horizontal and cross bracing members was designed and a centerline finite element simulation was created (Lewin & Sritharan, 2010). The braces were designed to be hollow, circular UHPC members that could be prestressed or post-tensioned for added tensile capacity. It was found that the designed UHPC bracing system was adequate for service level loads, which are expected to govern the design, and that other bracing options such as steel WT-sections may also be possible if verified. The centerline analysis identified force redistribution between the columns and bracing which resulted in lower column stresses and higher stresses in the braces (Lewin & Sritharan, 2010).

The main conclusion drawn from the four tower designs was that the UHPC lattice tower design offered a promising alternative to traditional steel or concrete shell tower design by offering a practical solution for alleviating transportation challenges while maintaining adequate performance standards (Lewin & Sritharan, 2010). Circular shell steel and concrete towers will continue to face logistical issues as hub heights continue to increase and shell diameters expand. In addition, the lattice tower was not governed by fatigue which may allow the tower life to be

extended beyond the current 20 year steel tower service life and provide further benefits for future wind installation (Lewin & Sritharan, 2010).

2.3.4 Iowa State University – Schmitz and Sritharan:

In 2012, Schmitz and Sritharan, of Iowa State University, continued work on the UHPC lattice tower concept by designing three 328 ft (100 m) lattice towers for a 2.5 MW Liberty turbine from Clipper Windpower (Schmitz, 2013). Due to feedback from the wind industry, the lattice tower with full wall braces was chosen over the horizontal UHPC braces designed by Lewin and Sritharan in order to fully enclose the wind tower and protect the internal tower components. The tower columns were subsequently modified to be hexagon in shape in order to provide a flat surface for connection of the wall braces. Due to the proprietary nature of wind tower loads, the loads for the 2.5 MW Liberty turbine were not published, however, loads of similar magnitude were derived for a 2.5 MW turbine from the loads provided by Lewin and Sritharan (Schmitz, 2013). The tower top loads and damage equivalent loads (DEL) are shown in Table 2.12 and Table 2.13.

Table 2.12. 2.5 MW turbine loads at top of tower

	Vx kips (kN)	Vy kips (kN)	Mx kip-ft (kN-m)	My kip-ft (kN-m)	Mz kip-ft (kN-m)
EWM50	127.5 (567)	169.1 (752)	6218 (8430)	3033 (4112)	3315 (4495)
EOG50	209 (930)	12.0 (54.7)	1955 (2650)	2882 (3908)	451 (611)

Table 2.13. 2.5 MW damage equivalent loads (DEL)

DEL Vx - kips (kN)	22.2 (98.7)
DEL My - kip-ft (Kn-m)	915 (4071)

In order to continue to improve the design of the lattice tower, high strength concrete (HSC) with a compressive strength of 13 ksi (89.7 MPa) was used in addition to UHPC to reduce overall tower costs (Schmitz, 2013). HSC sections add weight to the overall tower system because of larger concrete sections, however, due to the high material cost of UHPC, it was thought that the use of HSC could be economical (Schmitz, 2013). Three towers were designed with different combination of HSC and UHPC as shown in Table 2.14 where the connecting wall braces are referred to as panels. Each tower contained three stages of vertical, internal post-tensioning in the test unit columns (Figure 2.5). The first set of post-tensioning ran the full height of the tower, the second was terminated at 220 ft (67.1 m), and the third set was terminated at

110 ft (33.5 m). The amount of vertical post-tensioning for each stage was based on the magnitude of tower loads. The resulting tower designs are shown in Table 2.15 (Schmitz, 2013).

Table 2.14. Tower materials

Tower Name	Column Material	Panel Material
HCUP	HSC	UHPC
HCHP	HSC	HSC
UCUP	UHPC	UHPC

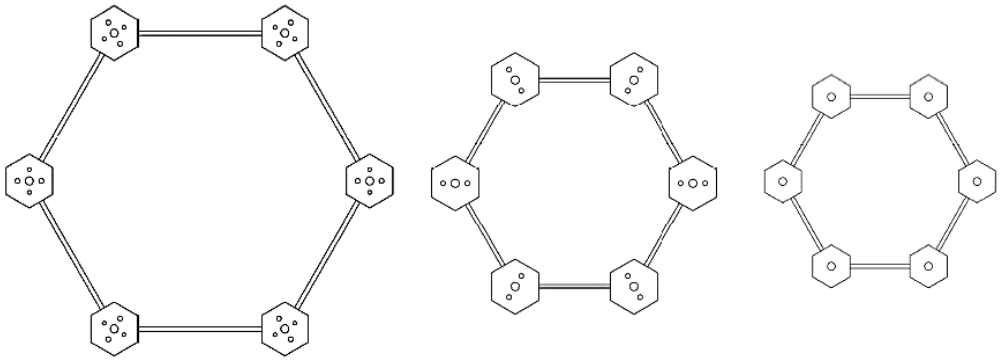

Figure 2.6. Cross-sections of lattice towers showing post-tensioning locations (Schmitz, 2013)

Table 2.15. Lattice tower geometry and tower properties

	HCUP	HCHP	UCUP
Column compressive strength, ksi (MPa)	f'c = 13 (89.7)	f'c = 13 (89.7)	f'c = 26 (179.3)
Panel compressive strength, ksi (Mpa)	f'c = 26 (179.3)	f'c = 13 (89.7)	f'c = 26 (179.3)
Vertical post-tensioning effective stress, ksi (MPa)	180 (1241)	180 (1241)	180 (1241)
Diameter at base, in. (m)	228 (5.79)	228 (5.79)	228 (5.79)
Column diameter at base, in. (mm)	36 (914)	36 (914)	25.5 (648)
Number of 0.6 in. diameter tendons, 0-110 ft (0-33.5 m)	402	402	390
Diameter at 110 ft (33.5 m), in. (m)	156 (3.96)	156 (3.96)	160 (4.06)
Column diameter at 110 ft (33.5 m), in. (mm)	36 (914)	36 (914)	25.5 (648)
Number of 0.6 in. diameter tendons, 110-220 ft (33.5-67.1 m)	366	366	354
Diameter at 220 ft (67.1 m), in. (m)	132 (3.35)	132 (3.35)	134 (3.40)
Column diameter at 220 ft (67.1 m), in. (mm)	29 (737)	29 (737)	20 (508)
Number of 0.6 in. diameter tendons, 220-319.5 ft (67.1-97.4 m)	198	198	210
Diameter at 322 ft (98.2 m), in. (m)	112.6 (2.86)	112.6 (2.86)	112.6 (2.86)
Column Diameter at 322 ft (98.2 m), in. (mm)	21 (533)	21 (533)	17 (431.8)
Material Volume, yd^3 (m^3)	378.2 (289.2)	451.7 (345.4)	318.3 (289.2)
Tower Weight, kips (kN)	1620	1907	1384
Fundamental Natural Frequency of Tower, Hz	0.32	0.34	0.293
Top Deflection, in. (m)	53.1 (1.35)	39 (0.99)	66.1 (1.68)

To further advance the lattice tower concept, three connection details for joining the panels and columns were designed and experimentally tested. The first connection was a bolted connection shown in Figure 2.6 that consisted of an embedded column plate, two embedded panel plates, and an angled connection plate. The column plate utilized shear studs to transfer the load to the column concrete while the panel plates utilized welded reinforcement for load transfer as shown in Figure 2.6 (Schmitz, 2013). The second connection detail was a UHPC wet joint which was utilized with the HCHP tower. A pocket was provided in each tower column and protruding rebar was embedded in both the panel and column (Figure 2.7). After placement and alignment of the columns and panels the pocket was filled with UHPC to provide continuity across the connection interface. The wet joint connection takes advantage of the shortened amount of development length required in UHPC (Schmitz, 2013). The final connection was a horizontal post-tensioned connection that utilized 0.6 in. (15.24 mm) diameter tendons installed in circumferential ducts around the test unit perimeter (Figure 2.8). The connection detail relied on the post-tensioning force and shear friction between the column and panels to generate sufficient connection capacity. A 0.75 in. (1.9 cm) layer of high strength epoxy was placed between each column and panel for the post-tensioned connection detail in order to ensure a smooth bearing surface between tower members (Schmitz, 2013).

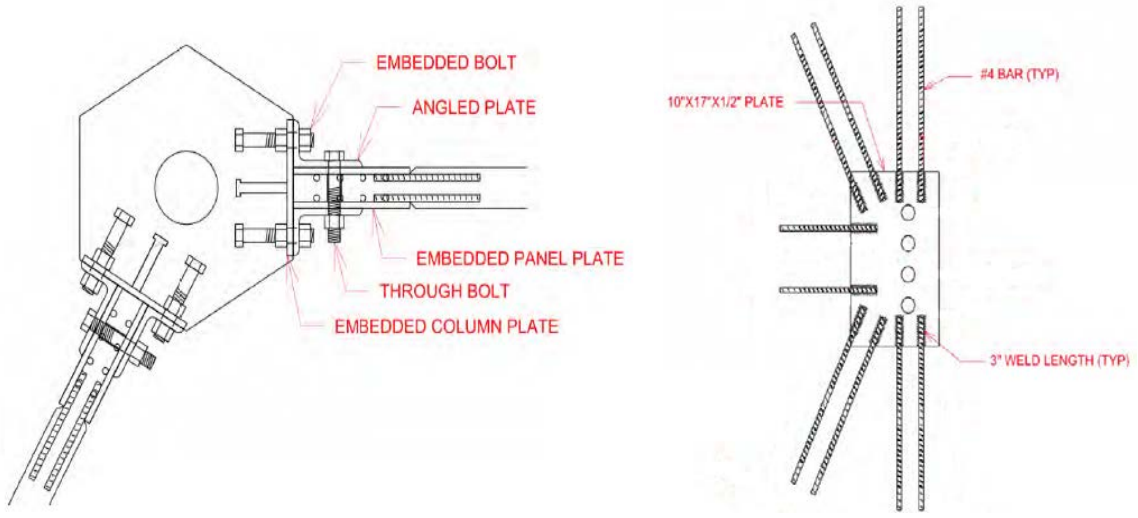

Figure 2.7. Bolted connection detail (left); panel embedded plate with welded reinforcement (right) (Schmitz, 2013)

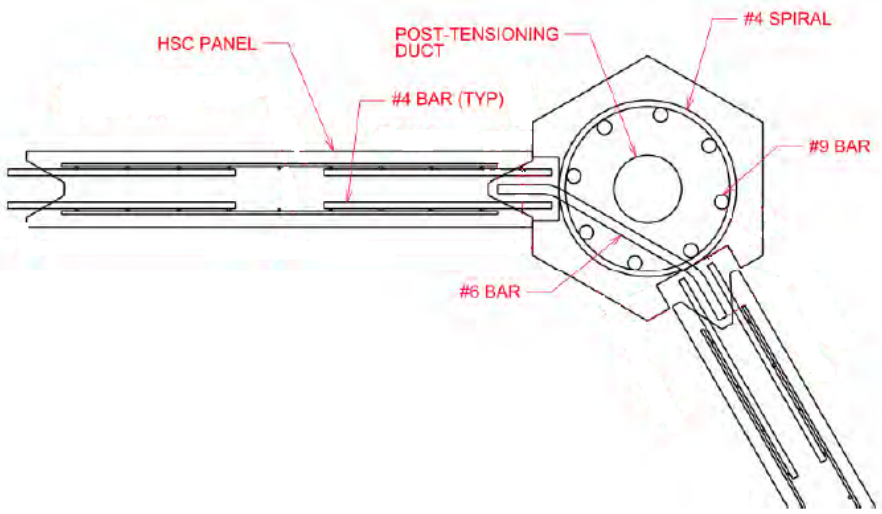

Figure 2.8. UHPC wet joint connection (Schmitz, 2013)

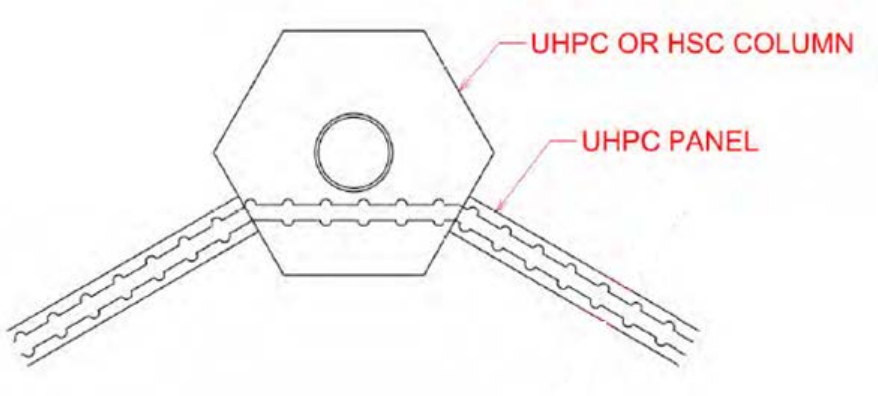

Figure 2.9. Circumferential post-tensioned connection (Schmitz, 2013)

Experimental testing of each connection was conducted in the Iowa State University Structural Laboratory. The test unit was a full scale section of a single side of each tower that consisted of two 12 ft (3.66 m) tower columns and a single 12 ft tower panel (Figure 2.9). The test unit sections corresponded to the top 12 ft of each tower and equivalent tower loads were calculated for lateral application to the test unit. The bolted connection was tested with the HCUP tower test unit, the wet joint with the HCHP tower test unit, and the post-tensioned connection with the UCUP tower test unit. The force displacement response of each connection is shown in Figure 2.10 - Figure 2.12. The bolted connection met the required load demands but generated a large amount of localized stresses and it was postulated that the connection may be difficult to construct in the field due to bolt hole tolerances (Schmitz, 2013). The UHPC wet joint performed well and provided a way to prevent column and panel separation that may occur in the

bolted or post-tensioned connections. However, under extreme loads it was observed that hairline cracks appeared at the wet joint interface in order to engage the rebar embedded in the joint. These cracks did not adversely affect the tower performance, but could be important to consider in environments that are highly corrosive such as marine locations (Schmitz, 2013). The UHPC wet joint also requires increased construction time to allow all the joints to cure. The post-tensioned connection had similar performance to the wet joint and no interface opening was observed in the test unit, even under extreme loads (Schmitz, 2013).

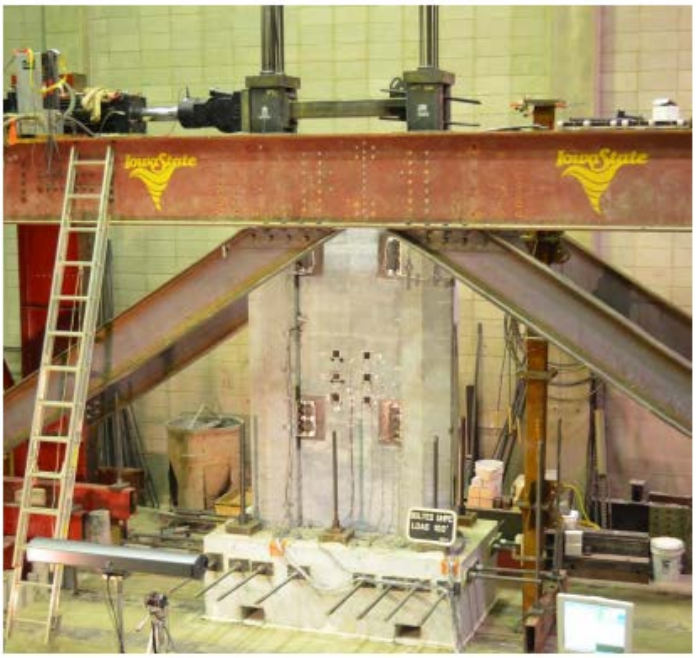

Figure 2.10. Test unit setup, bolted connection test (Schmitz, 2013)

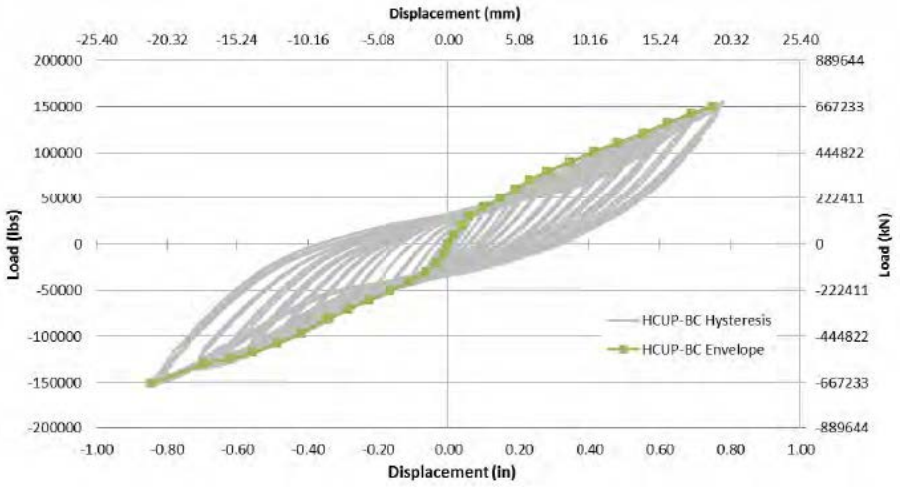

Figure 2.11. Bolted connection force-displacement response (Schmitz, 2013)

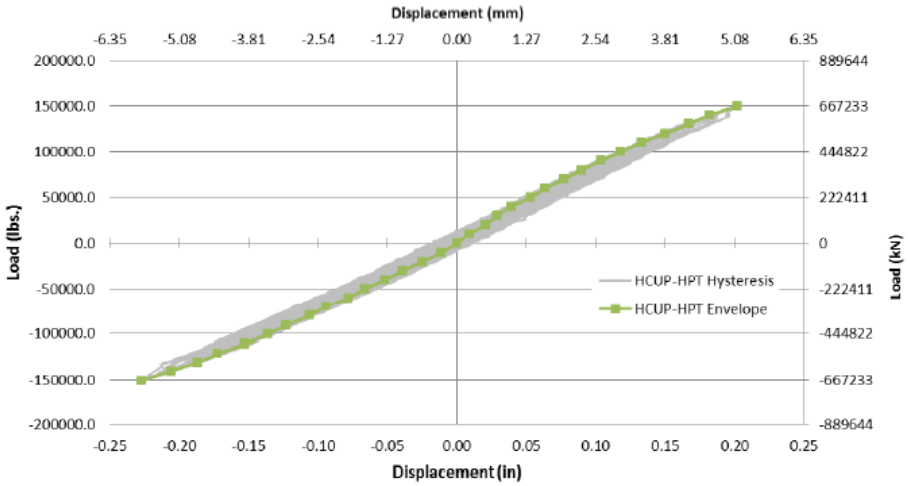

Figure 2.12. UHPC wet joint force-displacement response (Schmitz, 2013)

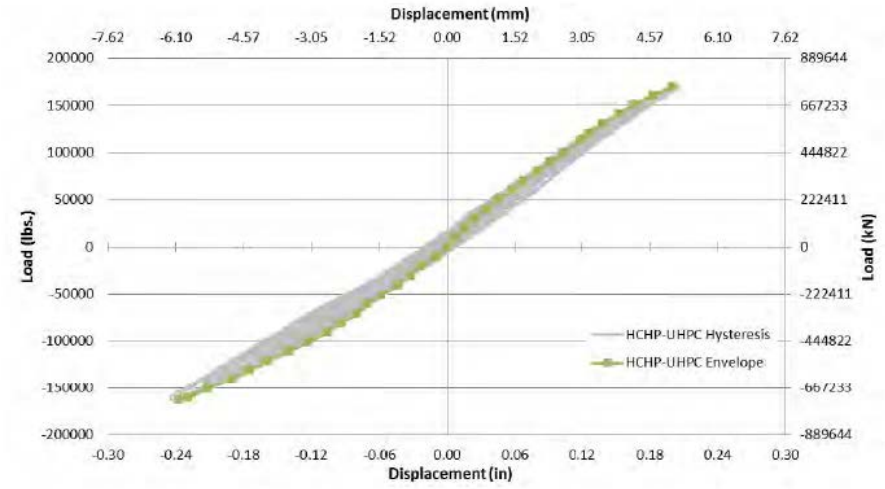

Figure 2.13. Post-tensioned connection force-displacement response (Schmitz, 2013)

The research at Iowa State University by Lewin, Sritharan, and Schmitz was successful in developing a new patented UHPC lattice tower technology (U.S. Patent No. 8,881,485, 2014) (U.S. Patent No. 9,016,012, 2015). It was found that panel bracing for the tower would be the most effective and that UHPC wet joint or horizontal post-tensioned connections provided exceptional load capacity and displacement performance. The HCUP tower was identified as a cost-effective solution that reduced the tower top deflection compared to the UCUP tower and reduced the tower weight in comparison to the HCHP tower. The researchers note that an aerodynamic analysis should be completed through computational fluid modeling or wind tunnel testing to further understand the effect of the hexagon tower shape on tower wind loads.

2.4 Prestressing tendon effects on tower natural frequency:

2.4.1 Introduction:

Many concrete tower systems contain prestressing tendons that are either prestressed or post-tensioned. The number and location of these tendons varies depending on the tower design. The following literature was reviewed in order to determine the effect of prestressing tendons and corresponding prestressed forces on the frequency of concrete members and by extension, tower structures.

2.4.2 Hamed and Frostig:

This paper presents a non-linear analytical model to evaluate the dynamic response of prestressed beams (Hamed & Frostig, 2006). The model is general in nature and the authors state that the model is valid for any boundary or continuity condition. Kinematic relations for the concrete use large displacements and moderate rotations to correctly model the compressive force provided by the tendons (Hamed & Frostig, 2006). The authors point out that the combined natural frequency of both the beam and tendon must be considered along with compressive force effects, changes in prestressing, and changes in tendon position (Hamed & Frostig, 2006). While full details of the complex numerical model can be found in the referenced article, the results of the model predict that prestressing does not affect the natural frequency of the concrete member regardless of the magnitude of applied prestressing force. (Hamed & Frostig, 2006).

2.4.3 Wang, Huang, and Wang

In this article, the authors state that that concrete beams that are axial loaded in compression decrease in stiffness, while steel tendons loaded in tension increase in stiffness (Wang & Huang, 2013). The article then proceeds to investigate the effects of prestressed and post-tensioned strands on a concrete beam using the experimental setup as shown in Figure 2.13. Five identical beams were fabricated with identical geometries and reinforcement details. Three of the beams had parabolic tendons with eccentricity of $e = 0$ at each end and $e = 8$ in. at the center of the beam. The other two beams contained straight tendons with a constant eccentricity of $e = 8$ in. (Wang & Huang, 2013). The impact hammer kit shown in Figure 2.14 was used to measure the beam frequency before stressing of the tendons, after stressing of the tendons but before grouting, and after grouting of the tendons. The frequencies for the first two vertical modes are recorded in Table 2.16 with $\omega b1$ representing the frequency before prestressing, $\omega p1$ representing the frequency after prestressing, and $\omega g1$ representing the frequency after grouting

(Wang & Huang, 2013). It can be observed that the natural frequency decreases after stressing for all the beams with parabolic tendons, regardless of the magnitude of prestressing force, and that the natural frequency of the beams with straight tendons does not change after tensioning. Therefore the authors conclude that straight tendons will not affect the concrete member frequency but parabolic tendons will reduce the overall frequency (Wang & Huang, 2013).

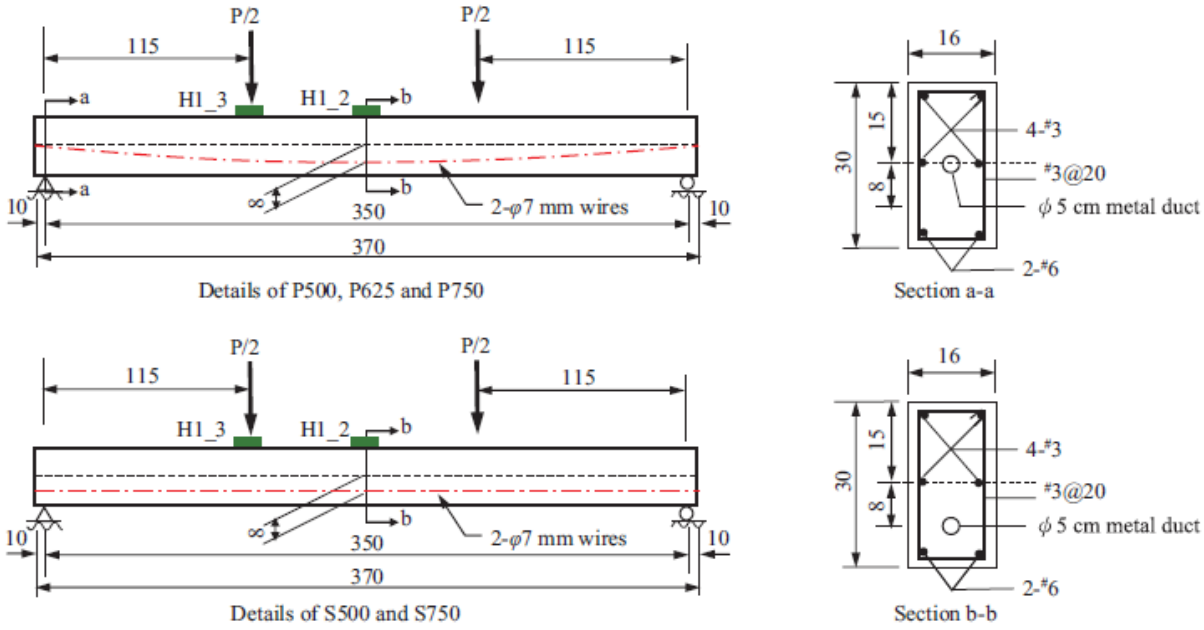

Figure 2.14. Experimental beam setup (Wang & Huang, 2013)

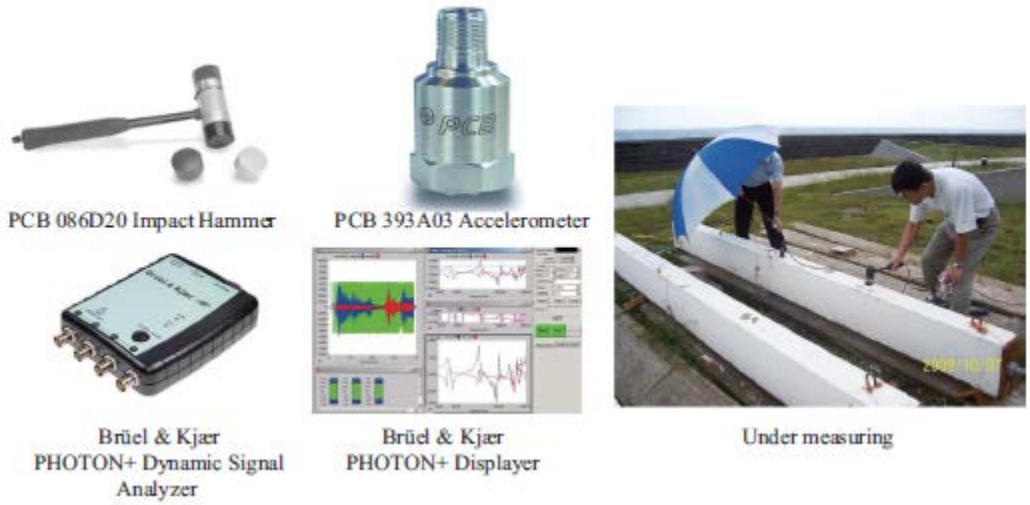

Figure 2.15. Accelerometer kit used to measure beam frequency (Wang & Huang, 2013)

Table 2.16. Frequency results from beam test (Wang & Huang, 2013)

Specimen Designation	Prestressing Force P_s (KN)	1st. mode (Hz)			2nd. mode (Hz)		
		ω_{b1}	ω_{p1}	ω_{g1}	ω_{b2}	ω_{p2}	ω_{g2}
P500	31.39	27.00	26.20	27.00	123.50	110.00	116.70
P625	39.24	33.80	32.00	43.50	132.20	130.00	140.00
P750	47.09	36.00	33.00	36.50	130.50	130.00	135.60
S500	31.39	33.00	33.00	23.30	131.00	120.00	116.70
S750	47.09	30.30	30.30	33.30	113.30	116.70	129.50

2.4.4 Miyamoto, Katsuji, Nakamura, and Bull:

This study explored the frequency effects of external tendons added to strengthen existing bridges. To investigate the dynamic behavior of external tendons, a numerical model was formulated, laboratory tests were conducted to measure frequency values, and an existing bridge was retrofitted (Miyamoto, Tei, Nakamura, & Bull, 2000). Details of the numerical model can be found in the referenced journal article. The laboratory testing included a 3 m long composite girder with external tendons as shown in Figure 2.15. Prestressing forces were applied to the tendons in three stages and an impulse hammer test was conducted after each increase in tensioning. Two different eccentricities were used for the parabolic tendons, one small and the other large in relation to the girder centroid with the same tendon angle. For both the numerical model and laboratory tests, it was found for small tendon eccentricities that the natural frequency of the girder decreased with increasing loads since the end of the tendon was closer to the centroid and the tendon force acted as an axial load. In contrast, for the tendon with the larger eccentricity, the natural frequency increased along with the member flexural rigidity due to the location of the tendon force being farther away from the girder centroid at the end of the beam causing flexural resistance instead of a true axial force (Miyamoto, Tei, Nakamura, & Bull, 2000). The change in frequencies corresponding to increased loads, are shown in the laboratory test results in Table 2.17 with specimen No. 1 and No. 2 corresponding to small eccentricities and No. 3 and No. 4 corresponding to large eccentricities (Miyamoto, Tei, Nakamura, & Bull, 2000).

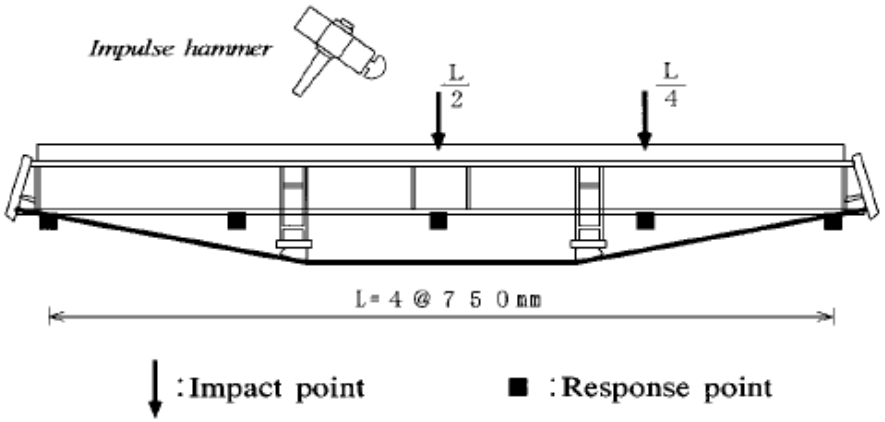

Figure 2.16. Experimental test setup with external tendons (Miyamoto, Tei, Nakamura, & Bull, 2000)

Table 2.17. Results from laboratory testing (Miyamoto, Tei, Nakamura, & Bull, 2000)

		1st Mode		2nd Mode		3rd Mode	
Specimen (1)	PS (kN) (2)	f_1 (Hz) (3)	h_1 (%) (4)	f_2 (Hz) (5)	h_2 (%) (6)	f_3 (Hz) (7)	h_3 (%) (8)
No. 1	Non-PS	56.32	8.54	174.51	7.64	453.25	3.90
	9.8	56.72	10.08	176.99	3.54	446.45	7.46
	29.4	54.42	11.98	172.96	7.56	437.10	2.55
	—	—	—	—	—	—	—
No. 2	Non-PS	53.40	10.21	173.24	3.94	432.47	0.48
	19.6	53.45	9.32	173.08	4.75	421.14	0.81
	39.2	53.22	9.89	172.29	5.13	—	—
	58.8	53.10	9.77	172.52	4.74	405.87	3.58
No. 3	Non-PS	52.18	14.56	159.64	7.54	374.78	3.63
	14.7	54.38	11.55	161.11	7.79	383.81	9.27
	19.6	54.06	10.96	161.70	7.20	—	—
	24.5	54.47	11.46	162.04	6.43	395.62	1.41
No. 4	Non-PS	51.60	12.23	174.19	5.00	395.64	0.20
	14.7	56.72	7.52	176.26	6.87	415.01	18.63
	19.6	56.41	8.09	177.23	7.21	410.47	14.63
	24.5	56.72	7.73	177.31	6.31	417.27	0.90

The findings developed in the numerical model and laboratory study where then applied to strengthen a single span, composite girder bridge with a length of 34.6 m (113.5 ft) and average width of 6.33 m (20.8 ft) (Miyamoto, Tei, Nakamura, & Bull, 2000). The depth of the bridge deck was increased and external tendons were added to provide additional strength. The tendons were 19.3 mm (0.76 in.) in diameter with a total prestressing force per girder of 1470 kN (330.5 kips) for a total bridge force of 4410 kN (991.5 kips). A schematic of the bridge is shown in Figure 2.16. An impact hammer test, similar to the test used in the laboratory study, was used to measure the natural frequency of the bridge before and after testing at multiple impact locations with test results shown in Table 2.18 (Miyamoto, Tei, Nakamura, & Bull, 2000). The test results showed a decrease in natural frequency after post-tensioning of the tendons which

aligns with findings from the numerical model and laboratory testing since the eccentricity of the external tendons in the retrofitted bridge was small.

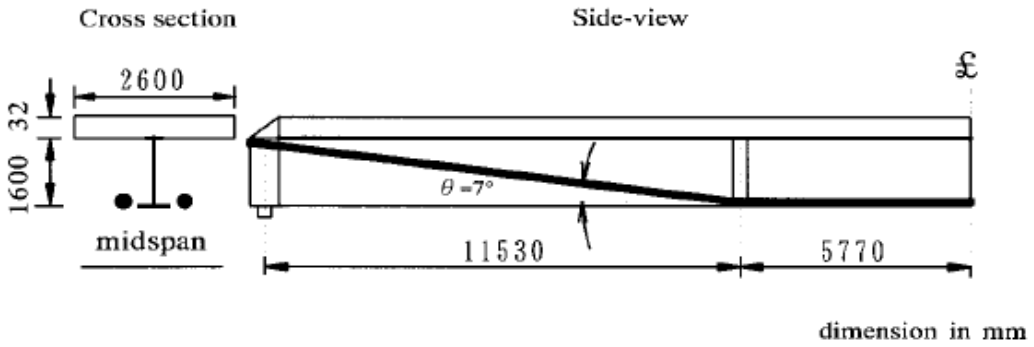

Figure 2.17. Bridge schematic for installation of external tendons (Miyamoto, Tei, Nakamura, & Bull, 2000)

Table 2.18. Test results for retrofitted girder (Miyamoto, Tei, Nakamura, & Bull, 2000)

Mode shape (1)	(a) Before Tensioning		(b) After Tensioning		(b)/(a)	
	f (Hz) (2)	*h* (%) (3)	*f* (Hz) (4)	*h* (%) (5)	*f*-ratio (6)	*h*-ratio (7)
1st flexural mode	3.49	0.081	3.18	0.670	0.91	8.27
1st asymmetrical torsion mode	4.77	1.135	4.72	0.399	0.99	0.35
2nd asymmetrical torsion mode	12.36	2.851	12.16	1.725	0.98	0.61
3rd flexural mode	20.30	6.003	19.66	4.183	0.97	0.70
3rd asymmetrical torsion mode	22.96	1.922	22.44	2.023	0.98	1.05

2.4.5 Conclusion:

The general findings regarding the effect of post-tensioned strands on the frequency of concrete structures from the reviewed articles was that parabolic tendons with eccentricities close to the member centroid decrease the natural frequency of the structure with increasing prestressed load. Parabolic tendons with large eccentricities increase the member frequency and flexural rigidity with increasing prestressing. It was also found that straight tendons appear to have negligible effect on the natural frequency of a structure regardless of the prestressing load.

2.5 Wind tower dynamic considerations:

2.5.1 Blade passing frequencies:

The natural frequency of a wind tower system must be considered with regard to 1P and 3P passing frequencies that are generated by the wind turbine blades. The 1P frequency results from the constant rotation of the group of 3 blades passing the tower, while the 3P frequency results from each individual blade passing the tower. Tower structures can be classified as soft-soft, soft-stiff, or stiff-stiff structures depending on where the tower natural frequency falls in

relation to the turbine 1P and 3P frequencies (Arany, Bhattacharya, Macdonald, & Hogan, 2016). The natural frequency of soft-soft towers falls below 1P, soft-stiff tower frequencies are between 1P and 3P, and stiff-stiff frequencies are above 3P. Typical onshore wind towers are designed to be soft-stiff because a tower with a frequency below the 1P value of onshore turbine blades would experience large deformations that would not be sustainable by the tower structure. Towers with frequencies above 3P are possible but use a large amount of material and are often not cost-effective (Arany, Bhattacharya, Macdonald, & Hogan, 2016). Therefore, soft-stiff towers are designed with frequencies between 1P and 3P with a working range typically set within allowable proximity to the blade frequencies to prevent resonance of the tower structure. An example of this design spectrum is presented in Figure 2.17 for different size wind turbines with the pink lines representing the upper and lower bounds and the red lines representing the allowable tower frequencies or working range.

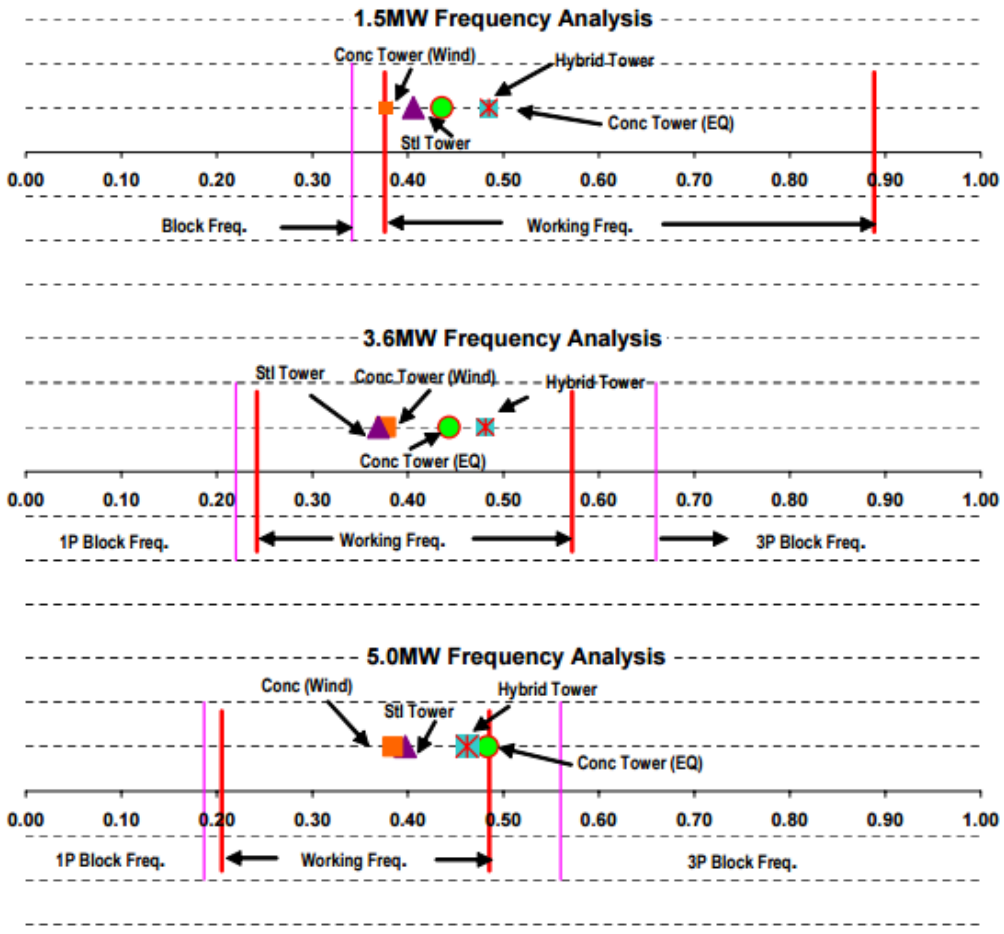

Figure 2.18. Example of allowable tower frequencies for different size turbines (Lanier, 2005)

2.5.2 Vortex shedding:

Vortex shedding must also be checked in wind tower design and is defined as "flow separations that occurs when large wake eddies are formed which reside near the downstream surface" (Simiu & Scanlan, 1986). Vortex shedding can result in a phenomenon known as "lock-in" where the wind speed causes the vortex shedding frequency to match the natural frequency of the structure resulting in large tower displacements in the across wind direction (Simiu & Scanlan, 1986). The lock-in phenomenon should be avoided by calculating the critical wind speed for vortex-induced response using Equation 2-1 and checking to ensure that this wind speed does not fall within the range of operating wind speeds for the specified wind turbine (Simiu & Scanlan, 1986).

$$V_{cr} = \frac{n*D}{St} \qquad \text{(Eq. 2-1)}$$

where:

V_{cr} = critical wind speed for vortex-induced response

n = natural frequency of tower structure

D = characteristic dimension of tower structure (average diameter of top third of tower)

St = Strouhal number – dependent on shape of tower cross-section

2.6 References:

Arany, L., Bhattacharya, S., Macdonald, J. H., & Hogan, S. J. (2016). Closed form solution of Eigen frequency of monopile supported offshore wind turbines in deeper waters incorporating stiffness of substructure and SSI. *Soil Dynamics and Earthquake Engineering*.

ASCE/AWEA. (2011). *Recommended Practice for Compliance of Large Land-based Wind Turbine Support Structures.* American Wind Energy Association and American Society of Civil Engineers.

GL, G. L. (2010). *Guideline for the Certification of Wind Turbines.* Hamburg, Germany.

Hamed, E., & Frostig, Y. (2006). Natural frequencies of bonded and unbonded prestressed beams - prestress force effects. *Journal of Sound and Vibration 295*, 28-39.

IEC, I. E. (2008). *IEC 61400-1: Wind Turbines - Part 1: Design Requirements (3rd Edition).* International Electrotechnical Commission.

Lanier, M. (2005). *LWST Phase I Project Conceptual Design Study: Evaluation of Design and Construction Approaches for Economical Hybrid Steel/Concrete Wind Turbine Towers.* Golden, CO: National Renewable Energy Laboratory.

Lewin, T., & Sritharan, S. (2010). *Design of 328-ft (100-m) Tall Wind Turbine Towers Using UHPC.* Ames, IA: Department of Civil, Construction, and Enviromental Engineering Report ERI-ERI-10336.

Miyamoto, A., Tei, K., Nakamura, H., & Bull, J. W. (2000). Behavior of prestressed beam strengthened with external tendons. *Journal of Structural Engineering, Vol 126,* 1033-1044.

Schmitz, G. (2013). *Design and experimental validation of 328 ft (100 m) tall wind turbine towers utilizing high strength and ultra-high performance concrete.* Ames, IA: MS Thesis, Iowa State University.

Simiu, E., & Scanlan, R. H. (1986). *Wind Effects on Structures.* New York: John Wiley and Sons.

Sritharan, S., & Lewin, T. (2015). *U.S. Patent No. 9,016,012.*

Sritharan, S., Lewin, T., & Schmitz, G. M. (2014). *U.S. Patent No. 8,881,485.*

Wang, T.-H., & Huang, R. (2013). The variation of flexural rigidity for post-tensioned prestressed concrete beams. *Journal of Marine Science and Technology, Vol 21 No. 3,* 300-308.

CHAPTER 3 – DESIGN AND CERTIFICATION OF HEXCRETE TOWERS

Descriptions prepared for submission to independent design certification company

Robert Peggar, Iowa State University

Sri Sritharan, Ph.D., Professor of Structural Engineering, Iowa State University

3.1 Abstract

As a part of the U.S. Department of Energy (DOE) sponsored project "Hexcrete Towers for Harvesting Wind Energy at Taller Hub Heights," six tall Hexcrete wind towers were designed for Siemens SWT 2.3-108 and SWT 3.2-113 turbines. The Hexcrete tower is a hexagon shaped, precast concrete wind turbine tower utilizing both High Strength Concrete (HSC) and Ultra High Performance Concrete (UHPC). In the following paper, the tower design process is described along with resulting tower properties. Tower erection details are also discussed with regard to constructability and cost reduction. Hexcrete pedestals are presented as a part of a tall foundation system for the purposes of design certification and prototyping. Benefits of the pedestals are discussed as a culmination of the entire design process and the first step in commercializing the Hexcrete tower technology.

3.2 Introduction:

The Hexcrete tower system is an innovative tower design, patented by Iowa State University that utilizes precast high strength concrete members connected by steel post-tensioning tendons (U.S. Patent No. 9,016,012, 2015) (U.S. Patent No. 8,881,485, 2014). As the name implies, the tower is hexagon in shape and is made up of six hexagon shaped columns and six connecting wall panels as shown in Figure 3.1. Circumferential tendons connect the column and panel members, while vertical post-tensioning tendons run through the tower columns and connect the tower sections. For the U.S. Department of Energy (DOE) sponsored project "Hexcrete Towers for Harvesting Wind Energy at Taller Hub Height," three all concrete and three hybrid concrete/steel towers were designed for Siemens SWT 2.3-108 and SWT 3.2-113 turbines with tower heights of 394 ft (120 m) and taller. The goal of the project was to help establish a tower design that minimized the overall Levelized Cost of Energy (LCOE) of a wind turbine while reliably and safely harvesting energy at taller hub heights. The project was successful and resulted in six tall tower designs that provided structural stability while reducing the overall LCOE by 0-9% when compared to a traditional 262 ft (80 m) steel tower. Following the completion of the project, Hexcrete tower pedestals were designed in order to prototype the

Hexcrete tower technology at a new or existing wind farm and provide opportunity for certification of the Hexcrete tower design. The following sections of this paper outline the tower design process, discuss dimensions and characteristics of the six tall tower designs, present details pertaining to tower construction and erection, and describe pedestal design and certification requirements.

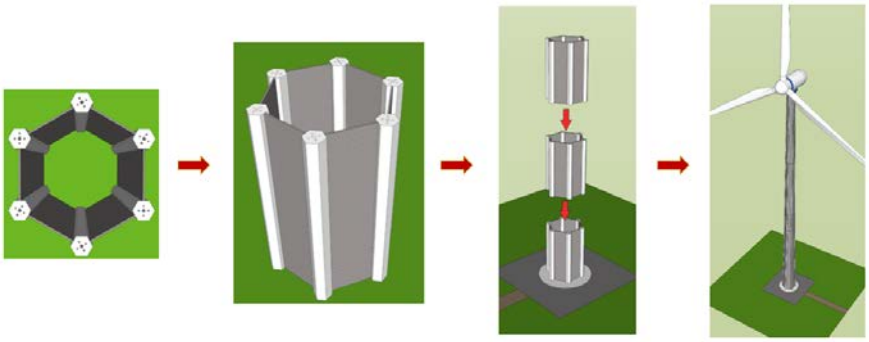

Figure 3.1. Hexcrete tower concept

3.3 Design process:

The design process for the tall Hexcrete towers is outlined in Figure 3.2. High Strength Concrete (HSC), with a compressive strength of 13 ksi (89.6 MPa), was used for the tower columns, and Ultra High Performance Concrete (UHPC), with a compressive strength of 26 ksi (179.3), was used for the tower panels. Geometry constraints for the towers were provided by Siemens and included the tower top diameter and the maximum allowable tower diameter for blade tip clearance. It should be noted that a base diameter constraint was not given by Siemens due to the modular nature of the Hexcrete tower which eliminates transportation of large tower

sections. The tower loads provided by Siemens and will be discussed in the next section along with guidelines for tower design.

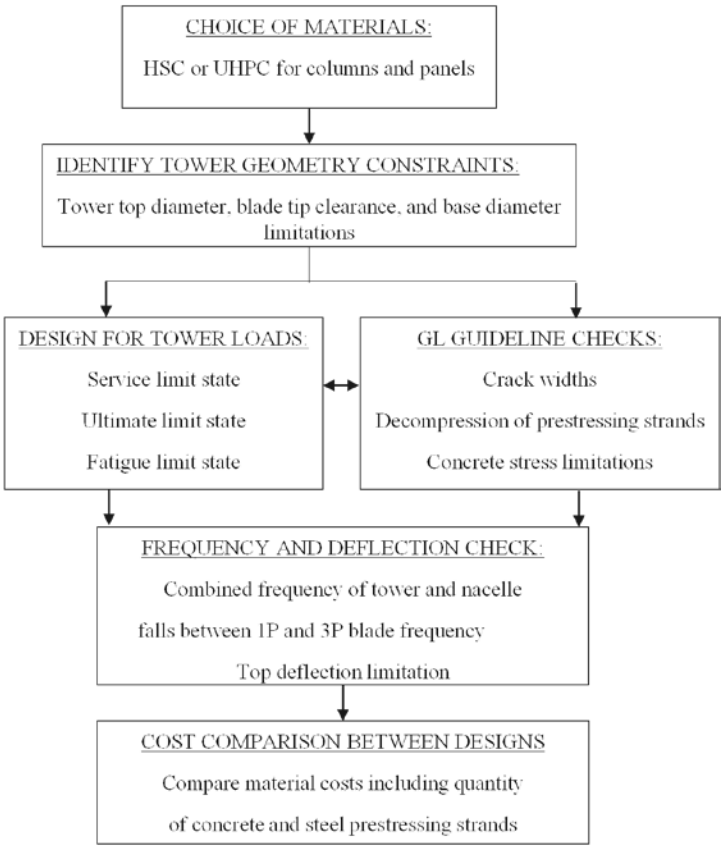

Figure 3.2. Hexcrete tower design process

3.4 Design loads:

Three specific tower hub heights and two turbine sizes were selected for design. A full concrete as well as a hybrid tower were designed for each tower combination for a total of six tower designs. The tower names, corresponding hub heights, and turbine sizes are shown in Table 3.1. The Siemens tower loads included loads generated from the turbine as well as direct wind loads on the tower structure. These loads, along with corresponding safety factors, were calculated according to guidelines set by the International Electrotechnical Commission (IEC). The Siemens load tables included shear in the x and y directions, moment in the x and y directions, torsion on the tower cross-section, and axial forces. Each type of load was provided at specified intervals along the height of the tower. Three specific load types were taken into account: service limit state (SLS) loads, which correspond to normal operation of the wind tower; ultimate limit state (ULS) loads, which include the maximum loads the tower will see due to extreme events; and fatigue

limit state (FLS) loads, which result from repeated cycles of back and forth movement over the life of the tower. Due to the proprietary nature of the tower loads, specific load values will not be disclosed in this report. However, example design loads are provided in the certification portion of this report.

Table 3.1. Description of tower design combinations

Tower Name	Hub Height	Turbine size	Rotor diameter
HT1/HT1 Hybrid	394 ft (120 m)	2.3 MW	354 ft (108 m)
HT2/HT2 Hybrid	459 ft (140 m)	2.3 MW	354 ft (108 m)
HT3/HT3 Hybrid	459 ft (140 m)	3.2 MW	370 ft (113 m)

3.5 Hexcrete design equations:

The concrete portion of Hexcrete wind turbine towers were designed for the SLS, ULS, and FLS limit states described in the previous section. Similar to typical precast concrete structures, the Hexcrete towers are first designed for service level loads and then checked for ultimate and fatigue load capacity. Since the calculations involve multiple variables and tower geometric properties, design of the Hexcrete towers was completed using Microsoft Excel and MathCAD software.

In the tower design process, service level overturning moments are examined in order to size the tower columns and determine the magnitude of required vertical post-tensioning. Columns are then checked for shear and fatigue capacity, and the vertical steel post-tensioning tendons are also checked for fatigue. The tension and compression caused by the service level overturning moment are then combined with service level torsional and shear loads to design the column to panel connections by quantifying the amount of required circumferential post-tensioning and thickness of the tower panels. The ultimate capacity of the tower is then checked to ensure durability under extreme wind events. Finally, the top deflection and frequency of the tower (combined with the nacelle) are checked to ensure that the dynamic response of the tower falls within the working frequency range of the 1P and 3P blade passing frequencies and meets vortex shedding requirements.

3.6 GL certification guidelines:

For concrete towers, design checks must be made for the following GL guidelines: section 5.4.3.4 part 1, section 5.4.3.4 part 2, and section 5.4.3.5 part 2. Design loads to check these specific cases were identified by the turbine manufacturer. For section 5.4.3.3 part 1, stress

is limited to 0.6 *fck* under the combination of DLC 1.5, 1.6, and 9.4 where *fck* corresponds concrete compressive strength. This is similar to the ACI guidelines discussed earlier. The columns in the Hexcrete tower experience the highest stresses due to post-tensioning were checked for this guideline with the supplied load information.

For GL section 5.4.3.4 part 2, crack widths must not exceed 0.2 mm for a combination of DLC 1.1 and 6.4 with a probability exceedance of $p_f = 10^{-2}$. The panels and columns in the Hexcrete towers were designed to remain uncracked for operational loads which happened to exceed the combination of DLC 1.1 and 6.4, thus meeting this requirement.

For GL section 5.4.3.5 part 2, the guidelines state that "verification of load-dependent stiffness reduction can be omitted for the calculation of natural frequencies when decompression is verified" for the combined load case of DLC 1.1 and 6.4 with a probability of exceedance of $p_f = 10^{-2}$. The load-dependent stiffness reduction refers to cracking of the concrete. Tests of the designed Hexcrete tower system show that the tower stiffness does not decrease under operational and extreme flexural loads. If the combination of DLC 1.1 and 6.4 had exceeded extreme flexural values a separate design check would have been made.

3.7 Hexcrete tower designs:

The full concrete Hexcrete tower designs were completed with the resulting dimensions and tower properties shown in Table 3.2. The designs included a single group of vertical post-tensioning strands that ran from the base to the top of the tower. Hexcrete hybrid towers were also designed with the transition from Hexcrete to circular steel sections at heights of 260 ft-306 ft (80 m-94 m) depending on the design. The hybrid designs offered improved tower performance in two ways: 1) hybrid designs reduced wind loads at the top of the tower by replacing the bluff body Hexcrete shape with a circular section 2) hybrid designs reduced the number of lifts needed at heights above 260 ft (80 m) since steel tubes are lighter than Hexcrete sections and can be lifted in longer sections. The reduced number of lifts shortens the crane time at each tower which results in cost savings during the erection process. Dimensions of the Hexcrete hybrid towers are given in Table 3.3. A complete set of erection and tower drawings were formulated for the HT1, HT2 hybrid, and HT3 towers but are not included in this report due to confidentiality.

Table 3.2. Full concrete Hexcrete tower dimensions

	HT1	HT2	HT3
Tower base diameter*, ft (m)	25.72 (7.84)	27.9 (8.50)	34.34 (10.47)
Tower top diameter*, ft (m)	10.50 (3.20)	10.50 (3.20)	11.97 (3.65)
Base column diameter, ft (m)	3.58 (1.09)	3.33 (1.02)	3.84 (1.17)
Top column diameter, ft (m)	3.08 (0.94)	3.09 (0.94)	3.58 (1.09)
Strands per column	70	76	92
Max deflection, ft (m)	4.4 (1.34)	2.10 (0.64)	1.84 (0.56)
Frequency (Hz)	0.35	0.266	0.318
Weight (tower only), kips (metric tons)	2868 (1301)	3536 (1604)	4277 (1941)

*Hexcrete tower diameters are measured from outside column edges

Table 3.3. Hybrid Hexcrete tower dimensions

	HT1 hybrid	HT2 hybrid	HT3 hybrid
Tower base diameter*, ft (m)	25.72 (7.84)	27.9 (8.50)	34.34 (10.47)
Diameter at concrete to steel transition, ft (m)	13.4 (4.09)	13.2 (4.03)	14.0 (4.27)
Base column diameter, ft (m)	3.58 (1.09)	3.33 (1.02)	3.84 (1.17)
Column diameter concrete to steel transition, ft (m)	3.28 (1.00)	3.14 (0.96)	3.76 (1.15)
Tower top diameter, ft (m)	7.4 (2.26)	7.4 (2.26)	8.9 (2.71)
Height of Hexcrete, ft (m)	260 (79.3)	305.75 (93.2)	284.5 (86.7)
Height of steel, ft (m)	124 (37.8)	144.85 (44.2)	166.1 (50.64)
Thickness of steel, in. (mm)	1.25 (31.8)	1.375 (34.9)	1.375 (34.9)
Strands per column	70	76	92
Frequency (Hz)	0.409	0.325	0.339
Weight (tower only), kips (metric tons)	2265 (1028)	2930 (1329)	3469 (1574)

*Hexcrete tower diameters are measured from outside column edges

3.8 Tower dynamic properties:

All the natural frequencies of the designed Hexcrete towers fell within the allowable 1P and 3P working range specified by Siemens, with the exception of the HT1 hybrid tower which had a frequency slightly above 3P. This difference in frequency was not considered significant enough to warrant redesign of the tower system, but if the HT1 hybrid was selected for

manufacturing, the design would need to be adjusted. Vortex shedding was also checked for each tower with an assumed Strouhal number of 0.2 for the Hexcrete shape and circular steel sections.

3.9 Tower construction and erection:

The Hexcrete tower utilizes a modular precast design which allows the tower designer to segment the tower to meet transportation and erection constraints. Cells or sections of the Hexcrete tower are built on the ground and consist of six precast columns and six precast panels with the section height determined by weight or length limitations. Weight limitations can occur due to transportation costs or lifting capabilities of the erection crane if an assembled section of the Hexcrete tower is too heavy. Length limitations can also be a factor for transportation. In order to segment the tower in a cost effective manner, each section was initially limited to a length of 53 ft which would fit on a standard flatbed semi-trailer and reduce transportation costs in comparison to traditional steel towers. It was found that the weight limit for lifting completed tower sections with the erection crane was the critical criteria for determining member sizes. Therefore, each tower was divided into sections along its height according to the lifting capacity of the cranes available for tower erection. A Manitowoc 16000 was chosen for stacking the Hexcrete tower cells (or sections) up to a height of 260 ft (80 m) with a cell weight limit of 240 kips (109 metric tons). For sections above 260 ft, a Liebherr 11350 was selected with a cell weight limit of 225 kips (102 metric tons). The tower sections, lengths, and corresponding weights are shown in Table 3.4 through Table 3.6 with the first tower section designed to be built in place with a length of 53 ft. In place erection for the first tower section allows heavier columns and panels since the crane will not have to lift an entire section.

Table 3.4. HT1 tower sections according to weight

Section Number	Section Height (ft)	Single Column Weight (kips)	Single Panel Weight (kips)	Total Section Weight (kips)
1	50	49.4	20.0	416.4
2	28	27.8	10.2	228.2
3	28	27.8	8.8	219.5
4	28	27.8	10.4	229.1
5	30	29.8	9.7	236.5
6	30	29.8	8.1	227.4
7	32	31.7	7.1	232.8
8	34	33.7	5.9	237.4
9	32	31.7	5.0	220.6
10	34	33.7	4.2	227.1
11	34	33.7	3.5	223.1
12	26	25.8	2.5	170.1

Table 3.5. HT2 tower sections according to weight

Section Number	Section Height (ft)	Single Column Weight (kips)	Single Panel Weight (kips)	Total Section Weight (kips)
1	53.1	54.4	38.3	557.0
2	23.3	23.4	16.3	237.8
3	23.9	24.0	15.2	236.0
4	24.9	24.9	14.3	235.2
5	26.6	26.0	13.7	237.6
6	27.9	27.1	12.6	238.9
7	29.5	28.2	11.2	237.6
8	31.8	30.0	9.7	238.0
9	31.8	29.5	7.7	223.7
10	33.1	30.4	6.8	223.3
11	34.8	31.5	6.0	224.8
12	36.4	32.6	5.1	224.8
13	37.4	32.8	3.7	219.3
14	36.1	31.1	2.9	203.4

Table 3.6. HT3 tower sections according to weight

Section Number	Section Height (ft)	Single Column Weight (kips)	Single Panel Weight (kips)	Total Section Weight (kips)
1	52.2	70.7	27.8	591.8
2	21.0	28.7	10.8	237.6
3	21.6	29.1	10.4	237.6
4	22.0	29.8	9.7	236.3
5	22.6	30.2	9.0	234.7
6	22.0	29.3	9.9	234.7
7	23.0	30.4	9.0	236.7
8	23.9	31.5	8.2	238.0
9	24.9	32.4	7.1	237.8
10	25.9	33.5	6.0	236.5
11	25.6	32.6	4.2	220.8
12	26.6	33.5	3.3	221.5
13	27.6	34.6	2.9	223.9
14	28.2	35.0	2.2	223.9
15	28.2	34.8	2.4	223.3
16	27.9	34.2	2.9	221.9
17	27.6	33.3	3.7	222.2

During discussions with industry partners regarding the erection process, it was found that the number of lifts required for each tower with the Liebherr crane was a major cost driver in the construction sequence. The Hexcrete hybrid towers minimize the number of lifts with the larger crane by replacing the upper portion of the tower above 260 ft (80 m) with traditional tubular steel shells. The steel shells are lighter which enables the use of fewer, longer sections and results in a smaller number of lifts for the Liebherr crane. Since the design of the Hexcrete towers was implemented to eliminate oversized transportation loads, each steel shell tube was limited to a length of 56 ft (17.1 m) in order to fit on a standard semi-trailer (56 ft includes three feet of overhang) as shown in Table 3.7 through Table 3.9 below. There is an option to make the steel shells a single piece if the oversized transportation costs do not outweigh the cost of additional crane lifts.

Table 3.7. HT1 hybrid tower sections according to weight (blue shades indicate steel sections)

Section Number	Section Height (ft)	Single Column Weight (kips)	Single Panel Weight (kips)	Total Section Weight (kips)
1	50	49.4	20	416.4
2	28	27.8	10.2	228.2
3	28	27.8	8.8	219.5
4	28	27.8	10.4	229.1
5	30	29.8	9.7	236.5
6	30	29.8	8.1	227.4
7	32	31.7	7.1	232.8
8	34	33.7	5.9	237.4
9	42	-	-	101.4
10	42	-	-	79.7
11	42	-	-	56.3

Table 3.8. HT2 hybrid tower sections according to weight (blue shades indicate steel sections)

Section Number	Section Height (ft)	Single Column Weight (kips)	Single Panel Weight (kips)	Total Section Weight (kips)
1	53.1	54.4	38.3	557.0
2	23.3	23.4	16.3	237.8
3	23.9	24.0	15.2	236.0
4	24.9	24.9	14.3	235.2
5	26.6	26.0	13.7	237.6
6	27.9	27.1	12.6	238.9
7	29.5	28.2	11.2	237.6
8	31.8	30.0	9.7	238.0
9	31.8	29.5	7.7	223.7
10	33.1	30.4	6.8	223.3
11	48.2	-	-	98.1
12	48.2	-	-	88.7
13	48.2	-	-	78.3

Table 3.9. HT3 hybrid tower sections according to weight (blue indicates steel sections)

Section Number	Section Height (ft)	Single Column Weight (kips)	Single Panel Weight (kips)	Total Section Weight (kips)
1	56.1	76.3	34.2	662.5
2	20.0	27.3	11.9	234.5
3	20.7	28.2	11.2	236.5
4	21.6	29.1	10.8	238.7
5	22.0	29.3	9.9	236.5
6	21.6	28.7	10.8	236.7
7	22.6	29.8	10.1	238.9
8	23.6	30.9	9.3	239.6
9	24.6	31.7	7.9	238.3
10	25.9	33.3	6.6	238.5
11	25.9	32.8	4.6	224.8
12	55.8	-	-	156.6
13	55.8	-	-	147.9
14	55.8	-	-	138.8

Another design innovation resulting from discussion with industry partners was implementation of a quick connect system between the stacked tower sections. Due to the vertical post-tensioning of the stacked Hexcrete sections, grout is required at each column to column interface. Industry professionals recommended that the connections between the tower sections not require grouting immediately following erection because waiting for grout to cure between each section would significantly prolong tower assembly. The section connection detail designed for HT1 used rebar splice couplers which were required to be grouted in place. To avoid the delays caused by grout, the quick connect tower system was developed. The system consists of high strength steel threaded bars that run along the interior of each column. The bars are attached to the columns during assembly of the tower section on the ground. When tower sections are stacked, the sections can quickly connect to the bars in lower tower sections by using threaded bar couplers. The bars do not need to be post-tensioned, but simply hand tightened. However, the bars can be post-tensioned after completion of the tower in order to reduce the amount of vertical post-tensioning in the tower columns. Keyways were also added to the connection design to provide guidance for setting the next tower section. The keyways provide additional connection shear capacity during erection (Figure 3.3).

The number of threaded bars need for each tower was determined based on construction wind loads along the tower as well as placement of the nacelle/rotor combination. The calculated wind loads were based on a maximum 3-sec gust of 50 mph (22.4 m/s) at an elevation of 33 ft (10 m) and utilized a safety factor of 1.5. The wind speed of 50 mph (22.4 m/s) was calculated based on a Mean Recurrence Interval (MRI) of 3-yrs according to ASCE 7-10 wind maps (American Society of Civil Engineers, 2010), and tower section loads were generated utilizing ASCE-7-10 guidelines for chimneys, tanks, and similar structures. Grouting of the column interfaces will still take place before the tower vertical post-tensioning is installed, but is not required until after erection of the entire tower, nacelle, and rotor. The quick connect system does not change the tower design or dimensions and is simply accomplished by installing steel weld plates at the ends of each column during casting. Steel brackets, which will guide the threaded bars along the columns length, are then welded to the plates before transporting the members to the job site (Figure 3.4). Due to the addition of the quick connect system, concrete transition rings were added to the tower design at location where the tower taper changes. The rings will be made of UHPC and will anchor the coupled threaded rods.

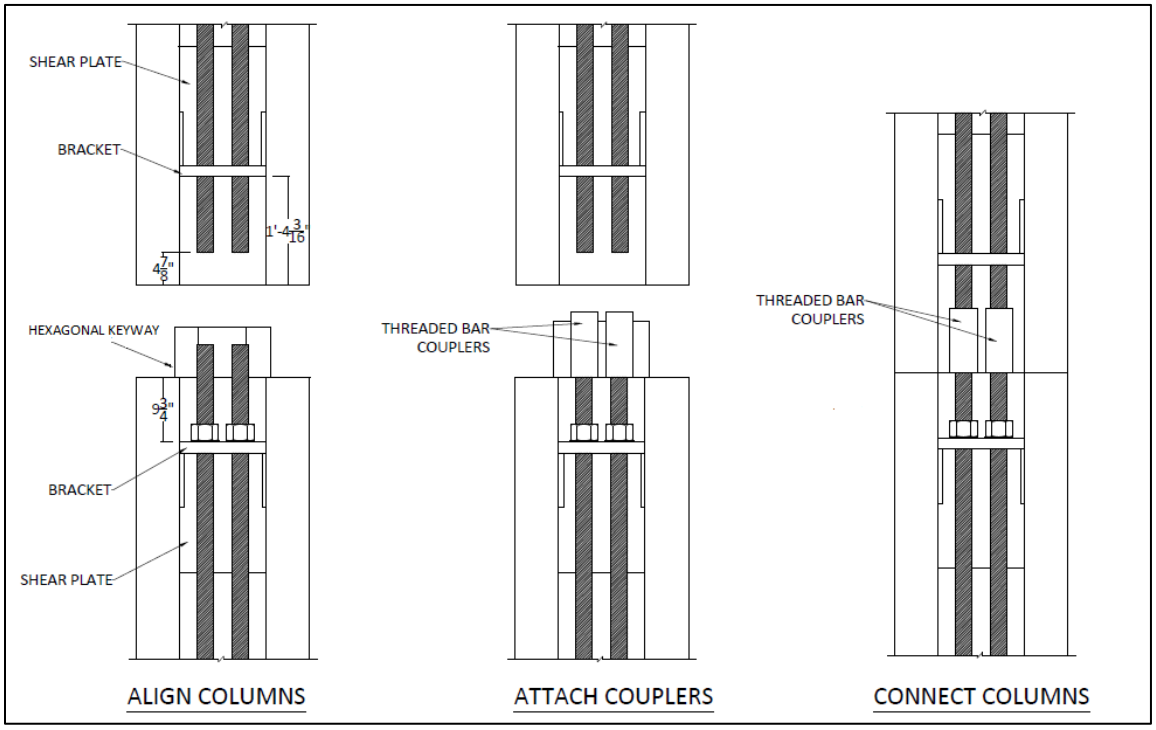

Figure 3.3. Quick connection between Hexcrete sections at columns utilizing threaded bars

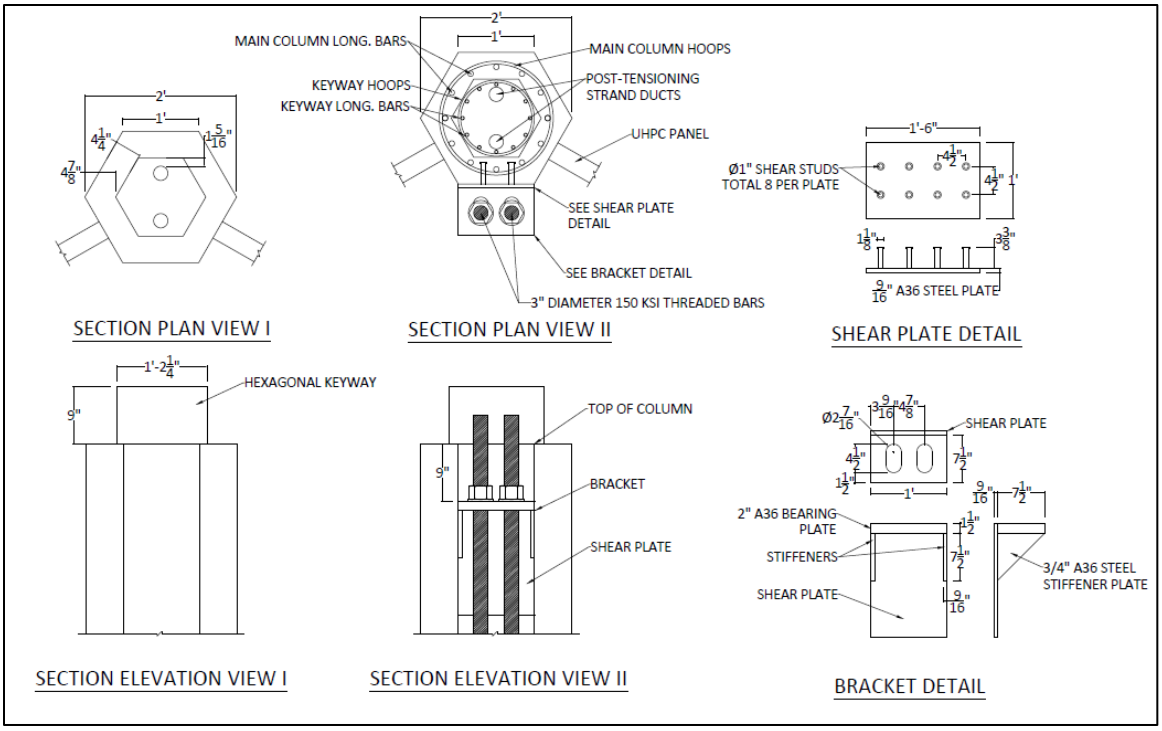

Figure 3.4. Details of quick connection for Hexcrete columns

3.10 Tall tower concept and design certification:

The next step in the evolution of the Hexcrete tower system is to design and build a prototype structure. In order to prove the tower concept, a Hexcrete pedestal was proposed. The pedestal would be 65 ft – 132 ft tall (20 m – 40 m) and support a traditional 262 ft (80 m) steel tower. The pedestal presents less risk to a potential wind farm owner than a full Hexcrete tower, provides an opportunity to test the tower concept through manufacturing, erection, and construction, and results in a 394 ft – 459 ft (120 m – 140 m) tower which can take advantage of increased wind speeds at higher elevations. It was also proposed to certify the Hexcrete pedestals as tall foundations where the pedestal would be considered part of the tower foundation system along with the typical wind tower spread footing. Therefore, for the purposes of prototyping and design certification, two Hexcrete pedestals were designed, one at 65 ft (20 m) and the other at 132 ft (40 m) for a generic 2.5 MW wind turbine. The pedestals were designed and analyzed using similar procedures to the towers described previously and documentation was submitted for certification including design equations, loads, and pedestal properties. Upon completion of certification and prototyping, specifics of the design detail may be released; however at this time further specifications are not able to be published.

3.11 Conclusion:

The Hexcrete tower system provides an innovative design that can utilize full concrete and hybrid tower systems to effectively lower the LCOE of a wind turbine tower. Six Hexcrete tall tower designs were presented along with a discussion of corresponding tower design principles, geometry, dynamic properties, and construction details. Two Hexcrete pedestals were also designed which provide a valuable opportunity for prototyping and design certification.

3.12 References

ACI Committee 318. (2011). *Building Code Requirements for Structural Concrete (ACI-318) and Commentary.* Farmington Hills: American Concrete Institute.

American Society of Civil Engineers. (2010). *Minimum Design Loads for Buildings and Other Structures.* ASCE and SEI.

Comite Euro-International Du Beton. (1990). *CEB-FIP Model Code 1990.* Lausanne: Thomas Telford.

GL, G. L. (2010). *Guideline for the Certification of Wind Turbines.* Hamburg, Germany.

Lanier, M. (2005). *LWST Phase I Project Conceptual Design Study: Evaluation of Design and Construction Approaches for Economical Hybrid Steel/Concrete Wind Turbine Towers.* Golden, CO: National Renewable Energy Laboratory.

Lewin, T., & Sritharan, S. (2010). *Design of 328-ft (100-m) Tall Wind Turbine Towers Using UHPC.* Ames, IA: Department of Civil, Construction, and Enviromental Engineering Report ERI-ERI-10336.

Schmitz, G. (2013). *Design and experimental validation of 328 ft (100 m) tall wind turbine towers utilizing high strength and ultra-high performance concrete.* Ames, IA: MS Thesis, Iowa State University.

Sritharan, S., & Lewin, T. (2015). *U.S. Patent No. 9,016,012.*

Sritharan, S., Lewin, T., & Schmitz, G. M. (2014). *U.S. Patent No. 8,881,485.*

CHAPTER 4 – HEXCRETE WIND TURBINE TOWERS – A FULL-SCALE TEST

A paper to be submitted to the ASCE Structural Journal

Robert Peggar, Iowa State University

Sri Sritharan, Ph.D., Professor of Structural Engineering, Iowa State University

4.1 Abstract

As installed wind energy capacity continues to grow across the United States (U.S.), the U.S. Department of Energy (DOE) plans to expand wind power to all 50 states. Tall wind turbine towers above 100-m are a practical solution to help achieve this goal. Since traditional steel towers face transportation and logistical challenges at these heights, Iowa State University (ISU) has developed a precast concrete wind tower known as the Hexcrete tower. The Hexcrete tower is hexagon in shape, and utilizes both High Strength Concrete (HSC) and Ultra-High Performance Concrete (UHPC) precast members. A 120-m tall Hexcrete tower was designed for a Siemens 2.3 MW turbine and a full-size section of the tower was assembled and tested at the Multi-Axial Subassemblage Testing (MAST) Laboratory in Minneapolis, Minnesota. The test unit successfully met operational and extreme loads within acceptable performance conditions which validated the tower design. Loads beyond design conditions were also applied to the test unit to evaluate the overall system strength, ductility, toughness, and reserve capacity. The performance of the tower system showed that the test unit was highly ductile and possessed a large reserve capacity when subject to large displacements. The experimental test also offered opportunities for improved design and proved the Hexcrete concept as an innovative alternative for towers with hub heights at or above 100 m.

4.2 Introduction:

Wind energy continues to increase across the United States with a total installed nationwide capacity of 73.9 GW (AWEA, 2015). However, the increase in installed capacity is mostly limited to wind rich regions such as the Midwest, Northeast, and Texas, with limited to no resources in the southeast U.S. The U.S. Department of Energy (DOE) continues to look for opportunities to expand wind energy to all 50 states in an effort to reduce reliance on traditional energy with large carbon footprints such as petroleum and coal (U.S. Department of Energy, 2015). Wind energy continues to become more cost effective and the presence of renewable electricity sources in markets such as the southeast U.S. can provide competitive energy

resources near highly populated areas. However, current wind technology is not economical for these new regions, and as a result, technical innovation is needed. One such innovation with great potential is the design and production of wind towers with hub heights above 100 m (328 ft). Wind speeds increase with height which results in faster, more consistent winds at higher elevations. Faster winds mean dramatically increased power production and winds at higher elevations are also more consistent resulting in the ability to produce wind energy for longer periods of time. In addition, taller towers facilitate the opportunity to utilize longer blades and turbines with greater nameplate capacity. An ongoing wind resource study at Iowa State University (ISU) shows that these tall tower benefits make wind energy viable in the southeast U.S. and also increase production capacity in wind rich regions. An economic tall tower solution has great potential to shape future wind energy production.

Current winds tower are constructed from hollow steel shells; however, at hub heights above 80 m (262.4 ft) steel shells face limitations. An 80 m steel tower base is typically around 4 m (13 ft) in diameter, but a 100-m tall tower would require the base to grow to around 5.5 m (18 ft) in diameter (Lewin & Sritharan, 2010). The larger base prohibits cost-effective transportation due to the height of highway overpasses and lane widths. Steel shells can increase in thickness instead of growing in diameter, but this would result in almost doubling the volume of steel even for 100 m tall towers, which significantly increases material costs (Lewin & Sritharan, 2010). Precast concrete shell towers have begun to be implemented in Europe by multiple companies and are cast in smaller segments than circular steel tower sections, typically combining three to four shells to make a full circular cross-section (Acciona WindPower, 2016). Precast concrete shells take advantage of readily available concrete materials, but require larger upfront costs due to the specialized formwork. In addition, transporting curved concrete sections may still require accommodations in semi-trailer type or size, which increases the tower cost. Concrete shells provide an improved tall tower solution, but there is potential for further advancement to reduce the overall tower cost.

In order to further realize the potential benefits of concrete towers, the Hexcrete concrete technology was developed by ISU (U.S. Patent No. 9,016,012 and 8,881,485). The Hexcrete tower is a hexagonal shape concrete tower that utilizes high strength concrete materials and precast concrete shapes that do not require curved sections. Additionally, the tower consists of six hexagonal shaped columns and six flat wall panels as shown in Figure 4.1. The columns and

panels are all sized to fit on a standard flatbed trailer to simplify transportation. Multiple column to panel connections were experimentally tested including a bolted connection, UHPC wet joint, and an unbonded post-tensioned connection. The unbonded post-tensioned connection was selected due to robust test performance. Unbonded vertical post-tensioning also runs through the columns to secure the tower to the foundation and provide structural continuity. The tower system may be fabricated using Ultra-High Performance Concrete (UHPC) members with a compressive strength of 179 MPa (26 ksi), High Strength Concrete (HSC) members with a compressive strength of 89.6 MPa (13 ksi), or a combination of the two depending on the desired tower cost, durability, or size limitations. Multiple Hexcrete towers were designed for hub heights at both 120 m (394 ft) and 140 m (459 ft).

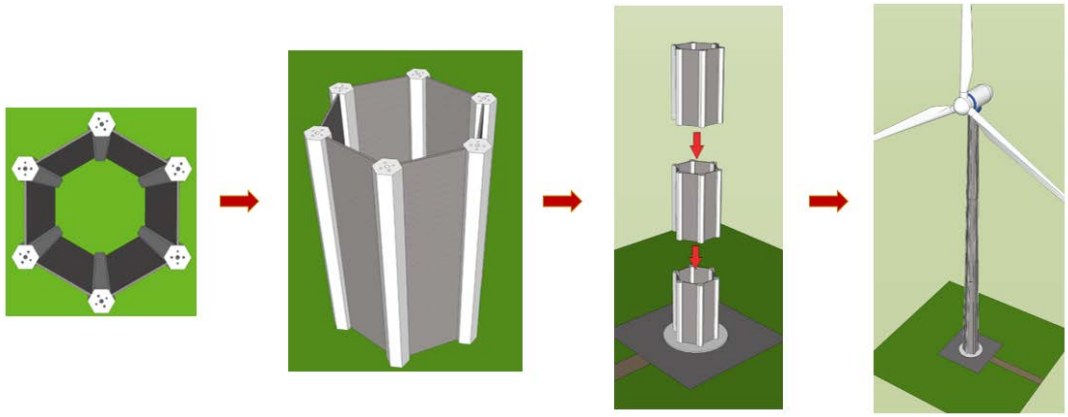

Figure 4.1. Hexcrete wind tower concept

To validate the Hexcrete design methodology and further evaluate tower performance, a proof test of a full scale tower segment was designed and tested at the Multi-Axial Subassemblage Testing (MAST) Laboratory in Minneapolis, Minnesota. In the following sections, a prototype Hexcrete tower design is presented, fabrication and construction of a full scale test unit is described as well as test unit instrumentation and loading details. The goal of the test was to evaluate the capacity of the test unit to resist required operational and extreme loads as well as identifying tower ductility, reserve capacity, and torsional loads response For design of wind towers, fatigue loads resulting from the dynamic response of the tower can also govern aspects of design. Therefore a separate fatigue test was conducted at Iowa State University with results that will be published in a subsequent paper. The MAST test provided an opportunity to evaluate the tower performance in regard to strength and stiffness, connection integrity, member

cracking, and overall tower behavior when subject to combined moment, shear, axial, and torsional loads.

4.3 Prototype tower:

The prototype tower designed by ISU was a 120 m (394 ft) tower designed for a Siemens SWT 2.3-108 turbine and referred to as the HT1 tower. Tower dimensions are shown in Table 4.1 along with tower weight and dynamic frequency. As part of the tower design process, industry input was sought to simplify the design process and develop feasible construction processes. The tower was originally designed with staged vertical post-tensioning in the tower columns. However, industry professionals recommended a single group of tendons for the entire tower height which would be installed after erection of the entire tower system. The single group of post-tensioning resulted in reserve capacity at the top of the tower since the critical tower section was at the tower base. The tower frequency range was specified by the turbine manufacturer.

Table 4.1. Dimensions of prototype tower

	Prototype (HT1)
Tower base diameter*, m (ft)	7.84 (25.72)
Tower top diameter*, m (ft)	3.20 (10.50)
Base column diameter, m (ft)	1.09 (3.58)
Top column diameter, m (ft)	0.94 (3.08)
Strands per column	70
Max deflection, m (ft)	1.34 (4.4)
Frequency (Hz)	0.35
Weight (tower only), metric tons (kips)	1301 (2868)

*Hexcrete tower diameters are measured from outside column edges

4.4 Test unit design:

The test unit was designed as a full-scale section of the prototype tower located at a height of 105 m (345 ft). This part of the tower was chosen based on the magnitude of the tower loads and the loading capacity of the MAST laboratory. The test unit section was 5 m (16.5 ft) tall and 2.4 m (8 ft) in diameter. The height of 5 m was selected based on crane weight limitations within the laboratory. Overall dimensions of the test unit are shown in Figure 4.2. The test unit utilized both HSC and UHPC in order to validate the performance of both types of concrete in the columns and panels of the Hexcrete tower system. Three columns and three panels were HSC and the other three columns and panels were UHPC. Using HSC and UHPC

also offered the opportunity to directly compare the performance of each material throughout the stages of testing.

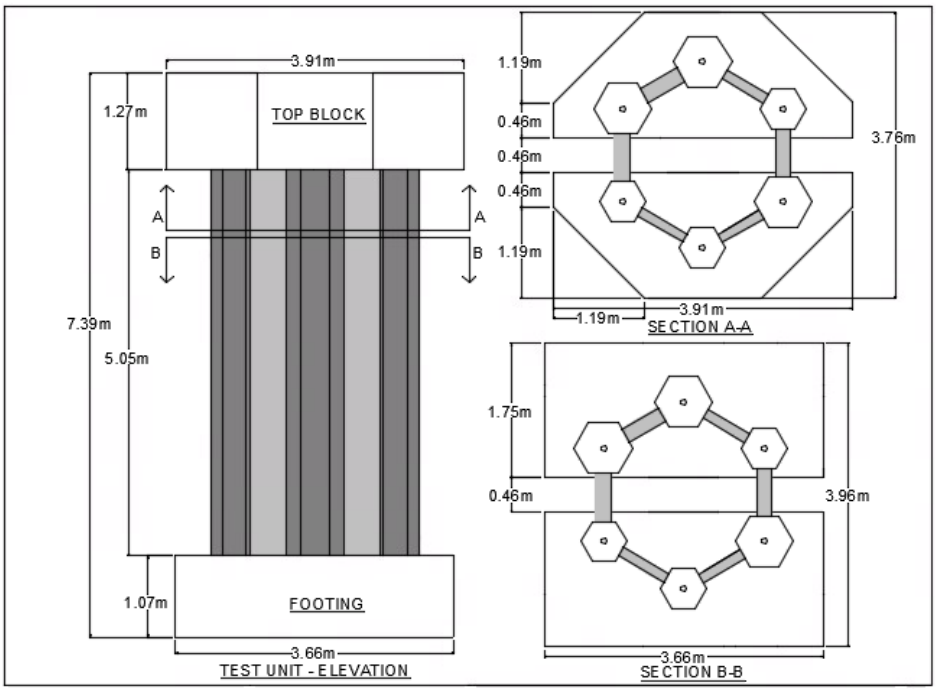

Figure 4.2. Test unit schematic

To increase structural capacity and provide economical connections between members, the Hexcrete tower consists of both circumferential and vertical unbonded post-tensioning. All post-tensioning tendons and anchorage locations were designed to follow code requirements for allowable stress limits from the American Concrete Institute (ACI) for both temporary and sustained loads. The circumferential post-tensioning of the tower was not designed to be installed around the entire tower perimeter. Instead, the tendons were divided into two overlapping groups in order to reduce the number of curves in each tendon as shown in Figure 4.3. The circumferential post-tensioning in the test unit consisted of 14 groups of four 15.24 mm (0.6 in.) 1862 MPa (270 ksi) relaxed tendons which translated to seven groups of tendons along the test unit height with an average spacing of 0.69 m (2.25 ft). The 120 m Hexcrete tower was designed with one set of vertical post-tensioning tendons per column which extend the entire height of the tower. The critical tower section, which determined the number of vertical tendons in the prototype structure, was located at the base of the tower. This resulted in reserve capacity at higher tower elevations. Since the test unit section was located at a height of 105 m, the number of vertical tendons in the test unit was reduced from the prototype tower design in accordance

with the test unit capacity demands which resulted in a group of twenty tendons in each test unit column.

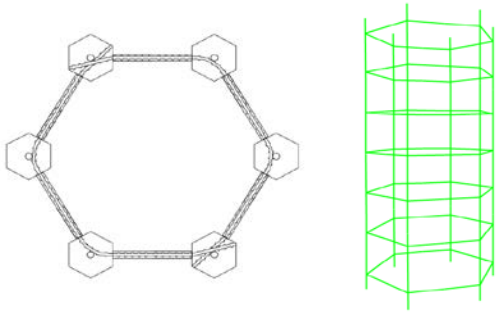

Figure 4.3. Radial tendon overlap layout (left); vertical and circumferential tendon locations along test unit height (right)

Two foundation blocks and two top reaction blocks were designed, and each block was connected to three tower columns. The reaction blocks anchored the vertical post-tensioning and also attached the tower test section to the strong floor and loading crosshead. The depth of the blocks was determined by the space necessary to ensure proper anchorage of each set of post-tensioning tendons. Load cells were fabricated to fit underneath the post-tensioning multi-strand anchors heads in the top blocks resulting in additional top block depth.

4.5 Test unit construction

Coreslab Structures in Omaha, Nebraska fabricated the precast concrete pieces for the test unit and then shipped the pieces to the MAST laboratory. Sixteen precast pieces were fabricated: three HSC columns, three HSC panels, three UHPC columns, three UHPC panels, two top reaction blocks, and two base reaction blocks. A 19 mm (0.75 in.) gap between each column and panel was included in the fabrication plans in order to allow for variation in casting of the concrete members. The test unit was assembled in two halves, due to space and lifting limitations within the lab. Each test unit half consisted of a single foundation block, three columns, two panels, and a single top block (Figure 4.4). A temporary support frame was constructed to hold the columns and panels in place during the construction process. For each half of the test unit, the base reaction block was placed first, followed by the columns and connecting panels. Grout was poured between the columns and reaction blocks and all members were temporarily attached to the support frame for stability. High strength epoxy was applied in this gap in order to provide a uniform bearing surface for the circumferential post-tensioning. No compression force was applied to the joint during the curing process. After curing of the epoxy,

six 12.7 m (0.5 in.) diameter tendons were utilized to temporarily connect the columns and panel so that the test unit half had adequate strength for positioning in the lab. After the epoxy cured overnight, the top block was placed and the vertical post-tensioning was installed. The vertical tendons were tensioned to an effective stress of 1124 MPa (163 ksi), followed by the removal of the support frame. The half test unit was lifted into its final test position and attached to the MAST strong floor. The second half of the test unit was constructed using the same method, moved into the correct position, and also attached to the strong floor.

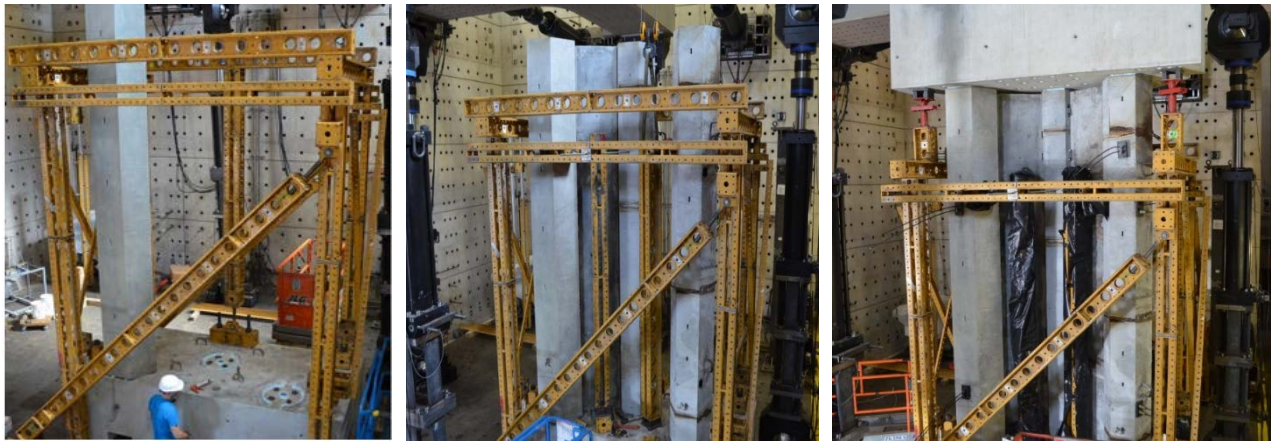

Figure 4.4. Construction of test unit half

When both halves of the test unit were positioned, the temporary post-tensioning between the columns and panels was removed, the final two panels were placed, and epoxy was installed at the column to panel joints. Due to constructing the test unit in halves, the connecting panels were not subject to pre-compression from the vertical post-tensioning in the columns, while the other four panels were pre-compressed. The absence of pre-compression in the connecting panels likely means that cracking will occur in the two connecting panels before the pre-compressed panels. After curing of the connecting panel epoxy, circumferential 12.7 mm diameter post-tensioning tendons were run through the columns and panels to connect the entire unit. The tendons were tensioned to an effective stress of 1145 MPa (166 ksi). The prototype design included 15.24 mm diameter radial tendons instead of 12.7 mm tendons. However, placement of the 15.24 mm radial tendons in the test unit was not possible due to the curvature of the post-tensioning ducts combined with the duct's corrugated inner surface. In the prototype tower this issue will easily be eliminated by increasing the duct size used for the radial post-tensioning. The assembly process of the prototype tower will also not be subject to the same space limitations experienced in the laboratory and the entire tower section of six columns and six panels will be

assembled as a single unit before installation of the vertical post-tensioning. This will result in pre-compress of all six panels and a more robust tower system.

Upon substitution of the 12.7 mm tendons, the design of the test unit was reexamined to understand how the smaller tendons would affect the test unit capacity. It was calculated that the reduction in post-tensioning would not have a significant effect on the capacity of the panel sections. However, the calculated connection capacity between the column and panel was reduced resulting in the possibility of cracking of the epoxy at the joint under extreme loads. After completion of the radial post-tensioning, the test unit was attached to the testing crosshead to allow load application.

4.6 Instrumentation:

The completed test unit was instrumented at multiple locations to allow adequate evaluation of the test unit behavior. Each column and panel was assigned a number along with each exposed column surface to allow clear labeling of recorded data (Figure 4.5). Instrumentation towers were added around the test unit perimeter and string potentiometers (string pots) were added to the towers to measure test unit deflection. Each string pot was labeled according to its column or panel number, column surface number (if applicable), and location (1-4) along the tower height. Tower height locations were 0 m (1), 1.68 m (5.5 ft) (2), 3.35 m (11 ft) (3), and 5.03 m (16.5 ft) (4) respectively. As an example, the resulting label for an individual string pot could be C1S2-1, which would corresponded to column 1, surface 2, and height position 1 of 0 meters. Before casting and erection of the precast test unit members, strain gages were attached to the reinforcement steel in a test unit base block, and also to rebar in a UHPC column, HSC column, UHPC panel, and HSC panel. The base block strain gages were installed on the steel containment stirrups located around the vertical post-tension anchors. The column strain gages were installed around the horizontal post-tensioning anchor locations, and the panel gages were installed at each panel base to monitor reinforcement strain.

Linear Variable Displacement Transducers (LVDTs) were attached to columns and panels to monitor gap opening between members. The LVDTs were labeled similar to the string pots by including the column or panel number, location regarding the upper (UL) or lower (L) part of the column or panel, and the column or panel surface number. Since the panels only have one surface, the panel surface number identified the orientation of the LVDT as shown in Figure 4.5. An LVDT number of C1L1 would then correspond to column 1, at the lower end of the

column, and at surface 1. LVDTs were also placed on the top and bottom reaction blocks to monitor any slip between the base blocks and floor or the top blocks and loading crosshead.

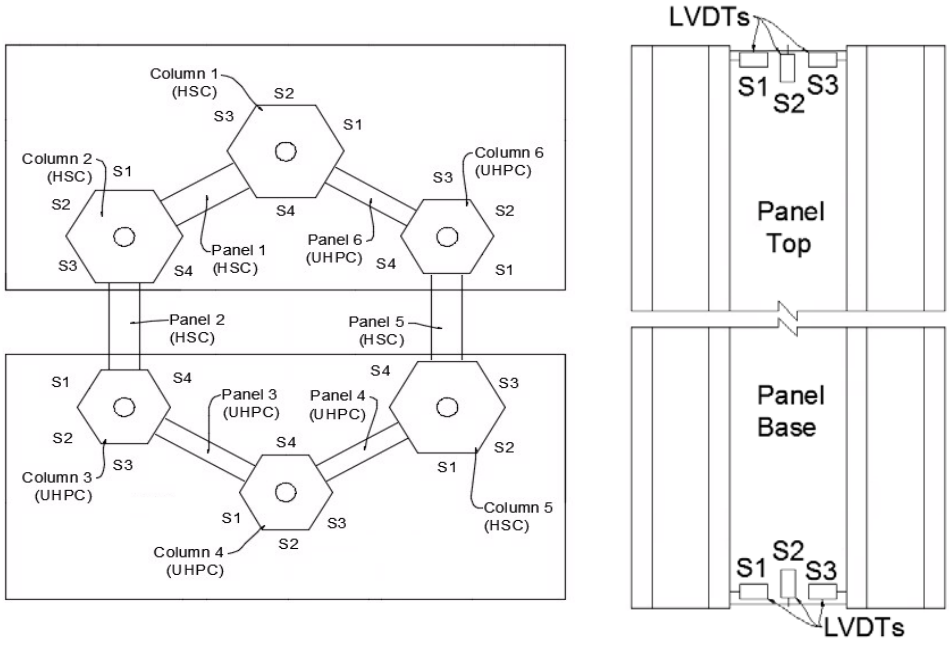

Figure 4.5. Column and panel number labeling (left); LVDT panel surface numbering (right)

Two steel load cells were fabricated and installed under the column post-tension multi-strand anchor heads to monitor column forces. Each load cell was a 16” x 16” x 16” hollow steel cube with 25.4 mm (1 in.) thick walls and 101.6 mm (5 in.) and 50.8 mm (2.5 in.) bearing plates on the top and bottom of the cube, respectively. Strain gage rosettes were attached to each side of the cube to monitor stress. The load cells were placed before post-tensioning of the tower system in order to effectively monitor post-tensioning losses. Surface strain gages were attached horizontally to a HSC and UHPC panel in order to monitor the change in panel surface stresses. A Northern Digital Inc. Optotrak 3D (referred to as NDI) camera system, utilizing multiple LED sensors, was positioned to observe the change surface strain for a section of one UHPC panel and one UHPC column. The LED location and layout are shown in Figure 4.6 and readings from the LEDs were collected at a frequency of 1 Hz.

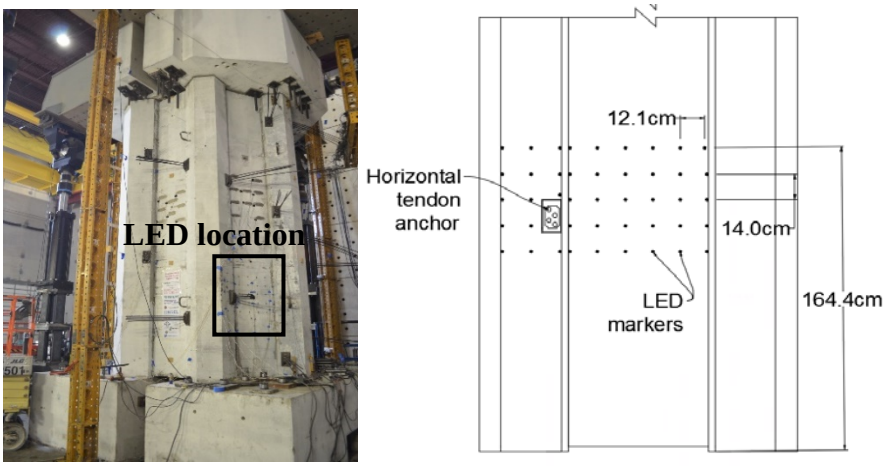

Figure 4.6. LED location (left) and layout (right)

4.7 Load protocol:

A loading protocol was developed based on loads obtained for the Siemens 2.3 MW-108 machine. The loads followed the International Electrotechnical Commission (IEC) document 61400-1, and corresponded to specified turbine operating conditions. Three controlling load cases were identified for application to the test unit and each corresponded to a governing shear, overturning moment, or torsional load. The first load case was IEC DLC 1.1 where the resultant loads are caused by atmospheric turbulence under normal tower operation. This load case generates the largest tower overturning moment for both operational and extreme load conditions. The second load case was IEC DLC 4.2 which corresponds to the wind turbine switching from power production to an idle or stand still position. The change in position generates the largest tower shear force at operational and extreme loads. The last load case was IEC DLC 2.2 which corresponds to an electrical fault in the control protection system and results in the largest tower torsional moment at operational and extreme conditions (International Electrotechnical Commission, 2005). Each controlling load case consisted of an applied shear, overturning moment, torsional load, and axial load. The test unit was displaced in four directions with both positive and negative magnitudes as shown in Figure 4.7 in order to allow opportunity to evaluate any difference in behavior between HSC and UHPC members. The loads were applied in 25% increments in each direction and cycled three times at 50% and 100% load magnitudes to allow proper evaluation of test unit response. A complete summary of operational and extreme loads is shown in Table 4.2. For defining the overload behavior of the test unit, large displacement cycles were applied, with the displacement magnitudes determined based on

the test unit performance during extreme loads. These cycles are further described in the testing observations.

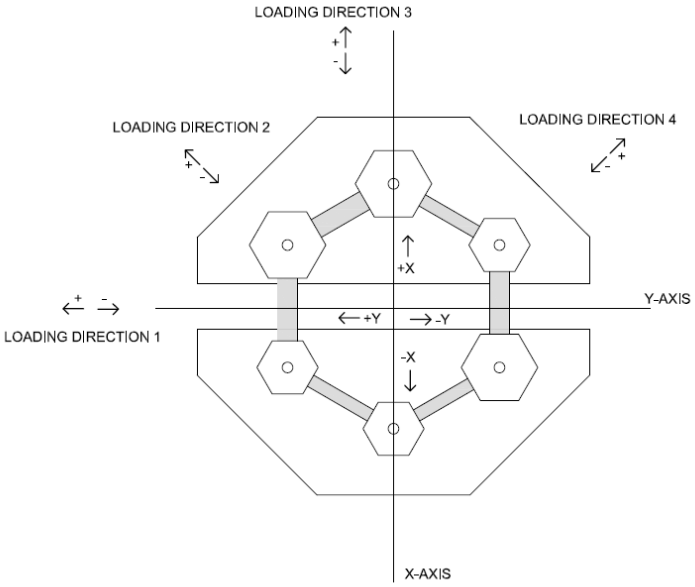

Figure 4.7. Loading directions

Table 4.2. Test unit load sequence

Operational limit state			
	Load Case	Load direction	Predominant load
Test 1	4.2	3	Base Shear - 544 kN (135 kips)
Test 2	4.2	1	Base Shear - 544 kN (135 kips)
Test 3	1.1	2	Base Overturning Moment - 9373 kNm (6912 k-ft)
Test 4	1.1	4	Base Overturning Moment - 9373 kNm (6912 k-ft)
Test 5	2.2	3	Base Torsion - 6522 kNm (4810 k-ft)
Test 6	4.2	3	Base Shear - 544 kN (135 kips)
Extreme limit state			
	Load Case	Load direction	Predominant load
Test 1	4.2	3	Base Shear - 787 kN (177 kips)
Test 2	4.2	1	Base Shear - 787 kN (177 kips)
Test 3	1.1	2	Base Overturning Moment - 11994 kNm (8846 k-ft)
Test 4	1.1	4	Base Overturning Moment - 11994 kNm (8846 k-ft)
Test 5	2.2	3	Base Torsion - 7647 kNm (5640 k-ft)
Test 6	4.2	3	Base Shear - 787 kN (177 kips)

4.8 Data measurement:

During testing, overall test unit force and displacement readings were available from the loading crosshead as well as the attached test unit instrumentation. After testing it was found that the horizontal (lateral) and torsional crosshead displacement readings were not fully accurate at small displacements due to the absence of hydraulic bearings in the horizontal actuators. The horizontal actuators contain mechanical bearings which create backlash when both shear and torsional forces are applied simultaneously and result in incorrect displacement readings at lower load values. For this reason, lateral and torsional measurements were collected using string pots and LVDTs for small displacements and the crosshead readings were referenced for large displacements.

4.9 Quantifying test unit response:

The test unit behavior was quantified in both the lateral and torsional directions using basic engineering mechanics and numerical equations. In the lateral direction, the numerical equation is derived from utilizing the principal of virtual work and applying a 1 kN virtual load laterally at the top of the test unit. Equation 4-1, shown below, is the resulting equation for lateral deflection due to shear and overturning moment. The shape factor for a hollow circular tube was used as an approximation for shear deformation. The torsional behavior of the tower was quantified using Equation 4-2 (Hearn, 1997), with the angle of twist corresponding to the torsional rotation at the top of the test unit section. For both the lateral and torsional response, some reduction in stiffness was expected due to the post-tensioning of the column and panel connections and the tensioning of the columns by the vertical tendons.

$$\Delta(z) = \int_0^z \frac{M}{\gamma * EI}(z - x)dx + \int_0^z \frac{V}{\gamma * G a_r} dx \qquad \text{(Eq. 4-1)}$$

where:

$\Delta(z)$ = deflection at height z along the test unit

z = height along test unit

M = applied moment at the base of the test unit

γ = stiffness reduction factor accounting for vertical post-tensioned connections

E = modulus of elasticity of test unit

I = moment of inertia of test unit

x = height along test unit where dummy load is applied

V = shear applied at base of test unit

G = shear modulus of test unit

a_r = modified test unit area based on shape (related to shear shape factor)

$$\theta(z) = \frac{Tz}{\gamma_T 4A^2 G} * \left[\frac{s_1}{t_1} + \frac{s_2}{t_2} + \frac{s_3}{t_3} + \cdots etc\right] \qquad \text{(Eq. 4-2)}$$

where:

θ(z) = torsional rotation at height (z) along the test unit

z = height along test unit

T = torsion applied at top of test unit

γ_T = torsional stiffness reduction factor accounting for vertical post-tensioned connections

A = area of test unit

G = shear modulus of test unit

s_n = width of column or panel *n*

t_n = thickness of each column or panel *n*

4.10 Test observations:

4.10.1 Operational loads:

Operational and extreme load values were applied to the test unit following the loading protocol outlined in Table 4.2. During operational loads, the Hexcrete tower remained elastic for both the operational and torsional displacements. The governing lateral and torsional displacements responses are reported in Figure 4.8 with the lateral response corresponding to DLC 1.1 and the torsional response corresponding to DLC 2.2. The numerical lateral and torsional stiffness responses, with appropriate stiffness reduction factors, are also included in the force-displacement plots. No cracking of the test unit members was observed until application of 100% of torsional load case DLC 2.2. Small 0.1 mm (0.004 in.) hairline cracks appeared in the two HSC connecting panels cracks (Figure 4.9) due to the absence of vertical pre-compression during the test unit construction. Cracking did not occur along the entire panel, but only in a few locations and the cracks were outlined with markers to allow for visibility. No other cracks were observed and all of the panel cracks closed upon removal of the test loading.

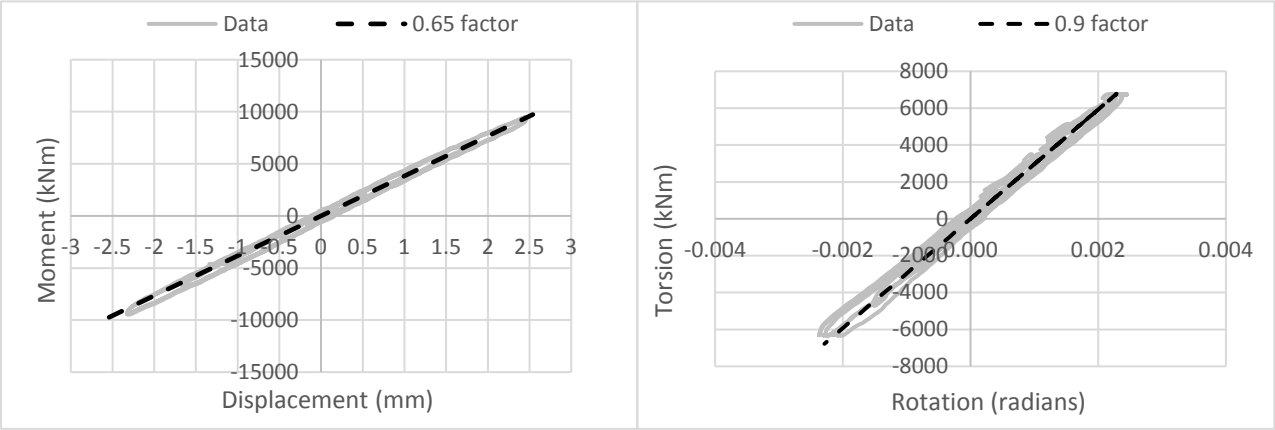

Figure 4.8. Operational lateral response (left); operational torsional response (right)

Figure 4.9. Hairline HSC connecting panel cracks

4.10.2 Extreme loads:

Following the completion of operational loads, extreme loads were applied to the test unit. The test unit behavior remained elastic in both the lateral and torsional directions with a slight reduction in stiffness observed in the torsional tower behavior, most likely due to the panel cracking during operational loading (Figure 4.10). No further cracking was observed until 75% of the torsional load case DLC 2.2 was reached. At this load level new torsional cracks appeared at the base of one of the HSC connecting panels and the cracks from operational torsion widened to 0.2 mm (0.008 in). As the extreme torsional loading increased to 100%, cracks appeared along the entire height of the connecting panels as well as in a single region of one UHPC column. The UHPC column cracks were localized around a horizontal PT anchorage location. Cracks were not observed on any of the other columns or panels and both the column and panel cracks closed upon removal of extreme loads.

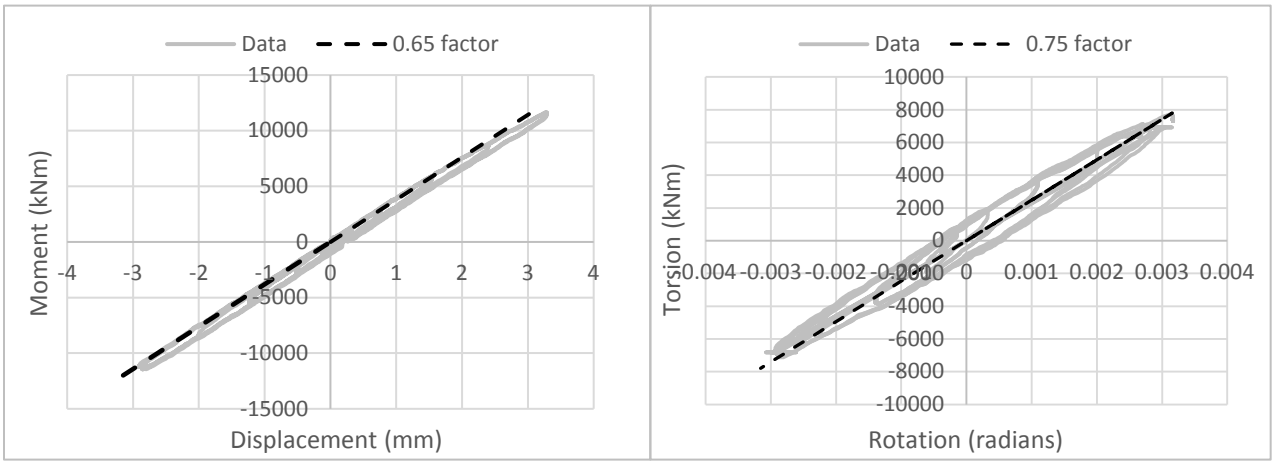

Figure 4.10. Extreme lateral response (left); extreme torsional response (right)

4.10.3 Capacity testing:

Since the test unit force-displacement response remained linear after the application of extreme loads, large magnitude loads were applied in order to measure the full capacity of the unit and also identify the failure mechanism of the tower system. To reach the test unit capacity, loads corresponding to the operational and extreme design envelopes were applied. A small number of 0.1 mm cracks were observed on the HSC connecting panels under the operational load envelope, but no further damage occurred. An elastic response was observed in the lateral and torsional test unit response with a minimal change in stiffness. However, at the extreme load envelope a drop in both torsional and lateral stiffness was observed as shown in Figure 4.11. Further cracking of the connecting HSC panels occurred and vertical cracks appeared in the epoxy joints appeared between multiple UHPC panels and the test unit columns.

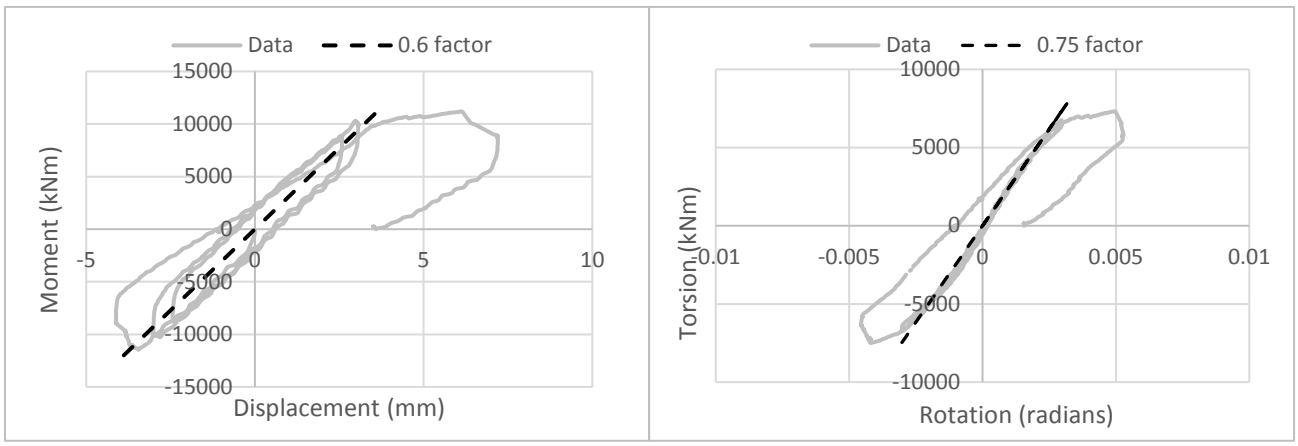

Figure 4.11. Operational envelope lateral (upper left) and torsional (upper right) responses; extreme envelope lateral (lower left) and torsional (lower right) responses

The test unit retained a large amount of load capacity after the decrease in stiffness, therefore, overturning moments of increasing magnitude were applied to overload the test unit. However, the force limit for the overturning moment of the testing actuators was reached with no further drop in stiffness. Therefore, to reach full capacity of the test unit and further investigate the torsional capacity of the Hexcrete design, large torsional displacements were applied. Damage to the test unit progressed steadily as the torsional displacement increased beyond the 0.005 radians (0.3 degrees) applied during the extreme envelope loading. Both HSC and UHPC columns experienced torsional cracking, new cracks continued to appear on the HSC panels, and the epoxy between all of the column and panel connections cracked diagonally or split vertically. No visible cracks occurred in the UHPC panels but gaps up to 6.35 mm (0.25 in.) opened between the UHPC panels and columns at the epoxy joint. Torsional loading of the test unit continued at 0.0035 radian (0.2 degree) displacement intervals until 0.07 radians (4 degrees) of rotation was reached. At a rotation of 0.07 radians, which was 23 times more rotation than was experienced under extreme torsional loads, spalling had occurred on both HSC and UHPC columns and the test was terminated due to damage to the foundation blocks. Damage to the test unit during the large displacement cycles is shown in Figure 4.12 along with the tower rotational displacement response measured at the crosshead. Much of the damage to the test unit was spalling of cover concrete which protects the steel reinforcement from corrosion. The cover concrete did not significantly affect the structural capacity of the test unit and the unit was still able to support the axial load simulating the weight of the nacelle and rotor after the completion of testing. The response of the test unit under large displacements demonstrated that the tower had sufficient ductility beyond extreme loads.

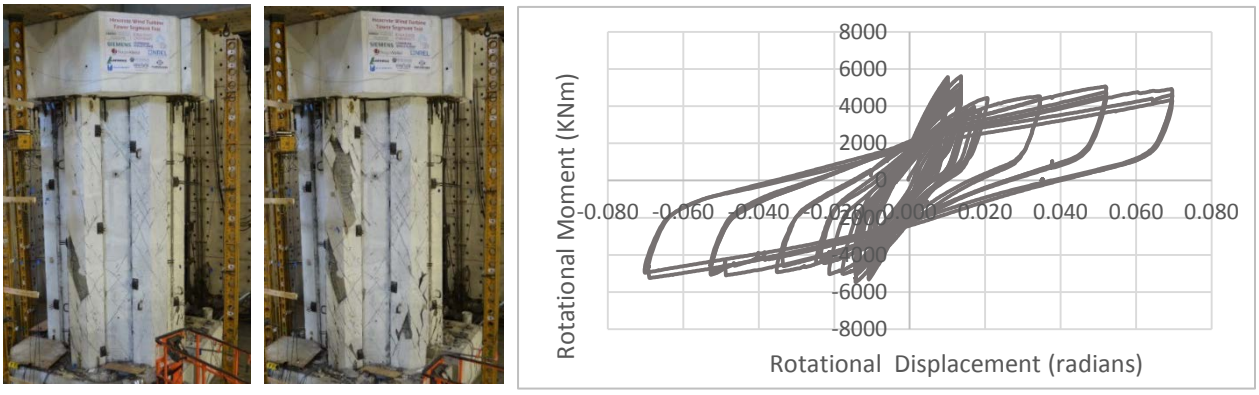

Figure 4.12. Test unit damage under large rotation cycles (left); large rotation force-displacement response (right)

4.11 Discussion of test observations:

The objective of the Hexcrete unit test was to validate strength capacity of the tower design process and demonstrate that the assembled precast pieces can act as a single unit to resist design loads in an elastic manner. Based on the performance of the test unit, it can be concluded that the test unit did act as a single unit and remained elastic through both operational and extreme loads. Slight softening of the unit began to occur under the operational envelope due to cracking of the two HSC connecting panels, and a more sizeable drop in stiffness occurred at the extreme envelope load level after separation occurred at the epoxy column to panel joints. The following sections discuss specific tower member behavior and the effect of member behavior on the overall test unit response.

4.11.1 Panel behavior:

Panel surface stresses were measured using the NDI camera system previously described. The NDI system used LED markers attached to the surface of Panel 3 (UHPC) to track surface movement and deflections which were then evaluated to define concrete surfaces stresses. The LED markers were installed after application of both the vertical and horizontal post-tensioning. Therefore, the panel pre-compression, caused by both sets of post-tensioning, was evaluated using a finite element model of the test unit created in SAP2000. The SAP2000 model was first verified by comparing changes in the SAP2000 panel stresses between load cases to the measured changes in NDI values. The changes in stress compared well with the NDI readings enabling the SAP pre-compression values to be applied to the NDI. Although stresses were only measured on a single UHPC panel, the multiple loading directions provided measurements representative of all six panels. Consideration was given to the effect of the increased HSC panel thickness on the adjusted stress values, and SAP2000 was also used as a reference for this adjustment. As a final check for UHPC to HSC panel stress conversion, the surface strain gage measurements attached to the HSC panel were compared to adjusted NDI readings and found to be very similar, thereby providing confidence in the adjusted results.

The prototype tower panels were designed to remain uncracked under both operational and extreme loads. However, cracking was observed in the HSC connecting panels under operational torsional loading. Investigation of the panel stresses showed that the absence of pre-compression in the connecting panels, due to the sequence of construction, caused premature cracking. Figure 4.13 shows the HSC connecting panel average principal stresses with standard

stress deviation bars for the six load cases shown in Table 4.2. The shear load cases (DLC 4.2) are Op 1 and Ex 1; overturning moment load cases (DLC 1.1) are Op 3 and Ex 3; and the torsional load cases (DLC 2.2) are Op 5 and Ex 5. As noted in the testing results, the panel cracking that occurred during operational loads was limited and did not occur across the entire panel height. This agrees with data at Op 5 showing that the average stress of the panel did not exceed cracking but the certain parts of the panel corresponding to the standard stress deviation were overstressed. At extreme envelope loads, the average stress in the connecting panels exceeded the cracking stress which explains the observed widespread cracking. The pre-compression due to the horizontal tendons was also examined to determine the impact of substituting 12.7 mm tendons for 15.24 mm tendons during the test unit construction. Figure 4.13 shows that the principal stress difference in the connecting panels, resulting from the change in tendon diameter, is negligible and that the vertical pre-compression controls the panel stress capacity. For comparison, panel principal stress values for the non-connecting panels are shown in Figure 4.14. The graph shows the impact that vertical pre-compression has on the tower system. All the test unit panels would have remained uncracked if all the columns and panels were circumferentially connected prior to installing the vertical post-tensioning.

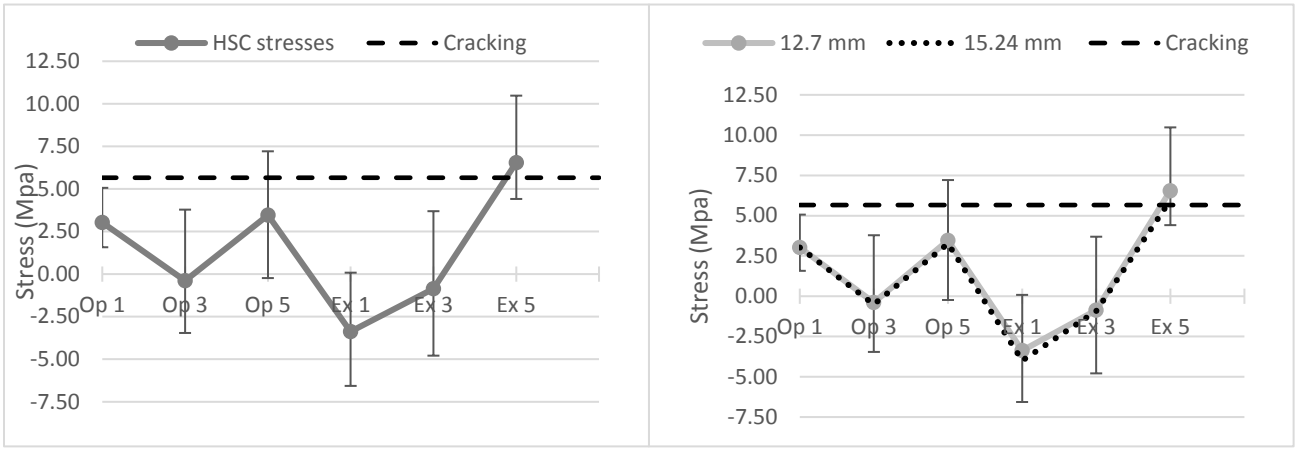

Figure 4.13. HSC connecting panel principal stresses with standard deviation (left); HSC connecting panel principal stresses with 15.24 mm tendons (right)

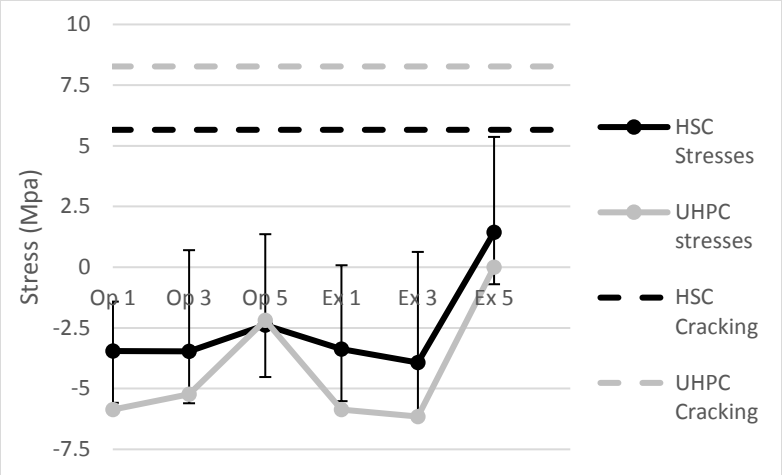

Figure 4.14. Principal stresses and principal stress deviation of pre-compressed panels

4.11.2 Column behavior:

The test unit columns anchored the horizontal post-tensioning and also contained the vertical pre-stressing strands. The only damage observed to the columns was cracking of a UHPC column (Column 6) around a single horizontal post-tensioning anchor location. Since this did not occur at any other column location, it is likely that the localized cracking was due to poor steel fiber distribution of the UHPC. The steel strain gages installed on the column rebar prior to casting were also examined and did not show any yielding of column reinforcement.

In addition to the overall force-displacement of the test unit, deflections along the height of the columns for increasing load magnitudes are shown in Figure 4.15. The nearly constant spacing between the deflection curves under increasing load reinforces the linear force-displacement relationship of the test unit under lateral loading. While Equations 1 and 2 accurately quantified deflection at the top of the test unit, the equations were overly conservative in calculating the deflection along the test unit height. Therefore, the SAP model created to predict panel pre-compression was utilized to better represent deflection along the height of the test unit (Figure 4.15).

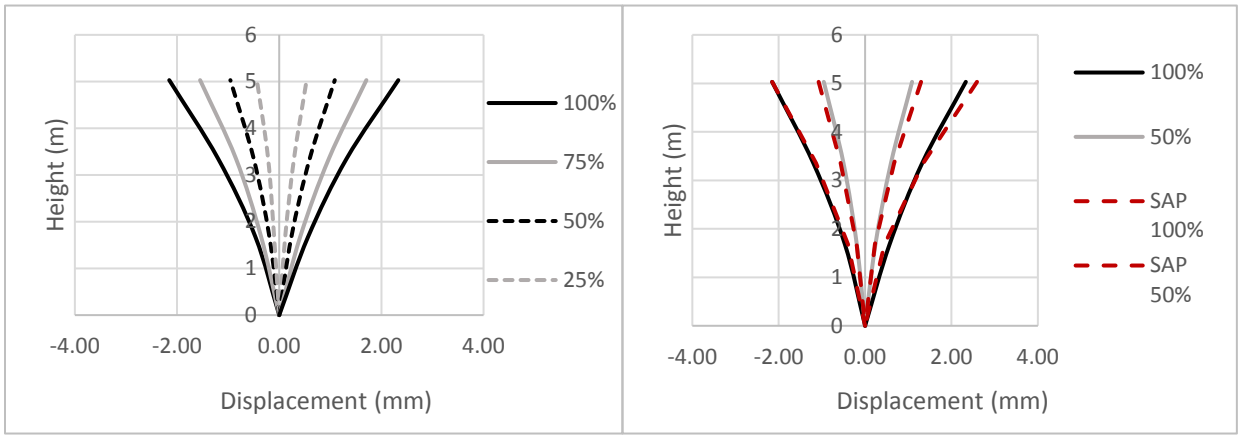

Figure 4.15. Displacement along column height as load increases (left); SAP prediction compared to measured data

4.11.3 Connection behavior:

The capacity of the horizontal post-tensioned connections between each column and panel were calculated using shear friction as shown in Equation 4-3 (ACI Committee 318, 2011). The first part of the equation accounts for the compression force of the post-tensioning steel across the connection and the second part calculates the contribution of concrete and epoxy bond known as adhesion. ACI specifies a strength reduction factor of 0.75 for *Vn*, but this factor was not considered for the test unit design in order to better understand the relation between the shear friction equation and measured test unit behavior. For each tested load case, column axial forces caused by gravity and overturning loads were measured by the installed column load cells and translated to an equivalent panel connection force using Equation 4-4 and 4-5. Torsion and shear connection forces were derived based on basic shear flow principles using Equations 4-6 through 4-8 (ACI Committee 318, 2011). The resulting connection loads for each load case are shown in Table 4.3 along with the calculated shear friction capacity of the column to panel joints based on Equation 3. The connection loads assume the worst case scenario in which shear and torsion are additive.

$$V_n = \mu A_{vf} f_y + A_c K_1 \qquad \text{(Eq. 4-3)}$$

where:

V_n = nominal shear capacity

μ = friction coefficient (assumed to be 0.6 for epoxy placed against hardened concrete that is not intentionally roughened)

A_{vf} = total area of PT tendons crossing connection interface

f_y = stress in PT tendons after jacking and PT losses

A_c = area of panel edge at connection interface

K_1 = bond strength of epoxy between the column and panel

$$\delta_{column} = \frac{PL}{A_g E} \qquad \text{(Eq. 4-4)}$$

where:

P = single column axial load + single column tension or compression from overturning moment

L = length of column

Ag = gross cross-sectional area of column

E = elastic modulus of column

$$P_{panel} = \frac{\delta_{column} * E_{panel} * A_{panel}}{L_{panel}} \qquad \text{(Eq. 4-5)}$$

where:

P_{panel} = equivalent panel connection force

E_{panel} = elastic modulus of panel

A_{panel} = area of panel

L_{panel} = length of panel

$$Vi = q * p_w \qquad \text{(Eq. 4-6)}$$

$$Ni = Vi * cot\theta * 0.5 \qquad \text{(Eq. 4-7)}$$

$$Di = Vi/sin\theta \qquad \text{(Eq. 4-8)}$$

where:

Vi = shear force acting at top of panel surface

q = shear flow resulting from torsional and shear loading (force/unit length)

p_w = panel width

Ni = connection force resulting from Vi

θ = angle of compression in concrete resulting from Vi (37.5 degrees for prestressed members)

Di = concrete diagonal compression resulting from Vi

Table 4.3. Column-to-panel connection loads and capacity

Load Case	HSC Panel calculated loads (kN)	HSC Panel connection capacity (kN)	UHPC Panels calculated loads (kN)	UHPC Panel connection capacity (kN)
Op. Lateral	2224	4355	2077	3434
Op. Torsion	2642	4355	2513	3434
Ex. Lateral	2224	4355	1997	3434
Ex. Torsion	3025	4355	2927	3434
OpEnv	3866	4355	3536	3434
Ex Env	4666	4355	4235	3434

As shown in Table 4.3, the capacity of the UHPC column-to-panel connection was slightly exceeded at operational envelope loading and a larger overloading occurred at extreme envelope loads. The large overloading caused opening of the epoxy joints at the UHPC panel connections and the subsequently observed drop in test unit stiffness. The HSC panel connection capacity was also exceeded at extreme envelope loads. LVDTs located on the outer surface of the panels, 25.4 mm (1 in.) from the panel top and bottom edges, were examined to verify the capacity calculations in Table 4.3. Table 4.4 shows LVDT data from Panels 4-6 for each load case with bold font indicating cracks. Cracking was defined as an opening greater than or equal to 0.1 mm (0.004 in.). LVDT measurements show that hairline cracks began to occur along the connection interface on all three panels during the operational torsional loads and the cracks reopened and grew under extreme torsion and envelope loads. The widening cracks for Panels 4 and 6 under operational and extreme envelope loading agree well with the capacity connections discussed above. It should be noted that Panel 5 is an HSC connecting panel that experienced torsional cracking at operational torsional loads which decreased the pre-compression due to post-tensioning and weakened the connection interface. However, an explanation is needed for the cracking of the epoxy interface for Panels 4 and 6 under operational and extreme torsion loads.

Table 4.4. LVDT measurements of column to panel joint opening (mm)

	P4L1	P4UL1	P5L1	P5UL1	P6UL1	P6UL3
Op. Lateral	0.05	0.03	0.08	0.05	0.05	0.05
Op. Torsion	0.09	**0.10**	**0.10**	0.09	**0.11**	0.08
Ex. Lateral	0.00	0.03	0.08	0.05	0.05	0.00
Ex. Torsion	**0.12**	**0.11**	**0.11**	**0.11**	**0.16**	0.09
OpEnv	0.08	**0.11**	**0.11**	**0.24**	**0.18**	0.07
Ex Env	0.08	0.05	**0.13**	**0.21**	**0.31**	**0.12**

The LVDT's listed in Table 4.4 were positioned approximately 25.4 mm (1 in.) from the top and bottom edge of the panel in close proximity to the vertical post-tensioning anchors in the test unit reaction blocks. A strut-and-tie model of a test unit panel (Figure 4.16) was created to investigate if transfer of the vertical post-tensioning forces from the columns to the panels caused any localized stresses at the panel edges. The strut and ties model indicated that the forces applied by the vertical post-tensioning resulted in a localized tension tie at the panel ends (Figure 4.16). The magnitude of the tension tie caused an increase in tensile stress of 11.03 MPa (1.6 ksi) along both the top and bottom edges of the panel. This increase in tensile stress, although not large enough to cause cracking in the UHPC panels, was great enough to cause vertical tensile cracks at the interface between the lower strength epoxy and UHPC panel at operational and extreme torsional loads.

Since the test unit was originally designed for 15.24 mm radial tendons instead of the 12.7 mm tendons installed during construction, the capacity of the connections was recalculated for the larger tendon size. The increased column to panel connection capacity is shown in Table 4.5 and it can be observed that for the 15.24 mm tendon, the UHPC panel connection capacity is not exceeded until extreme envelope loads. Therefore, it is possible that the drop in test unit stiffness at extreme envelope loads may not have occurred or may have been smaller if the 15.24 mm tendons were able to be installed.

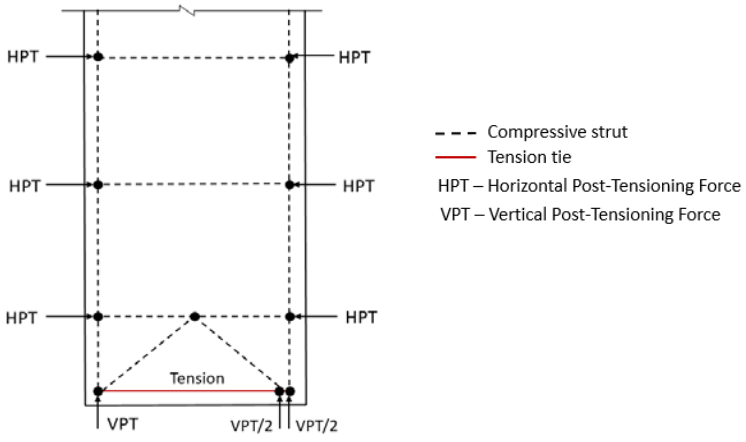

Figure 4.16. Strut and tie model for top and bottom of panel

Table 4.5. Column to panel connection loads and capacity for 15.24 mm tendons

Load Case	HSC Panel calculated loads (kN)	HSC Panel connection capacity (kN)	UHPC Panels calculated loads (kN)	UHPC Panel connection capacity (kN)
OpEnv	3608	5205	3938	4262
Ex Env	4321	5205	4754	4262

4.12 Conclusions:

The MAST test provided an opportunity to evaluate the tower performance in regard to design stiffness, connection integrity, member cracking, and overall tower behavior. The Hexcrete test unit remained elastic under both operational and extreme loads as demonstrated by a linear force-displacement response. Stiffness reduction factors for the Hexcrete system, due to column vertical post-tensioning connections, were found to be 0.65 for lateral loads and 0.9 for torsional loads before cracking of the structure. Damage of the test unit was mostly limited to the two HSC connecting panels due to the test unit construction sequence and resulting absence of vertical pre-compression. In field application of the Hexcrete tower system, this will not be an issue since an entire hexagon section will be fabricated before application of the vertical post-tensioning. The other panels in the test unit did not experience cracking, and the column-to-panel connections were found to have sufficient capacity to resist connection forces until the application of envelope loading. To prevent separation of the column to panel connections under envelope loads, the size or spacing of the horizontal post-tensioning can be adjusted to meet the necessary connection capacity. Finally, it was found that additional tensile stresses were generated at the top and bottom of the test unit panels due to the transfer of the column vertical post-tensioning force. This stress increase resulted in hairline cracks at the column to panel interface. In future Hexcrete designs, this cracking can be avoided by relocating horizontal post-tensioning closer to the edge of the panels to counteract this additional force.

The strength test of the Hexcrete tower validated the tower design by showing that the unit responded as a single system. Furthermore, opportunities for improvement of the design were identified and the knowledge gained from the test will help further advance Hexcrete tower performance. By making the adjustments noted above, the Hexcrete tower system has the capability to be a viable wind tower solution and an important part of extending wind energy to all 50 states.

4.13 References:

Acciona WindPower. (2016, July). *Concrete Towers*. Retrieved from Acciona WindPower: http://www.acciona-windpower.com/technology/concrete-towers/

ACI Committee 318. (2011). *Building Code Requirements for Structural Concrete (ACI-318) and Commentary.* Farmington Hills: American Concrete Institute.

AWEA. (2015, December). *U.S. wind industry leaders praise multi-year extension of tax credits*. Retrieved from American Wind Energy Association: http://www.awea.org/MediaCenter/pressrelease.aspx?ItemNumber=8254

Hearn, E. (1997). *Mechanics of Materials 2, 3rd Edition.* Woburn, MA: Butterworth-Heinemann.

International Electrotechnical Commission. (2005). *Wind turbines - Part 1: Design requirements.* Geneva, Switzerland: International Electrotechnical Commission.

Lewin, T., & Sritharan, S. (2010). *Design of 328-ft (100-m) Tall Wind Turbine Towers Using UHPC.* Ames, IA: Department of Civil, Construction, and Enviromental Engineering Report ERI-ERI-10336.

Sritharan, S., & Lewin, T. (2015). *U.S. Patent No. 9,016,012.*

Sritharan, S., Lewin, T., & Schmitz, G. M. (2014). *U.S. Patent No. 8,881,485.*

Twigden, K., Sritharan, S., & Henry, R. (2017). Cyclic testing of unbonded post-tensioned concrete wall systems with and without supplemental damping. *Engineering Structures*, 406-420.

U.S. Department of Energy. (2015). *Wind Vision: A New Era for Wind Power in the United States.*

U.S. Energy Information Administration. (2017, April 3). *U.S. States: State Profiles and Energy Estimates*. Retrieved from Independent Statistics and Analysis, U.S. Energy Information Administration: https://www.eia.gov/state/maps.php?src=home-f3

4.14 Acknowledgements:

The information, data, or work presented herein was funded in part by the Office of Energy Efficiency and Renewable Energy, U.S. Department of Energy, under award number DE-EE0006737 (http://sri.cce.iastate.edu/hexcrete/). Additional funding and in-kind support have also been obtained from Iowa Energy Center and Lafarge North America Inc. of Chicago, Ill., respectively. Members of the project team include Sri Sritharan, Ming-Chen Hsu, David Jeong, Julienne Krennrich, Shibin Lin, Hart Wibowo, Robert Peggar, Bin Cai, Phil Barutha, Ali Nahvi, and Cheng-Hao Wu of Iowa State University; Suraj Musuvathy and Sanjeev Srivastava of Siemens Corp.'s Corporate Technology; Todd Culp of Coreslab Omaha; Markus Wernli and

Miranda Hagadorn of BergerABAM Inc.; and Jason Cotrell and Tyler Stehly of the National Renewable Energy Laboratory.

4.15 Disclaimer:

CHAPTER 5 – FINITE ELEMENT ANALYSIS AND NUMERICAL METHODS FOR HEXCRETE WIND TURBINE TOWERS

A paper to be submitted to the ASCE Structural Journal

Robert Peggar, Iowa State University

Sri Sritharan, Ph.D., Professor of Structural Engineering, Iowa State University

5.1 Abstract

The Hexcrete wind tower is an innovative hexagon shaped, precast concrete wind tower developed by Iowa State University (ISU) for wind towers above 328 ft (100 m). Six tall Hexcrete wind towers were recently designed for Siemens SWT 2.3-108 and SWT 3.2-113 turbines. Finite element models were created in the program SAP2000 with the goal of better characterizing Hexcrete tower behavior. Numerical methods were also developed to simplify design of the Hexcrete tower force-displacement response and predict member strains. The finite element analysis and numerical methods were verified from an experimental full-scale Hexcrete section test for a variety of test loads including both operational and extreme load conditions, as well as large section displacements. It was found that the finite element model was able to effectively replicate the behavior of the experimental test unit and was then extended to the complete tower system to identify critical tower dynamic properties. The simplified numerical methods were also found to be adequate approximations of the Hexcrete test unit but further validation is needed for application to the full tower system. This validation may be possible in design of a prototype Hexcrete tower structure in the near future.

5.2 Introduction:

The Hexcrete wind turbine tower is a new design for tall wind turbine towers above 328 ft (100 m) and was designed and patented by Iowa State University (ISU). A project funded by the U.S. Department of Energy (DOE) was recently completed which resulted in the design of six tall wind towers for heights of 394 ft (120 m) and 49 ft (140 m) as well as experimental verification of the tower design process. In order to supplement the design of the Hexcrete tower systems, finite element models and simplified numerical analysis processes were created.

Finite element analysis was performed in the Computers & Structures, Inc. (CSI) program SAP2000 version 17, while numerical models derived from reviewed literature and fundamental engineering principles. The finite element analysis and numeric models were verified by comparing results for a variety of load cases to experimental laboratory testing of a

full size Hexcrete wind tower section. The following sections of this paper detail the modeling techniques utilized for finite element analysis, discuss finite element verification, describe simplified numerical model formulations, and outline accuracy of the numerical models in comparison to measured experimental data. The paper concludes with specific recommendations related to finite element and numerical models for tower systems.

5.3 Finite element analysis:

5.3.1 Hexcrete tower system:

The Hexcrete tower system is an innovative tower design, patented by Iowa State University that utilizes precast high strength concrete members connected by steel post-tensioning tendons (U.S. Patent No. 9,016,012, 2015) (U.S. Patent No. 8,881,485, 2014). As the name implies, the tower is hexagon in shape and is made up of six hexagon shaped columns and six connecting wall panels as shown in Figure 5.1. Circumferential tendons connect the column and panel members, while vertical post-tensioning tendons run through the tower columns and connect the tower sections.

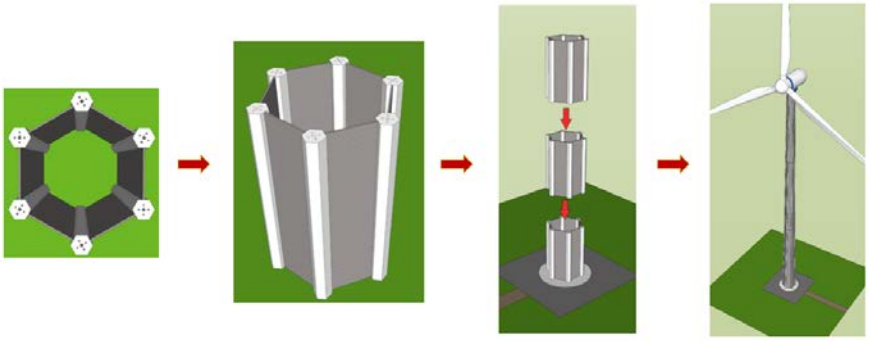

Figure 5.1. Hexcrete tower concept

5.3.2 Modeling techniques:

The program SAP2000 was chosen to analyze the Hexcrete tower system based on the ability to easily produce a centerline model of the entire tower system as well as the capability of the program to include staged construction in the model analysis. Staged construction is important due to the modular nature of the Hexcrete tower design as well as the high amount of post-tensioning in the construction process. Material properties were defined first in the modeling process and included High Strength Concrete (HSC), Ultra High Performance Concrete (UHPC), and seven wire, relaxed steel tendons. Properties of each material are shown in Table 5.1. Hexcrete columns were then defined as frame elements using the section designer

option to specify a hexagon shape (Caltrans hexagon). The hexagon dimensional and reinforcement properties were then set according the tower design geometry with a standard column longitudinal reinforcement ratio of 1.5%, spiral transverse reinforcement consisting of #5 (#16 metric) bars with 3 in. (76.2 mm) spacing, and 1.5 in. (38.1 mm) of clear cover. These reinforcement details were kept constant for all towers. SAP2000 provides built-in models for confined concrete based on the assigned column concrete parameters. For each column, HSC was utilized for cover concrete and the SAP2000 confined model "Core 1" was used with HSC as the reference material strength. If a column was tapered along its length, it was classified as a non-prismatic section and the taper was defined in terms of column end parameters, column length, and variation of stiffness properties (SAP values EI33 and EI22). A parabolic stiffness variation was assigned to tapered column sections.

Table 5.1. SAP2000 material properties

	HSC	UHPC	Steel tendons
f'c/fy, ksi (MPa)	13 (90)	26 (179)	270 (1862)
Elastic modulus (E), ksi (MPa)	6499 (44811)	7449 (51361)	29000 (199955)
Shear modulus (G), ksi (MPa)	2708 (18672)	3104 (21402)	11154 (76907)
Unit weight, pcf (kN/m^3)	150 (23.56)	150 (23.56)	490 (76.97)

The Hexcrete connecting panels were defined next using area elements. The area elements provide the option to specify wall thickness as well as shell, membrane, or plate behavior. For the Hexcrete panels, a thick shell formulation was used in order to consider shear stresses transverse to the panel surface as opposed to thin shells which do not account for these stresses. SAP2000 also provided the option to define the panels as layered elements where rebar in the panels can be included for analysis. However, this option was not utilized since the tower panels will have minimal reinforcement due to the combination of high tensile capacity materials (HSC and UHPC) and the use of circumferential post-tensioning which introduces pre-compression panel forces.

Steel post-tensioning tendons were then defined using the built in SAP tendon module. The area of each group of tendons was specified and the tendon modeling option was selected. Tendons can be modeled as loads or elements in SAP2000. For tendons modeled as loads, the

program converts the forces in the tendons to equivalent end loads and does not measure the forces along the tendon length during analysis. Tendons modeled as an element are treated similar to a frame object in that forces and displacements along the tendon length are measured and reported throughout the analysis process. For the vertical post-tensioning in the tower system, the tendons were modeled as elements in order to observe the resultant stresses and forces along the height of the tendon and corresponding column sections. For the circumferential post-tensioning, the tendons were modeled as loads since the tendons were short and equivalent end loads provided adequate pre-compression information.

In the Hexcrete tower system, a 0.75 in. (19 mm) layer of epoxy is placed between the tower columns and panels to provide a smooth bearing surface and additional bond strength prior to circumferential post-tensioning. The circumferential post-tensioning provides a large amount of connection capacity between the columns and panels. However, since the circumferential tendons were modeled as loads, a method was needed to transfer the loads between the column and panels. It was assumed that the column to panel connection would act as a fixed connection until decompression of the post-tensioning strands occurred, and it was also advantageous to the tower designer to observe the forces in the connection region following the application of tower loads. For these reasons, linear links were used to connect the columns to the panels. The linear links were assigned a uniform stiffness (10^5 k/in.) in all six degrees of freedom and resultant link forces and stresses were provided from the analysis output. For connection behavior after decompression, the stiffness of the links can be manually adjusted or non-linear properties can be introduced; however, this was not done immediately because the combination of loads resulting in tendon decompression was approximated but not fully determined because of the bonding behavior of the installed epoxy layer. A finalized section of the Hexcrete tower system is shown in Figure 4.18. The tower base is restrained only at the columns with pinned connections.

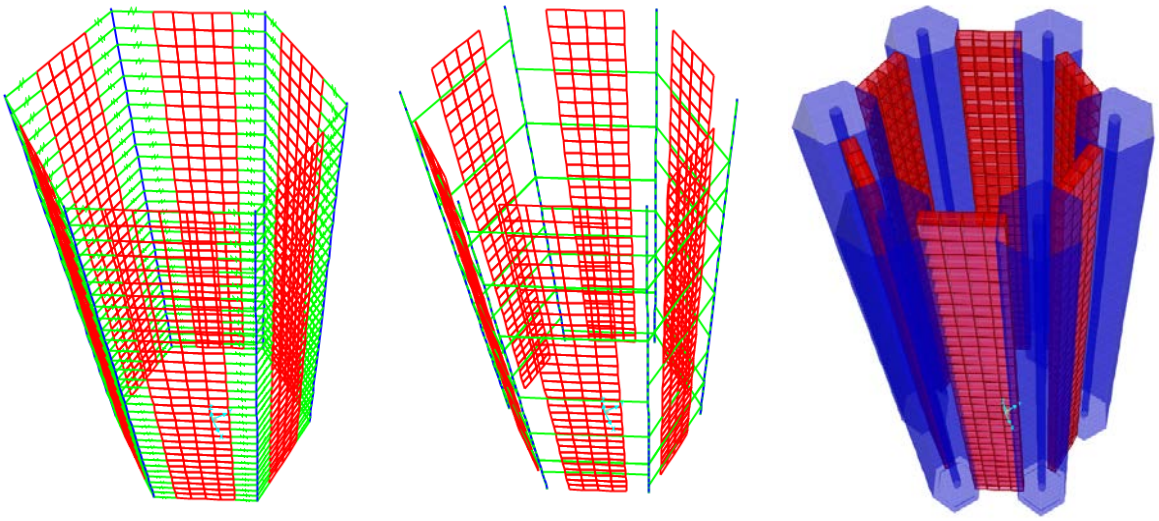

Figure 5.2. Hexcrete tower section: links (left), circumferential PT (middle), 3D view (right)

5.3.3 Tower models:

Six Hexcrete towers were designed and subsequently modeled in SAP2000 to evaluate the tower dynamic properties. Each of the tower corresponded specific hub heights and turbine sizes (Table 5.2). Three of the towers were fully fabricated from concrete (Table 1) while three were hybrid towers with circular steel at the tower top. All six towers utilized HSC columns and UHPC panels with vertical post-tensioning amounts varying according to each design. Details of the tower geometry are shown in Table 5.3 and Table 5.4. The steel shell at the top of the hybrid towers was modeled using a thin shell element composed of A992 steel with a yield stress of 50 ksi (345 MPa) and ultimate stress of 65 ksi (448 MPa).

Table 5.2. Hexcrete tower designs

Tower Name	Hub Height	Turbine size	Rotor diameter
HT1/HT1 Hybrid	394 ft (120 m)	2.3 MW	354 ft (108 m)
HT2/HT2 Hybrid	459 ft (140 m)	2.3 MW	354 ft (108 m)
HT3/HT3 Hybrid	459 ft (140 m)	3.2 MW	370 ft (113 m)

Table 5.3. Full concrete Hexcrete tower designs

	HT1	HT2	HT3
Tower base diameter*, ft (m)	25.72 (7.84)	27.9 (8.50)	34.34 (10.47)
Tower top diameter*, ft (m)	10.50 (3.20)	10.50 (3.20)	11.97 (3.65)
Base column diameter, ft (m)	3.58 (1.09)	3.33 (1.02)	3.84 (1.17)
Top column diameter, ft (m)	3.08 (0.94)	3.09 (0.94)	3.58 (1.09)
Strands per column	70	76	92
Max deflection, ft (m)	4.4 (1.34)	2.10 (0.64)	1.84 (0.56)
Frequency (Hz)	0.35	0.266	0.318
Weight (tower only), kips (metric tons)	2868 (1301)	3536 (1604)	4277 (1941)

Table 5.4. Hexcrete hybrid tower designs

	HT1 hybrid	HT2 hybrid	HT3 hybrid
Tower base diameter*, ft (m)	25.72 (7.84)	27.9 (8.50)	34.34 (10.47)
Diameter at concrete to steel transition, ft (m)	13.4 (4.09)	13.2 (4.03)	14.0 (4.27)
Base column diameter, ft (m)	3.58 (1.09)	3.33 (1.02)	3.84 (1.17)
Column diameter concrete to steel transition, ft (m)	3.28 (1.00)	3.14 (0.96)	3.76 (1.15)
Tower top diameter, ft (m)	7.4 (2.26)	7.4 (2.26)	8.9 (2.71)
Height of Hexcrete, ft (m)	260 (79.3)	305.75 (93.2)	284.5 (86.7)
Height of steel, ft (m)	124 (37.8)	144.85 (44.2)	166.1 (50.64)
Thickness of steel, in. (mm)	1.25 (31.8)	1.375 (34.9)	1.375 (34.9)
Strands per column	70	76	92
Frequency (Hz)	0.409	0.325	0.339
Weight (tower only), kips (metric tons)	2265 (1028)	2930 (1329)	3469 (1574)

Due to the size of the tower systems, a coarse mesh was used for the column frame and area elements with a single element height ranging from 3 ft – 4ft (0.61 m – 1.22 m). For this reason, local stresses within the tower system were not examined, instead the tower global dynamic response and deflection were evaluated. In order to accurately model the dynamic response of an entire wind turbine tower, the nacelle and rotor weights were modeled as a lumped mass at the rotor neutral axis (RNA) location which was specified by the turbine manufacturer. The lumped mass was connected to the top of the tower by body constraints which allowed equal displacement at the tower top in all six degrees of freedom. A full concrete and hybrid tower model are shown in Figure 4.19.

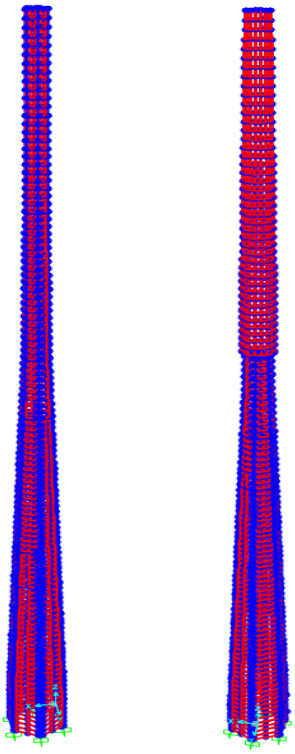

Figure 5.3. HT3 full concrete SAP model (left); HT3 hybrid SAP model (right)

5.3.4 Test unit model:

A full scale section of a Hexcrete tower was designed and experimentally tested (Figure 4.20). The test unit was 8 ft (2.44 m) in diameter and 16.5 ft (5.03 m) tall. The test unit included three 30 in. (0.76 m) diameter HSC columns, three 24 in. (0.61 m) diameter UHPC columns, three 8 in. (0.20 m) thick HSC panels, and three 5 in. (0.13 m) thick UHPC panels. The different column and panel sizes resulted from the strength of each material and provided opportunity to compare the performance of the two types of concrete. Groups of twenty 270 ksi (1862 MPa) relaxed 0.6 in. (15.24 mm) diameter tendons were installed in each test unit column and the circumferential post-tensioning consisted of seven groups of four 0.5 in. (12.7 mm) tendons with an average spacing of 2 ft (0.61 m).

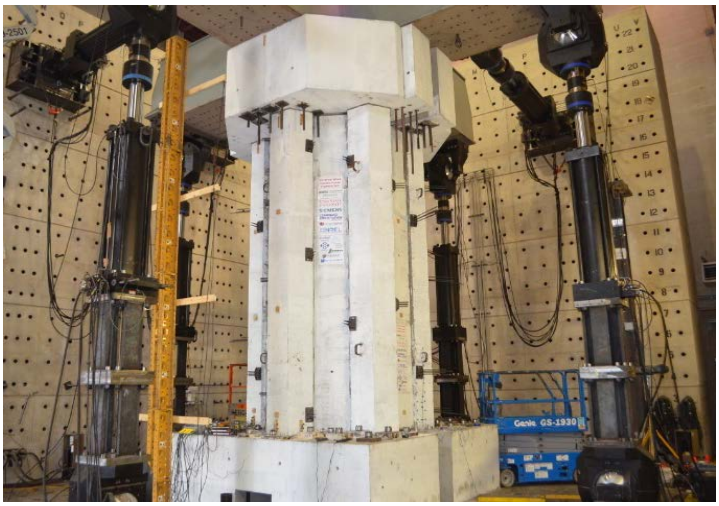

Figure 5.4. Hexcrete tower test unit

A SAP2000 model was created to investigate local section stresses, predict test unit behavior, and compare the modeling techniques to experimental testing results. A finer mesh than used in the tower model was used for the frame and area elements with an average element height of 6 in. (152.4 mm). The test unit and column diameters were prismatic with the corresponding SAP model shown in Figure 4.21. The foundation blocks and reaction blocks were omitted from the SAP model and replaced with simpler elements. The foundation blocks were replaced with a pinned constraints at each column base while the two reaction blocks were replace with a single, concrete frame element crosshead.

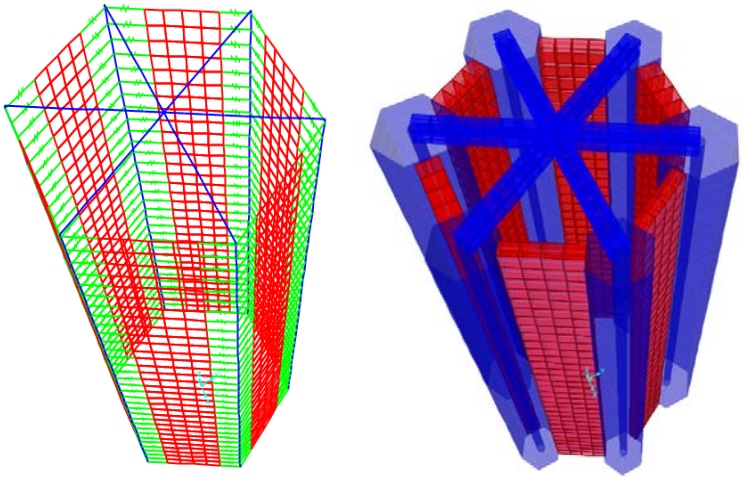

Figure 5.5. SAP2000 test unit model

5.3.5 Model verification and modification:

The loads applied to the experimental test unit were input into the SAP model and the response of the overall test unit as well as individual members was compared. Before the SAP model was run, material properties resulting from concrete cylinder tests were input into the model to match experimental testing conditions (Table 5.5). The test unit performed well under the designed operational and extreme loads with a linear force-displacement response; however, premature cracking in two of the HSC panels occurred during high torsional loads due to the laboratory erection sequence. Discussion of full test unit results can be found in (Peggar and Sritharan 2017, soon to be published). For the purposes of this report, test unit data corresponding to SAP model verification will be discussed with the overall stiffness of the tower examined first, followed by the individual member response.

Table 5.5. Test unit material properties based on concrete cylinder tests

	HSC	UHPC	Steel tendons
f'c/fy, ksi (MPa)	12 (83)	24 (165)	270 (1862)
Elastic modulus (E), ksi (MPa)	6244 (43052)	6876 (47410)	29000 (199955)
Shear modulus (G), ksi (MPa)	2602 (17941)	2865 (19754)	11154 (76907)
Unit weight, pcf (kN/m^3)	150 (23.56)	150 (23.56)	490 (76.97)

5.3.5.1 Test unit stiffness:

The force-displacement response of the SAP2000 test unit model was compared to the test unit data in both the torsional and lateral displacement directions for operational and extreme loads. It was found that the SAP model had a greater stiffness than the experimental test unit (Figure 4.22). The Hexcrete tower system consisted of multiple members that were post-tensioned together. The post-tensioned connections, while idealized as rigid, allow some flexibility in the tower system due to the interfaces between members. The SAP centerline model does not account for this flexibility but models all member connections as rigid which results in a stiffer SAP model. It may be possible to better capture the interface flexibility in a full 3D model of the system; however, for simplification purposes the column and panel element properties were modified in SAP by using factored values as shown in Table 5.6 with 1.0 representing the original property value. The member stiffness factors were derived by isolating column and panel stiffness values and subsequently iterating until the model behavior matched experimental

data. The stiffness factors differ between operational and extreme loads due to cracking that was experience in two of the panels at the end of operational loading. The resulting operational force displacement response of the test unit is shown in Figure 4.23 and the extreme force-displacement response is shown in Figure 4.24.

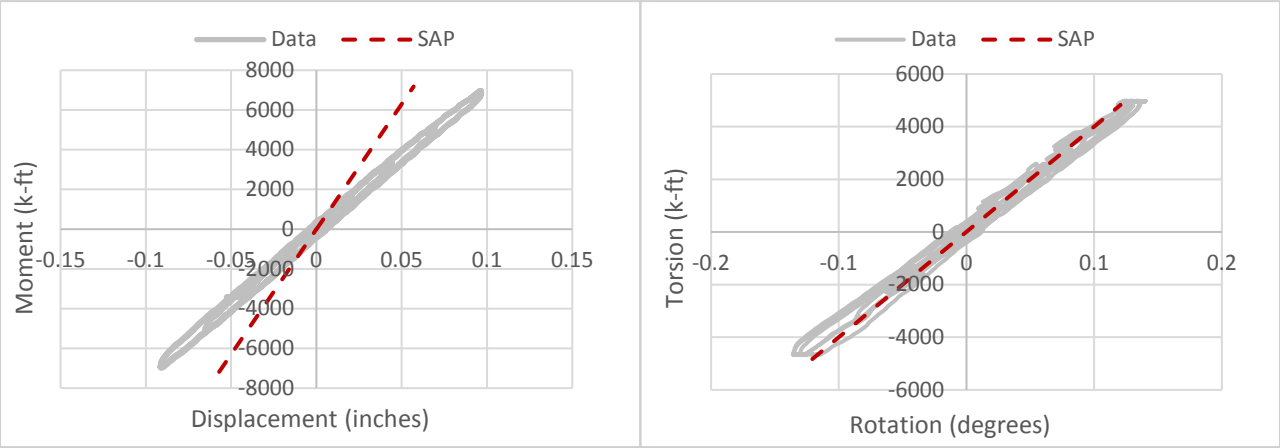

Figure 5.6. Force-displacement comparison of SAP model and test unit data for both the lateral (left) and torsional (right) directions under operational loads

Table 5.6. Column and panel section property modifiers

Column Section Property	Operational Factor	Extreme Factor
Cross-section (Axial) Area	0.60	0.60
Shear Area in 2 Direction	0.60	0.60
Shear Area in 3 Direction	0.60	0.60
Torsional Constant	0.9	0.90
Moment of Inertia about 2-axis	0.60	0.60
Moment of inertia about 3-axis	0.60	0.60
Panel Section Property	**Operational Factor**	**Extreme Factor**
Membrane f11 modifier	0.70	0.50
Membrane f22 modifier	0.70	0.50
Membrane f12 modifier	0.70	0.50

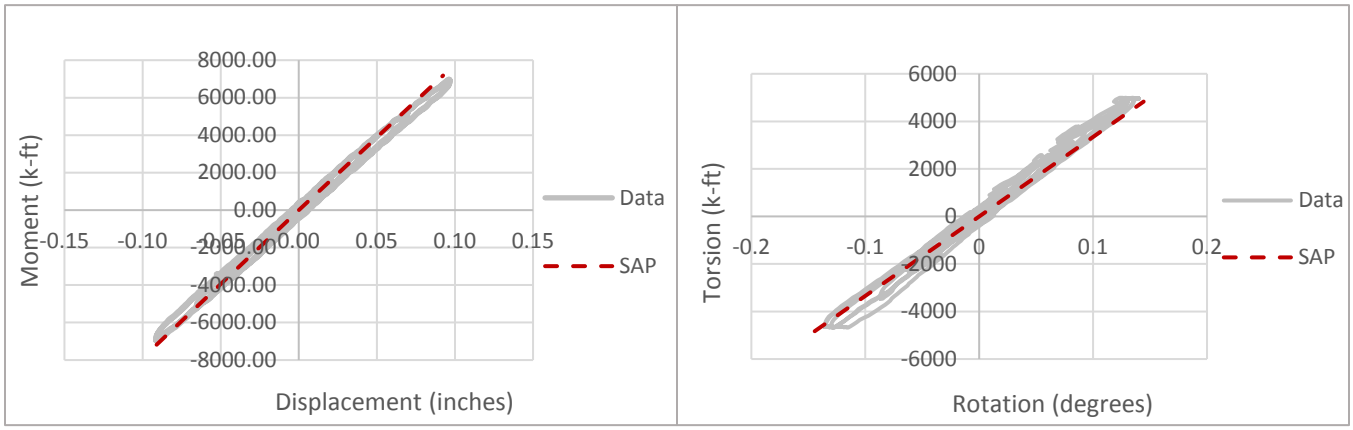

Figure 5.7. SAP comparison of operational loads

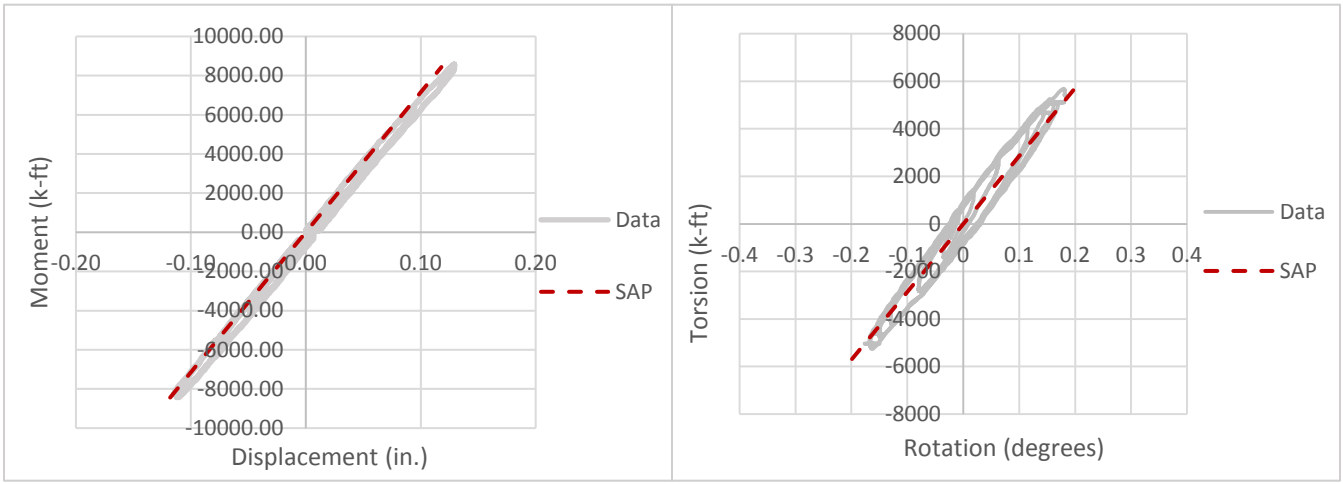

Figure 5.8. SAP comparison for extreme loads

5.3.5.2 Test Unit Columns:

Column deflections in the test unit were measured by string potentiometers (string pots) along the height of the test unit columns. The largest column deflections occurred during high lateral loads and are compared to the SAP model at 50% and 100% load levels in Figure 4.25. The SAP model compared well with the measured deflections with the exception of the positive deflection under 100% extreme loads. At this load level, deflections from the SAP model deviate slightly from the measured data at the base of the test unit columns. This is thought to be due to the effects of localized cracking in the two previously mentioned HSC panels which allowed the base of the columns to have slightly larger deflections. Since this difference in deflection was small, and the column top deflection was equal, the SAP model was not further adjusted.

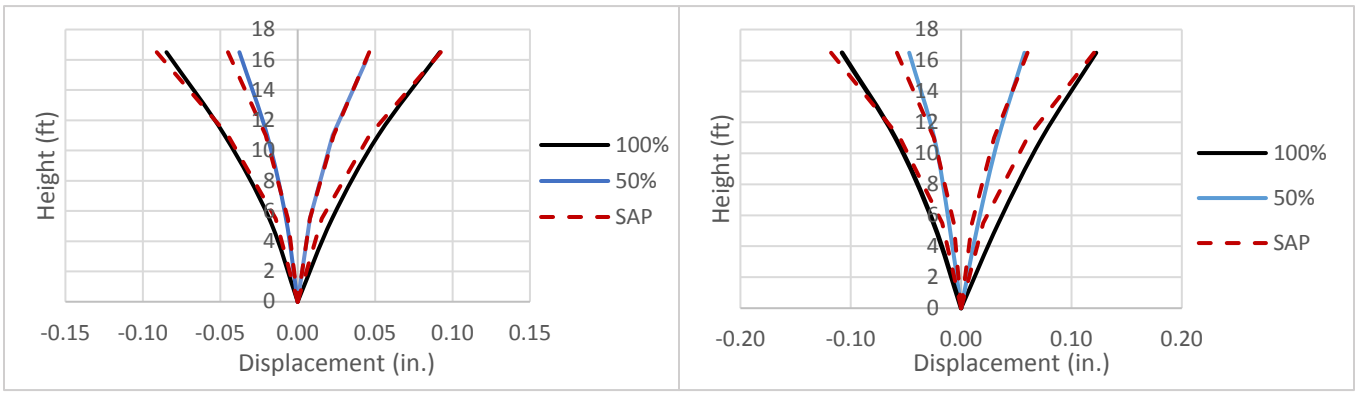

Figure 5.9. Lateral column deflections under operational (left) and extreme loads (right)

5.3.5.3 Panel stresses:

Surface stress measurements of the test unit panels were taken using a 3D Optotrack camera system which utilizes multiple LED sensors. The camera system is referred to as the NDI system and the location of the LED sensors is shown in Figure 4.26. SAP average principal panel stresses were compared with the NDI principal stresses as shown in Figure 5.11. The abbreviations used in the graph are listed in Table 5.7 and refer to test unit load cases. It can be observed the SAP stresses match fairly well with the measured values and are conservative in predicting a higher principal stress value where deviation occurs from the measured data.

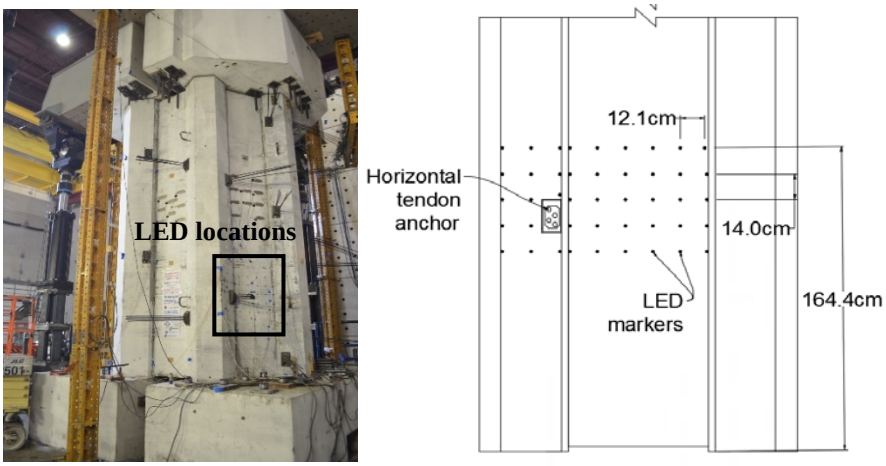

Figure 5.10. LED location (left) and layout (right)

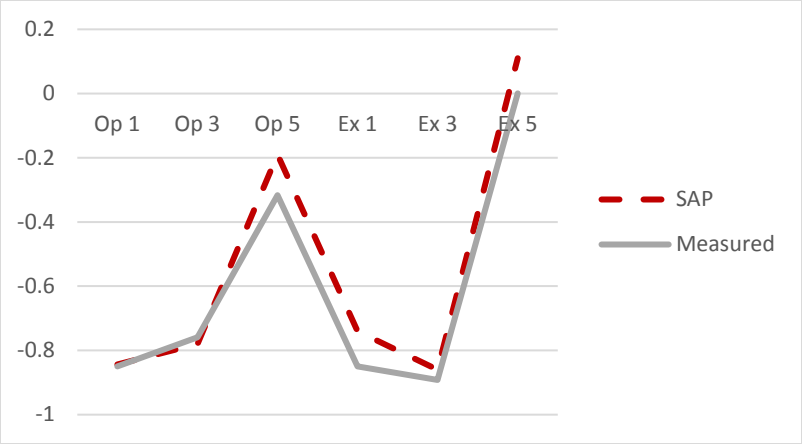

Figure 5.11. Comparison of SAP average principal stresses with measured values

Table 5.7. Load case details

Abbrev.	Load type	Predominant load
Op 1	Operational	Shear
Op 3	Operational	Overturning moment
Op 5	Operational	Torsion
Ex 1	Extreme	Shear
Ex 3	Extreme	Overturning moment
Ex 5	Extreme	Torsion

5.3.6 SAP test unit simulations:

After verification of the SAP model by the comparisons previously shown, model simulations were run to investigate increased spacing of circumferential tendons and the use of all HSC panels for the entire test unit. The simulations were run separately with the verified test unit modeling details. For increased tendon spacing, the space between each tendon was doubled from 2.5 ft (0.76 m) to 5 ft (1.52 m) and the number of tendons was increased from four to eight. In this way, the capacity of each column to panel connection would remain the same but a small number of post-tensioning ducts would be needed in the precast members. Average horizontal pre-compression stresses in the panels were examined (Table 5.8) along with panel principal stresses. The pre-compression stresses from the increased tendon spacing were slightly higher and the resulting panel principal stresses for each load case were lower due to the higher pre-compression values (Figure 5.12).

Table 5.8. Pre-compression of panels due to circumferential tendon spacing

	Original	2x spacing
σx	-0.87	-0.98
σy	-1.64	-1.65
τxy	0.04	0.01

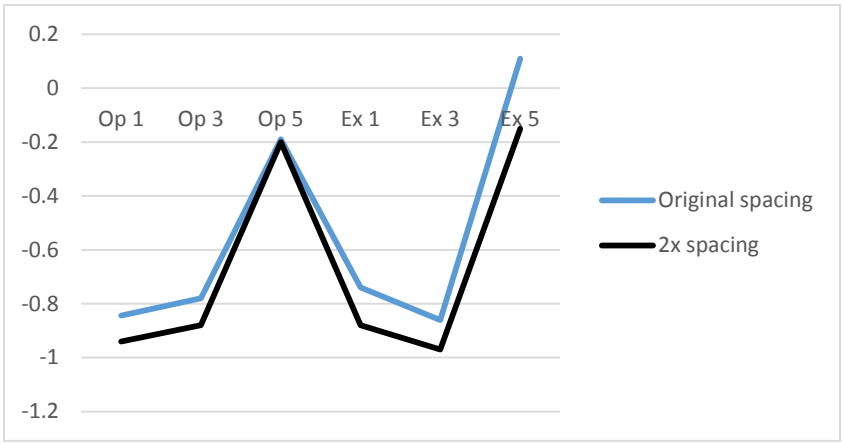

Figure 5.12. Principal stress comparison for circumferential tendon spacing

The higher pre-compression of the doubled tendon spacing is due to the location of stress measurement in SAP. The location of stress measurement corresponded to the center of the measured NDI values, and was used for both tendon spacing configurations at a location 2 ft (0.61 m) from a circumferential tendon. Due to the close proximity of the measurement location and increased number of tendons, the stress from the tendon was slightly higher than the original tendon spacing configuration. Other stress locations were examined and it was found that on average the pre-compression stresses between each the two spacing configurations were equivalent with slight deviations depending the distance of the measurement location from the tendons.

For the second simulation, all HSC panels were used in the test unit. It was found that the HSC panels had higher stresses than the UHPC panels as was expected due to the increased panel thickness which results in reduced pre-compression from vertical and circumferential tendons. The higher stresses were still below the allowable tensile stress units of the panels. Therefore HSC panels can be utilized in the Hexcrete tower designs as long as consideration is given to the amount of necessary pre-compression in relation to panel thickness. The only

drawback to the increased panel thickness is increased tower weight which can increase erection costs.

5.3.7 Tower design modifications resulting from test unit SAP model:

5.3.7.1 Tower stiffness:

As a result of the reduced stiffness found in the SAP test unit model, the SAP tower models were reexamined to investigate the effect of the reduced stiffness on tower natural frequencies. When the stiffness factors found in the test unit model were applied, it was found that for three of the six designed towers, the full concrete HT2, full concrete HT3, and the HT3 hybrid, the adjusted natural frequencies were below the lower limit of the acceptable design frequency range (Table 5.9). The HT3 hybrid natural frequency was close enough to the acceptable range that slightly increasing the Hexcrete panel thickness from 4 in. (101.6 mm) to 6 in. (152.4 mm) allowed the tower to meet the specified design standards. For the full concrete HT2 and HT3 towers, deflections at service level and ultimate loads were investigated since large deformations are generally the result of tower frequencies below the acceptable design range. As expected, the top tower deflections listed in Table 5.10 were found to be larger than those typically observed in wind tower design; therefore, the turbine manufacturer would need to approve these deflections or the tower would need to be redesigned before proceeding with tower fabrication.

Table 5.9. Adjusted tower design natural frequencies

	HT1	HT1 hybrid	HT2	HT2 hybrid	HT3	HT3 hybrid
Original	0.35	0.409	0.266	0.325	0.318	0.339
Reduced stiffness	0.274	0.325	0.217	0.264	0.234	0.294

Table 5.10. Tower deflections from adjusted tower designs

	HT2 full concrete	HT3 full concrete
Service level deflection, in. (m)	48.7 (1.24)	52.5 (1.33)
Ultimate level deflection, in (m)	59.3 (1.51)	63.9 (1.62)

5.3.7.2 Panel material and PT spacing:

As a result of the test unit simulations regarding post-tensioning tendon spacing and HSC panels, it is recommended that the standard spacing for circumferential post-tensioning be increased to allow the use of fewer ducts in precast tower members. The number of tendons

should be determined based on the column to panel connection capacity, spacing of the tendons will depend on the desired size of circumferential post-tensioning duct. The use of HSC panels is recommended as a possible tower option depending on the cost savings in material in contrast to the increased erection costs due to higher tower weight. In some cases it was found that the use of HSC panels slightly increased the tower natural frequency; however, the change in frequency was not significant enough to recommend implementation of HSC solely for this purpose.

5.4 Numerical modeling:

Finite element analysis is a useful tool, but the time and computational power required to input the model parameters and process output data is not always available. Therefore, numerical models were formulated to assess the force-displacement behavior of the tower, predict panel principal stresses, define tower section behavior, and calculate the failure loads or displacements of the structure. The goal of the numerical calculations is to provide equations that can be applied using basic math software and accurately predict tower response characteristics.

5.4.1 Force-displacement response:

Numerical equations were formulated for the test unit force-displacement response in both the lateral and torsional directions. In the lateral direction, Equation 5-1 was derived utilizing the principal of the virtual work and applying a 1 kip (4.45 kN) virtual load laterally at the top of the test unit while considering shear and overturning moment. The shape factor for a hollow circular tube was used as an approximation for shear deformation. The torsional response of the test unit (Equation 5-2) was formulated (Hearn, 1997) with the angle of twist corresponding to the torsional rotation at the top of the test unit section. A stiffness reduction factor of 0.60 was applied (reflects SAP analysis findings) for lateral displacement under operational loads based test data (Figure 4.29), while the torsional stiffness reduction factor was found to 0.9 under operational loads. For extreme loads, after operational panel cracking, the torsional stiffness reduction factor dropped to 0.75. If panel cracking does not occur under extreme loads, than the lateral and torsional stiffness factors should remain the same for extreme load events. Non-linear force-displacement behavior will be further addressed by the failure mechanism analysis located in a subsequent section.

$$\Delta(z) = \int_0^z \frac{M}{\gamma * EI}(z - x)dx + \int_0^z \frac{V}{\gamma * Ga_r}dx \qquad \text{(Eq. 5-1)}$$

where:

$\Delta(z)$ = deflection at height *z* along the test unit

z = height along test unit

M = applied moment at the base of the test unit

γ = stiffness reduction factor accounting for vertical post-tensioned connections

E = modulus of elasticity of test unit

I = moment of inertia of test unit

x = height along test unit where dummy load is applied

V = shear applied at base of test unit

G = shear modulus of test unit

a_r = modified test unit area based on shape (related to shear shape factor)

$$\theta(z) = \frac{Tz}{\gamma_T 4A^2 G} * \left[\frac{s_1}{t_1} + \frac{s_2}{t_2} + \frac{s_3}{t_3} + \cdots etc\right] \quad \text{(Eq. 5-2)}$$

where:

$\theta(z)$ = torsional rotation at height (z) along the test unit

z = height along test unit

T = torsion applied at top of test unit

γ_T = torsional stiffness reduction factor accounting for vertical post-tensioned connections

A = area of test unit

G = shear modulus of test unit

s_n = width of column or panel *n*

t_n = thickness of each column or panel *n*

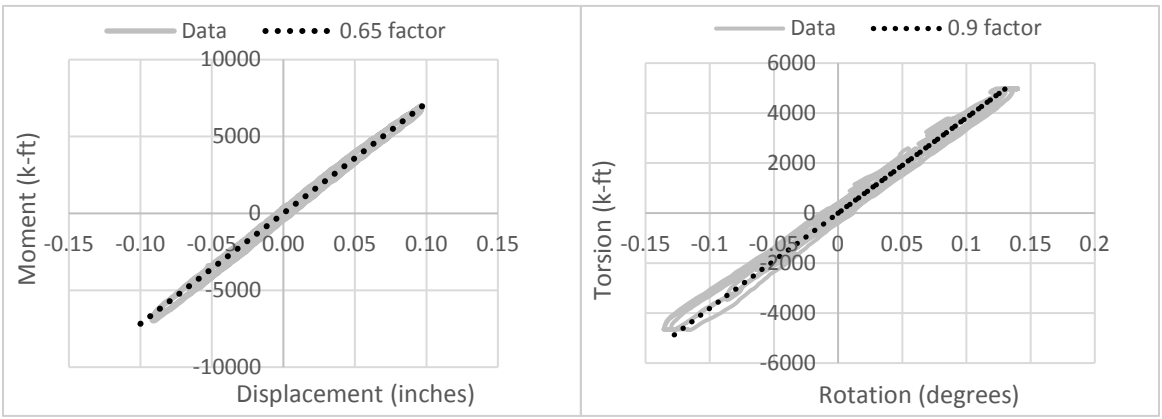

Figure 5.13. Test unit operational load data vs. numerical equations

5.4.2 Panel stresses:

The thickness of Hexcrete panels at a given tower location is determined by examining the principal stresses that result from the applied tower loads. Equation 5-3 describes the relationship between panel principal stresses and the critical material stress which typically corresponds to the tensile strength of the concrete. Equation 5-4 through Equation 5-9 provide a numerical method for estimating the panel average principle stresses based on the column and panel geometric properties. The method assumes that cracking has not occurred in any of the tower panels under operational and extreme loads which aligns with current Hexcrete design standards. Comparison of the numerical method predictions to experimentally measured results are shown in Figure 5.14 with Op 1, Op 3, and Op 5 corresponding to operational shear, moment, and torsional load cases respectively with similar notation for extreme loads. The graph shows that the numerical method is slightly conservative in predicting panel stresses with the exception of load case Ex 5 where a significant amount of panel cracking had already occurred in two of the test unit panels. A limited number of hairline panel cracks had also occurred at load case Op. 5 during testing but did not significantly affect the panel principal stresses. In future design of Hexcrete wind towers, the panels will be designed to remain uncracked under both operational and extreme tower loads.

$$\phi\sigma_{cr} \geq \sigma_p \qquad \text{(Eq. 5-3)}$$

where:

ϕ = strength reduction factor taken of 0.5

σ_{cr} = tensile strength of concrete

σ_p = principal stress caused by applied tower loads

$$\sigma_p = \frac{\sigma_x+\sigma_y}{2} \pm \sqrt{\left(\frac{\sigma_x-\sigma_y}{2}\right)^2 + \left(\tau_{xy}\right)^2} \qquad \text{(Eq. 5-4)}$$

where:

σ_x = stresses due to horizontal post-tensioning (PT)

σ_y = stresses due to vertical post-tensioning, applied overturning moment, and axial loads

τ_{xy} = shear stress from applied shear and torsional loads

Further definition:

$$\sigma_x = \frac{P_{effective}}{1.2*t*s} \quad \text{(Eq. 5-5)}$$

$P_{effective} = P_{jacking} - P_{losses}$

t = panel thickness

s = average spacing of horizontal PT strands

$$\sigma_y = \frac{\delta_{column}*E_{panel}}{L_{panel}} \quad \text{(Eq. 5-6)}$$

$$\delta_{column} = \frac{PL}{AE} \quad \text{(Eq. 5-7)}$$

P = single column vertical PT force + single column axial load + single column tension or compression from overturning moment

L = length of column

A = cross-sectional area of column

E = elastic modulus of column

E_{panel} = elastic modulus of panel

L_{panel} = length of panel

$$\tau_{xy} = \frac{q}{t} \quad \text{(Eq. 5-8)}$$

$$q = \left(\frac{T}{2A_t} + \frac{VQ}{I}\right) \quad \text{(Eq. 5-9)}$$

T = torsional load applied to tower section

A_t = area enclosed by midline of entire tower section

V = shear load applied to tower section

Q = first moment area for applied shear load

I = moment of inertia for tower section

t = panel thickness

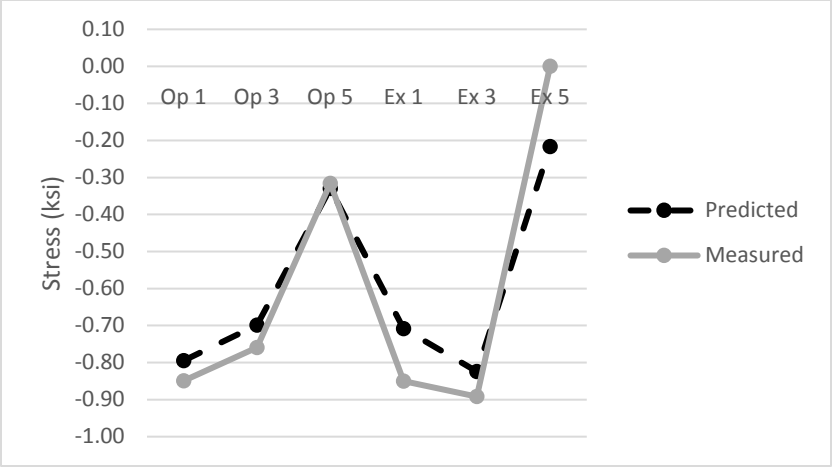

Figure 5.14. Measured vs. predicted panel stresses

5.4.3 Hexcrete tower flexural analysis:

For design and analysis of the Hexcrete tower subject to flexure, two different methodologies were utilized for linear and non-linear tower response. In both methodologies, it is assumed that the tower panels do not participate as compression or tension areas since the tower panels are not structurally connected vertically along the height of the tower. For linear response, an uncracked section analysis was applied based on basic stress equations where the stress in the test unit columns, σ_c, was found by using Equation 5-10. The stress in the vertical post-tensioning tendons was assumed to be the effective stress resulting from jacking of the tendons during erection. This approach was used until decompression of the vertical tendons occurred. Decompression was assumed to occur when Equation 5-11 was true of the tower section. Strain in the columns and vertical tendons was then calculated based on basic mechanics properties for converting from stress to strain.

$$\left(\frac{(F*N)+P}{(A*N)}\right)+\frac{M}{S}=\sigma_c \qquad \text{(Eq. 5-10)}$$

where:

F = single column vertical PT force after jacking and long term losses

N = number of columns

P = applied axial load of tower section

A = single column net area (accounts for voids due to PT ducts)

M = overturning moment applied to tower section

S = section modulus of tower cross section

$$F \leq \frac{(M*A)}{(S)} - \frac{P}{N} \qquad \text{(Eq. 5-11)}$$

For the non-linear tower analysis, an iterative displacement method first developed by Lewin was implemented assuming that decompression of the tower vertical tendons had already occurred and that a gap would open at a critical load location due to tendon decompression (Lewin & Sritharan, 2010). The first step in the analysis process was to define a critical tower rotation value corresponding to the magnitude of gap opening at the critical tower section. The tower rotation value depends on an assumed neutral axis depth at the critical section (Figure 5.15) which should be less than the critical section tower diameter (the neutral axis is an iterative value). The assumed neutral axis value and corresponding rotation were then input into Equation 5-12 to solve for the maximum column compression strain. Equation 5-12 treated the entire Hexcrete tower as a single hollow column and equated the critical section rotation to a constant plastic curvature over the plastic hinge length, *Lp* (Thomas & Sritharan, 2004). This method allows approximation of a maximum column strain for specific load and gap values without the need for calculating the ultimate tower capacity.

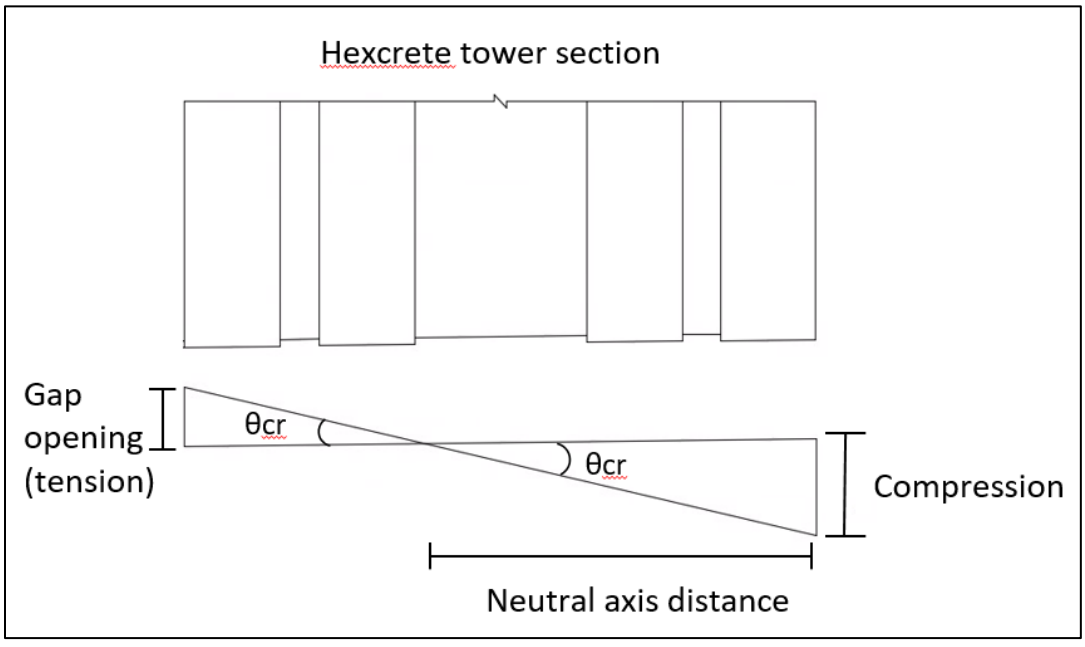

Figure 5.15. Gap opening, critical rotation, and neutral axis depth of Hexcrete tower section

$$\epsilon_{cmax} = c_{NA}\left(\frac{\theta_{cr}}{L_p} + \frac{M_{cr}}{0.6EI_{cr}}\right) \qquad \text{(Eq. 5-12)}$$

where:

ϵ_{cmax} = maximum column strain for given rotation and neutral axis values

c_{NA} = assumed neutral axis depth

θcr = rotation at critical section resulting from gap opening magnitude and assumed neutral axis

Lp = plastic hinge length, assumed to be 0.06L where L is equal to the distance of the critical section from the top of the tower

Mcr = moment at critical section

E = elastic modulus of tower columns

Icr = moment of inertia of tower columns at critical section

Based on the assumptions that plane sections remained plane within the Hexcrete tower, that the tower concrete experienced a linear strain distribution, and that the maximum column strain occurred at the edge of the outermost column, average strain values for each column were calculated using a linear strain profile and similar triangles (Figure 5.16). If the outermost column experienced a strain higher than 0.003 it was assumed that the ultimate load condition was reached for the tower structure. The calculated column strains were then converted to column stresses and column forces.

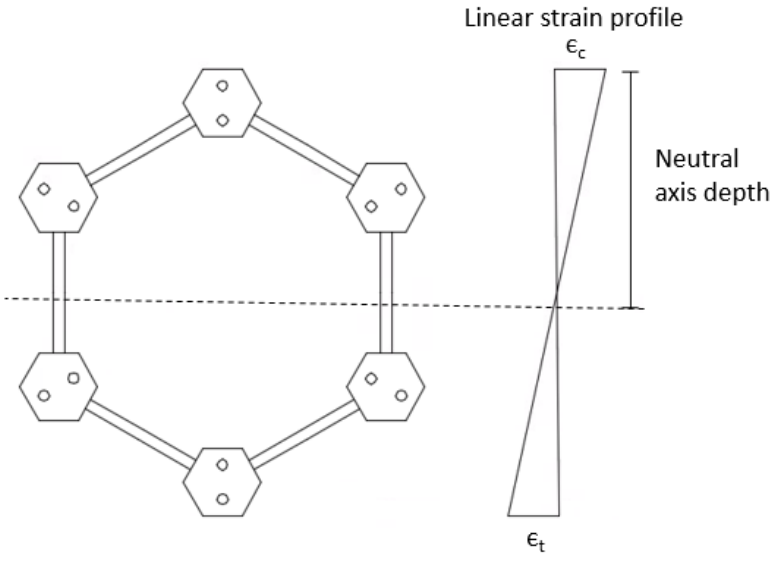

Figure 5.16. Linear strain distribution for tower critical section

Next, the elongation of the tower tendons due to rotation at the critical tower section were calculated based on the assumed neutral axis depth, corresponding critical rotation, and tendon location (Figure 5.17). The rotational elongations were then divided by the original tendon length, L_T, to calculate the tendon. Strain was then converted to stress and added to the effective stress due to tensioning of the tendons. If the resulting stress value exceeded 230 ksi, the strand would no longer act in a linear manner and the tower was considered to have reached its ultimate capacity. Tendon stresses were then converted to tendon forces.

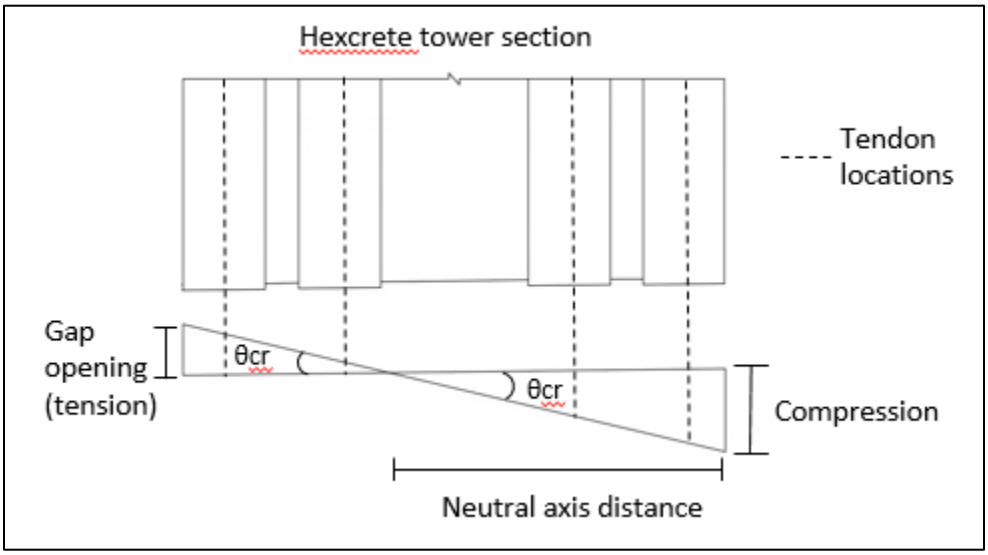

Figure 5.17. Tendon location in relation to critical rotation and neutral axis depth

Once column and tendon forces were calculated, force equilibrium was checked by summation of the column compression, tendon tension, and applied tower axial forces. If equilibrium was achieved, the assumed neutral axis depth was correct. If not, the neutral axis depth was iterated until equilibrium was reached.

The non-linear tower numerical method was then compared to the experimental test unit results. Before experimental testing, load cells were installed between the top of two test unit columns and the vertical tendon multi-strand anchors. Since the numerical method provided strain values for both test unit columns and tendons, the strain in a vertical tendon anchored to a load cell was examined. A test unit load case corresponding to tendon decompression was selected and the critical section was found to be located at the base of the test unit columns. Gap opening at the base of the selected column was measured by a Linear Variable Displacement Transducer (LVDT). Test unit properties were input into the non-linear model and the neutral

axis depth was iterated until force equilibrium was obtained. The resulting tendon strain was converted to force and compared to the load cell measurements (Figure 5.18). The graph shows that the numerical method values are typically within 2 to 3 kips of the measured data at high load values, which provides confidence in the accuracy of the numerical method.

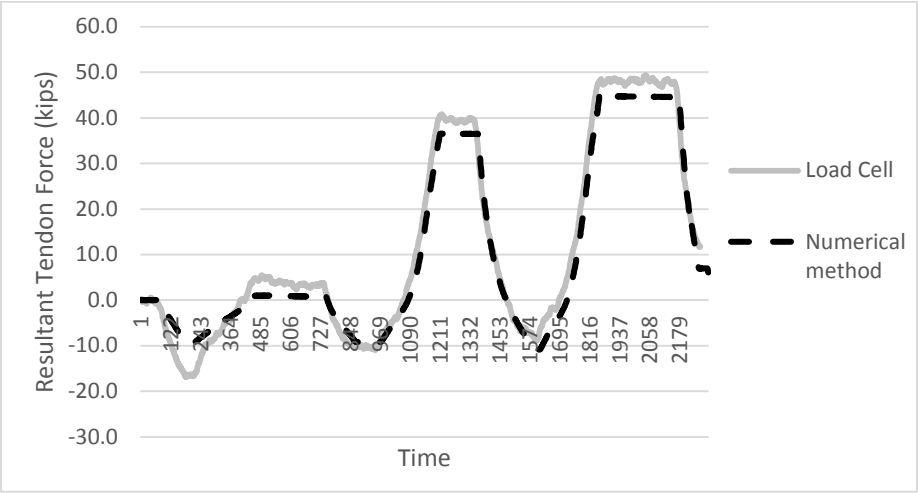

Figure 5.18. Comparison of measured and non-linear anaylsis tendon forces

5.5 Conclusion:

In order to better understand the behavior of the Hexcrete tower system, finite element centerline models of the designed tower systems and Hexcrete experimental test unit were created in SAP2000. The same modeling technique was used for both the towers and test unit and the test unit was then validated using experimental data for multiple load cases. The Hexcrete test unit was more flexible than the created SAP model due to the post-tensioning of multiple precast concrete members. The SAP models were subsequently adjusted to match the test unit data and then applied to the full Hexcrete tower system. In examining the SAP tower models, it was found that two of the tower designs, the full concrete HT2 and HT3 towers, did not meet the necessary frequency requirements. Both towers experienced large displacements at the top of the towers under operational and extreme loads and will require changes in tower design. Simulations were also run in the verified SAP models to investigate the effects of increasing the vertical spacing of the circumferential post-tensioning and using HSC panels. It was found that the spacing of the tendons could be doubled without detrimental effects to the tower system.

Numerical methods were also created to simplify the initial tower design process. The derived equations calculated the deflection of the tower system, predicted panel stresses, and

quantified the tower flexural behavior. Each numerical method was formulated and compared to Hexcrete test unit data for verification. The methods were found to be an effective alternative to finite element models for preliminary estimation of Hexcrete tower behavior. Opportunity for further refinement of these methods may be possible during future development of a Hexcrete prototype structure.

5.6 References:

ACI Committee 318. (2011). *Building Code Requirements for Structural Concrete (ACI-318) and Commentary.* Farmington Hills: American Concrete Institute.

Computer and Structures, I. (2014). Structural and Earthquake Engineering Software, SAP2000 Version 17.

Hearn, E. (1997). *Mechanics of Materials 2, 3rd Edition.* Woburn, MA: Butterworth-Heinemann.

Lewin, T., & Sritharan, S. (2010). *Design of 328-ft (100-m) Tall Wind Turbine Towers Using UHPC.* Ames, IA: Department of Civil, Construction, and Enviromental Engineering Report ERI-ERI-10336.

Sritharan, S., & Lewin, T. (2015). *U.S. Patent No. 9,016,012.*

Sritharan, S., Lewin, T., & Schmitz, G. M. (2014). *U.S. Patent No. 8,881,485.*

Thomas, D. J., & Sritharan, S. (2004). *An Evaluation of Siesmic Design Guidelines Proposed for Precast Jointed Wall Systems.* Iowa State University.

Twigden, K., Sritharan, S., & Henry, R. (2017). Cyclic testing of unbonded post-tensioned concrete wall systems with and without supplemental damping. *Engineering Structures*, 406-420.

CHAPTER 6 – SURFACE PRESSURE ANALYSIS OF HEXCRETE WIND TURBINE TOWERS

A paper to be submitted to a Wind Engineering Journal

Robert Peggar, Iowa State University

Sri Sritharan, Ph.D., Professor of Structural Engineering, Iowa State University

6.1 Abstract

The Hexcrete wind turbine tower is an innovative, hexagon shaped, precast concrete wind tower design. The Hexcrete design utilizes precast concrete columns and wall panels that can be easily transported, thereby eliminating the transportation challenges of large steel sections. However, the bluff body hexagon shape results in higher surface pressures along the height of the tower when compared to traditional circular steel towers. In addition, the unique Hexcrete design contains protruding column sections resulting in a ribbed hexagon shaped instead of a smooth hexagon surface. Therefore, a Hexcrete tower design was evaluated for wind loads according to American Society of Civil Engineers (ASCE) 7-10 guidelines for chimneys, tanks, and other structures. The results were compared to a previously run Computational Fluid Dynamic (CFD) analysis for the same Hexcrete tower. Surface pressures resulting from the ASCE calculations were examined with specific attention given to the effect of the ASCE shape coefficient, *Cf*, in relation to the CFD results. It was found that the ASCE method, with a hexagon shape coefficient, was adequate to predict the total base overturning moment of the Hexcrete tower system, but attention should be given to localized surface pressures at the top of the Hexcrete tower resulting from closely spaced column members. The results from the Hexcrete tower analysis were also compared with an equivalent diameter circular tower to quantify the difference in tower wind loads.

6.2 Introduction:

As wind towers continue to grow taller, new innovative designs emerge to overcome existing logistical and transportation challenges with current steel tower technology. The Hexcrete wind tower, developed at Iowa State University, is one such technology. The tower is a hexagonal shaped, precast concrete tower system that utilizes six concrete columns connected by six concrete flat wall panels. As part of a previously study funded by the U.S. Department of Energy (DOE), three Hexcrete towers were designed for heights above 328 ft (100 m). Full scale strength and fatigue laboratory testing verified the tower design methodology, and the

technology was found to be cost competitive with current steel technology at heights above 328 ft. A Computational Fluid Dynamic (CFD) analysis was performed for one of the towers in order to compare the base overturning moment of the Hexcrete tower to an equivalent diameter circular tower. The subsequent sections of this report will further discuss the fluid-structure interaction between the wind and Hexcrete tower surface, more specifically, the wind drag coefficients that result in tower surface pressure and tower loads. Since a wind tunnel test has not yet been performed, results from the CFD study will be discussed and CFD data, in the form of static surface pressures, will be examined and a compared to code equations set forth by the American Society of Civil Engineers (ASCE) in load document ASCE 7-10. This comparison provides a frame of reference for the design of Hexcrete tower systems in relation to current code standards and also identifies any potential challenges posed by the unique Hexcrete shape. Full verification of the wind and tower interaction will require wind tunnel testing, but this study will serve as a preliminary baseline investigation. The following sections of this report will include details of the ASCE 7-10 code requirements, a summary of results from the code calculations, and comparison of code derived surface pressure data with the CFD findings. Finally, recommendations regarding the Hexcrete tower system in relation to the ASCE 7-10 code will be provided.

6.3 Background:

As part of the DOE funded project for designing Hexcrete towers for heights above 328 ft, a CFD analysis was run to examine the interaction of the wind with the Hexcrete tower surface and compare base overturning moments with an equivalent diameter circular tower. Both towers analyzed in the CFD study were 394 ft (120 m) tall and designed for loads corresponding to a Siemens SWT 2.3 MW-108 machine. The towers were subject to an extreme wind speed model (EWM) corresponding to International Electrotechnical Commission (IEC) guidelines. Selection of the wind speed model was in accordance with wind speeds at hub height for a Class IIB turbine assumed to be located in Iowa. The CFD model simulated 150 seconds of wind load on the tower and the dynamic overturning moments were collected. Flow field interaction results from the study are shown in Figure 5.1. It is important to note that wind loads on the tower surface typically only account for roughly 30% of the total tower loading. The majority of the tower loads are generated from operation of the wind turbine (blades, hub, and nacelle). The

CFD simulation did not account for these additional loads but was limited solely to wind and tower interaction.

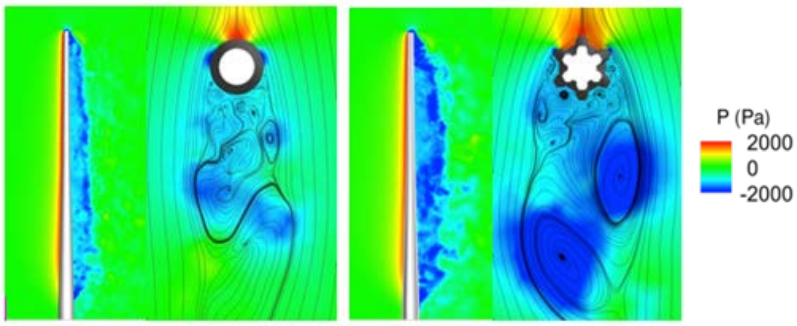

Figure 6.1. Tower flow field interaction

In structural design codes, wind drag coefficients, known as shape factors, are prescribed for different tower shapes in order to correctly calculate surface pressure values. In ASCE 7-10, shape factors for a hexagon shaped tower are twice the magnitude of a circular tower. The current ASCE hexagon drag coefficients also assume a regular hexagon shape; however, the Hexcrete tower contains protruding column elements in addition to the hexagon shape as shown in Figure 6.2. Furthermore, the Hexcrete tower tapers as the height of the tower increases and the taper in tower diameter results in narrower connecting wall panels between the columns. The narrower panels cause the column to be closer together which could affect the surface drag and also result in varying drag coefficients along the tower height. It is important accurately characterize the drag coefficients for design of the Hexcrete tower system for two reasons:

1.) Determining the magnitude of the drag coefficients along the tower height will enable a more accurate definition of tower loads along the tower height which may allow optimization of certain tower members and result and reduce tower costs.

2.) An appropriate shape coefficient for the Hexcrete tower can be defined in accordance with ASCE 7-10 values to expedite integration of the technology into the current wind tower market.

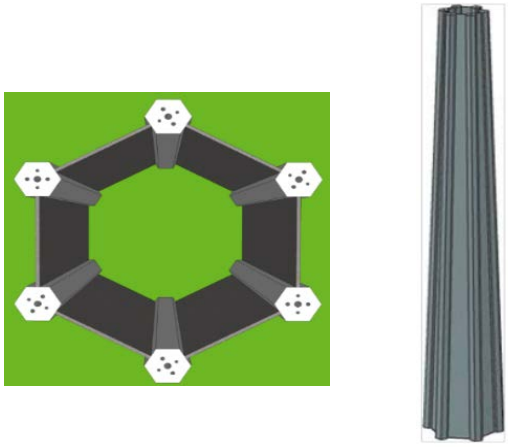

Figure 6.2. Hexcrete plan view showing protruding columns (left); tapered tower (right)

6.4 Modeling technique:

A numerical model was created based on the ASCE 7-10 design code. The model included tower geometry, an extreme wind speed profile, tower frequency, tower location information, and drag coefficients representing wind and tower interaction. The HT2 geometry was modeled and analyzed in two directions as shown in Figure 6.3 since each direction provided a different surface area for wind interaction. A simplified discussion of the main model inputs and variables is presented below along with how each variable relates to the final numerical solution. The tower was evaluated based on the ASCE 7-10 prescribed method for tanks, chimneys, and other structures.

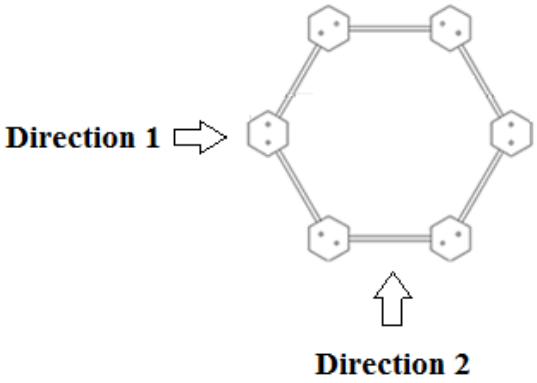

Figure 6.3. Two directions for analyzing drag coefficients and surface pressures

6.4.1 Input variables:

n_t – tower natural frequency; this variable contributes to the deflection of the tower system under wind loads

B_1 – base diameter of the tower

h – total height of tower

z_1 – height at which tower drag coefficients and velocity pressures are evaluated

The code allows the entire tower system to be evaluated at once; however, since the tower tapers, it was decided to evaluate the tower at intervals along the height to capture any change in drag coefficient. The integrals were determined by how tower was segmented for erection. For onsite erection, the tower was segmented into 14 sections with an average section length of 32.1 ft (9.8 m). Specific segment lengths are listed in Table 6.1 along with the corresponding z_1 values which are measured from the ground level to the mid-height of each section.

Table 6.1. Tower segment lengths

Section	Length (m)	Length (ft)	z1 (ft)
1	16.2	53.0	26.6
2	7.1	23.3	64.7
3	7.3	24.0	88.3
4	7.6	25.0	112.8
5	8.1	26.5	138.5
6	8.5	28.0	165.8
7	9.0	29.5	194.5
8	9.7	31.8	225.1
9	9.7	31.8	256.9
10	10.1	33.0	289.3
11	10.6	34.8	323.1
12	11.1	36.5	358.8
13	11.4	37.5	395.8
14	11.0	36.1	432.6

A_f – tower surface area being evaluated for drag coefficients; since the tower was evaluated in intervals, the surface area of each interval was calculated separately to accurately reflect any change in tower wall panel width.

6.4.2 Calculation parameters:

A_f – tower surface area; same as input variable above but listed here because it is also a main calculation parameter

gF – gust factor; captures dynamic response of tower considers, n_t, B_1, and h

qz – velocity surface pressure resulting from wind

Cf - force or drag coefficients

6.4.3 Result variables:

qz x gF x Cf - total surface pressure of tower sections (units of psf)

F_1 – force on tower system at specified location z_1 (units of kips)

In order to correctly evaluate the Hexcrete tower system using code equations, the following assumptions were made:

1.) As mentioned previously, the evaluated Hexcrete tower system will be located in Iowa. This informs the reference wind speed for the model as well as terrain characteristics.

2.) The wind tower is located in terrain that is considered surface roughness category C in the ASCE 7-10 code. This corresponds to open terrain with scattered obstructions (normal condition for wind towers in Iowa).

3.) The Hexcrete tower will be classified as a Category II structure which means that the structure is not designed to be operable in emergency situations such as earthquakes or other natural disasters.

In the model, four calculation parameters determine the force on the tower system: the gust factor (*gF*), tower surface area (*Af*), velocity wind surface pressure (*qz*), and force or drag coefficient (*Cf*). All four parameters depend on the input variables which correspond to the tower geometry features. The tower geometry used in the numerical ASCE model matched the tower geometry in the CFD analysis. The tower geometric properties included the tower natural frequency (n_t), base diameter normal to the wind direction (B_1), total tower height (h), height of tower where drag coefficients are being evaluated (z_1), and the surface area of each tower section (A_f). These attributes contributed to the dynamic response of the tower system captured by the gust factor (*gF*). For non-flexible buildings with natural frequencies greater than 1 Hz, *gF* is equal to 1.0, but for flexible structures such as wind towers, *gF* is often greater than one (Simiu & Scanlan, 1986). The variable z_1 was located at the mid-height of each tower section, and A_f, the surface area of the each section, was calculated normal to the wind direction. The velocity

surface pressure (*qz*) is derived from the assumed wind profile (Figure 6.4) and other factors such as the wind surface exposure factor (*Kz*), which is determined based on the height above ground since terrain effects lessen and unobstructed wind exposure increases; wind directionality factor (*Kd*), which assumes that a certain percentage of the surface area is fully normal to wind direction; and topographic factors (*Kzt*), which account for any terrain obstructions to the wind. In short, the wind resource is evaluated along with any terrain or topographic disturbance which would cause a change in wind speed before reaching the tower surface. The final factor analyzed is the force coefficient (*Cf*) which is also known as the drag coefficient. *Cf* is determined by the shape of the structure as well as the tower base diameter parallel to the wind (L_1) and tower height (*h*). As discussed in a previous section, this is the value that is being investigated for the Hexcrete tower system. Once all four variables, *gF*, *Af*, *qz*, and *Cf* are found, the corresponding tower force (F_1) can be obtained by multiplication.

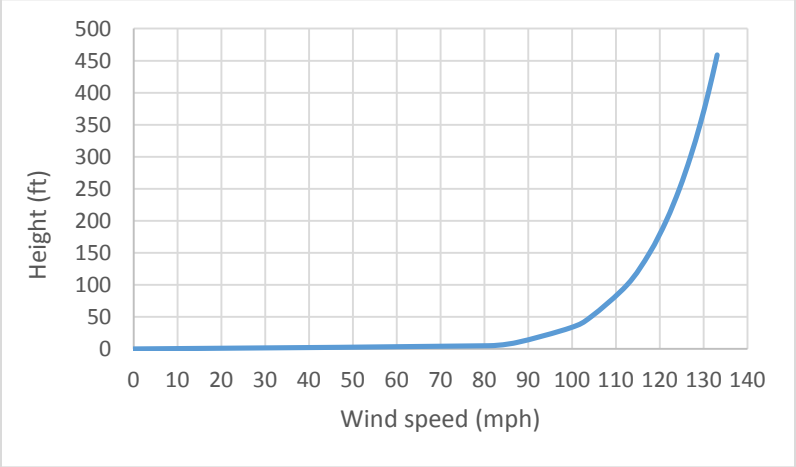

Figure 6.4. Wind profile (EWM) applied to CFD and ASCE equations

6.5 Results:

The calculated tower surface pressures for both ASCE 7-10 equations and the static CFD analysis are shown in Figure 6.5 and Figure 6.6. It is worth noting that for the numerical model the surface pressure does not change between the two directions due to the model formulation since the minimum base dimension L_1 is the same for both directions. Similarly, the static CFD surface pressure between the two directions is very similar until Section 10 at the top of the tower (Figure 6.7). The base overturning moments were calculated for both ASCE 7-10 (direction 1) and the static CFD data for comparison to the previously reported dynamic CFD response (Table 6.2).

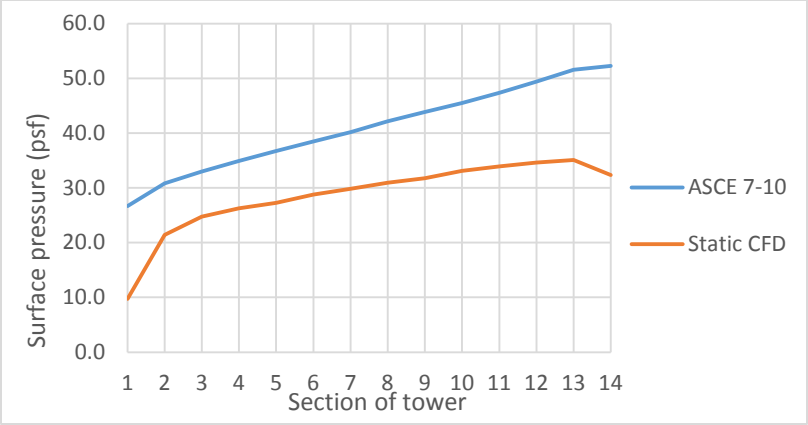

Figure 6.5. Surface pressure comparison for direction 1

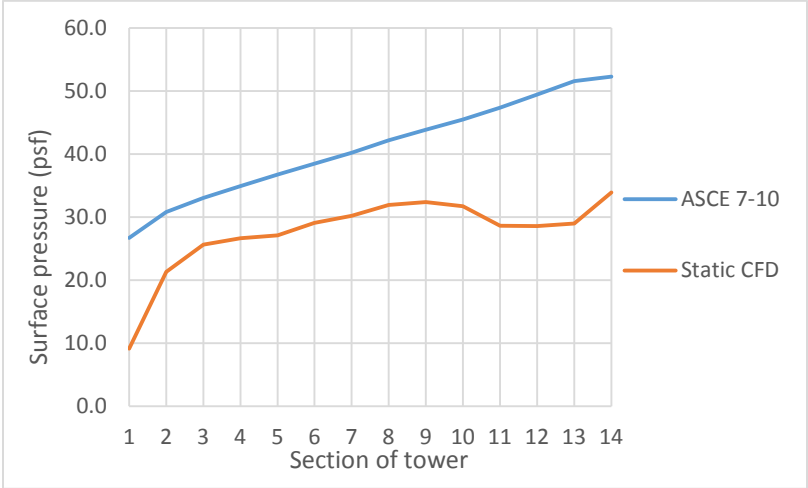

Figure 6.6. Surface pressure comparison for direction 2

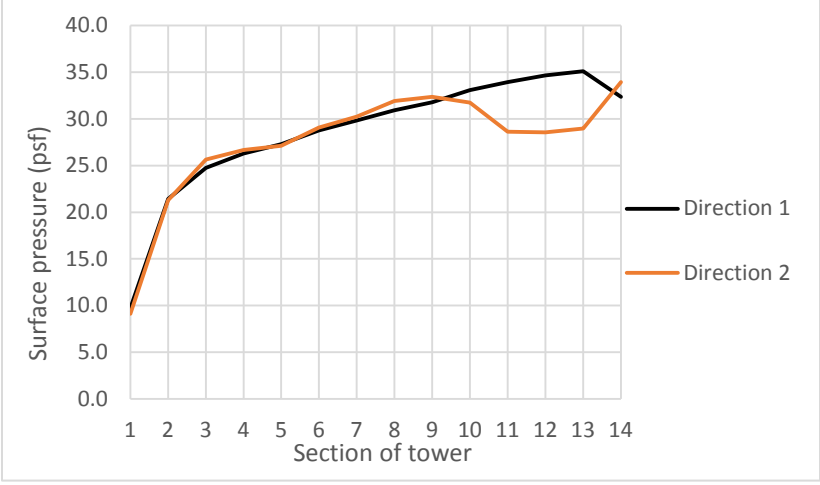

Figure 6.7. Static CFD comparison between direction 1 and direction 2

Table 6.2. HT2 base overturning moments

	Dynamic CFD (k-ft)	Static CFD (k-ft)	ASCE 7-10 (k-ft)
HT2	67708	49265	70323

It can be observed that the base overturning moment for ASCE 7-10 is relatively close (4% difference) to the dynamic CFD results, but that the static CFD results are significantly lower. The reason for this discrepancy is that the surface pressures for the static CFD model were calculated for only the windward side of the tower in order to be consistent with ASCE 7-10 code guidelines for chimneys, tanks, and other structures. Therefore, the static CFD calculations were rerun to also account for the leeward side of the wind tower. In addition, the ASCE 7-10 values were also rerun to include leeward tower pressure in order to determine the magnitude of increase in the code values. The ASCE 7-10 calculations were performed with assumption that the wind tower is fully enclosed. The resulting surface pressures are shown in Figure 6.8 and Figure 6.9 with base overturning moments recorded in Table 6.3. After including leeward pressure, the static CFD base moment almost exactly matched that of the dynamic CFD results while the ASCE 7-10 leeward code calculations overestimated the base moment by 17%. Based on these results it was determined that the ASCE 7-10 values used for comparison would correspond to only the windward side of the tower.

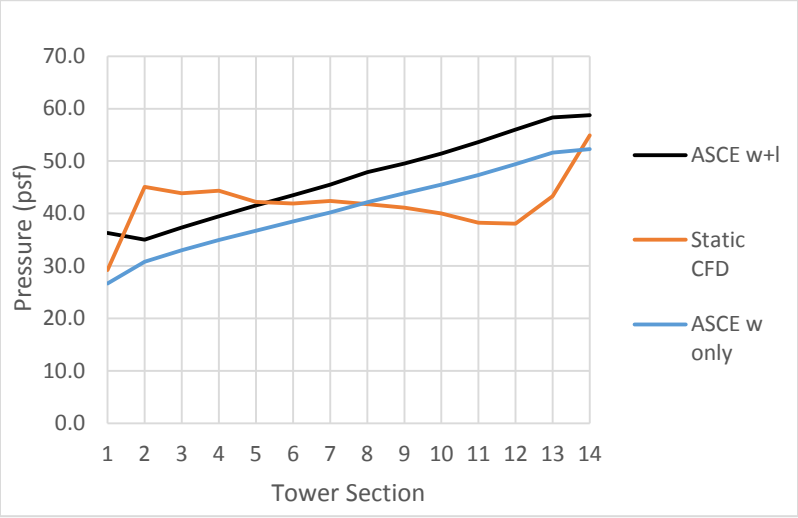

Figure 6.8. HT2 surface pressures accounting for windward and leeward tower surfaces (direction 1)

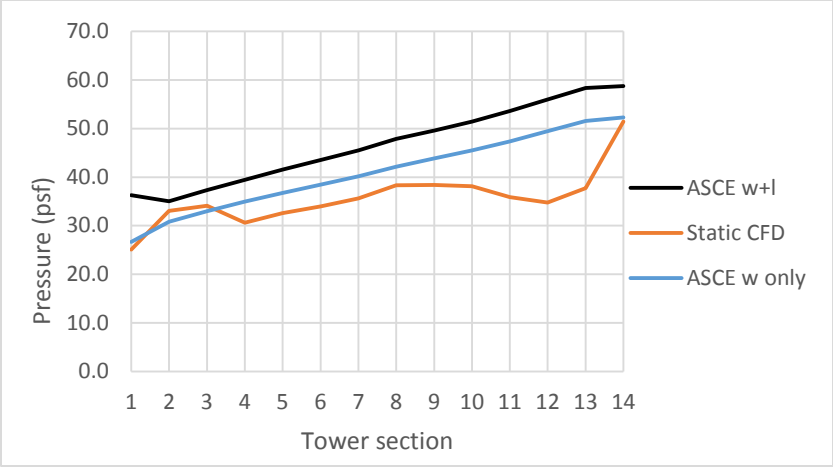

Figure 6.9. HT2 surface pressures accounting for windward and leeward surfaces (direction 2)

Table 6.3. HT2 base overturning moments including leeward pressure

	Dynamic CFD (k-ft)	Static CFD (k-ft)	ASCE 7-10 w+l (k-ft)	ASCE 7-10 w only (k-ft)
HT2	67708	67856	79762	70323

6.6 Discussion of results:

Accuracy of the results presented above assume the dynamic CFD base moment values as a baseline reference. The initial results that compared only the windward surface versus the combined windward and leeward surfaces of the Hexcrete tower provided evidence that the ASCE 7-10 method for evaluating chimneys, tanks, and other structures adequately evaluates the base overturning moment of the Hexcrete tower system. The calculated ASCE 7-10 base overturning moment with only windward pressure was only 4% greater than moment measured by the dynamic CFD analysis. The leeward pressure results overestimated the base moment by 17%. These results also indicate that the current hexagon drag coefficient is adequate to predict Hexcrete tower base moments even with the presence of the protruding tower columns.

Comparison of the surface pressures for the two different HT2 loading directions show that direction 1 loading result in higher tower forces. When comparing the ASCE HT2 direction 1 calculations to the static CFD results, the HT2 surface pressures are underestimated for the lower half of the tower and overestimated along the remaining tower height. However, the ASCE and CFD average surface pressures along the height of the tower are very similar (Figure 6.10). For design purposes, it is recommended that the tower average ASCE surface pressure be used to

calculate tower forces along the tower height until sections 13 and 14 where consideration should be given to localized tower pressures. Utilizing the average surface pressures enables a lower surface pressure to be used in design of tower sections 9-12 which may provide opportunity for tower cost reduction.

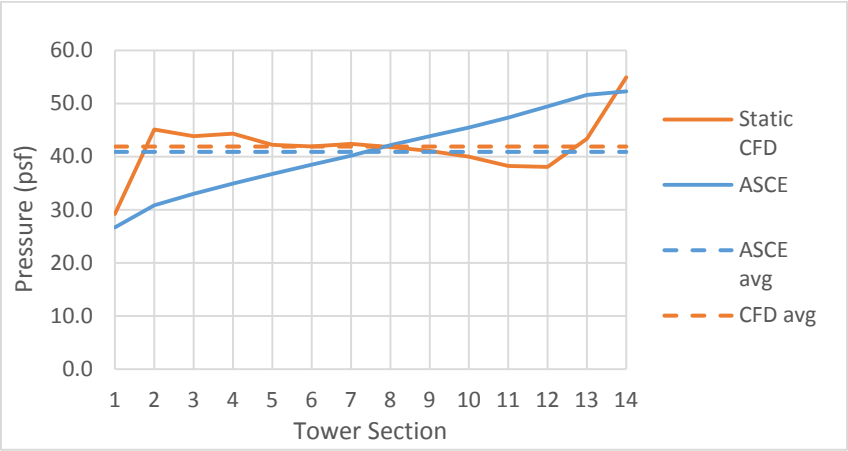

Figure 6.10. Average tower surface pressures

The static CFD model overturning moment is a close approximation of the dynamic CFD analysis which was expected. For the static CFD surface pressures results, pressure values along the tower height from tower section 2 to section 12 are almost constant. The increase in pressure over section 1 at the base of the tower can be attributed to surface obstructions at ground level that give way to less obstructed airflow at the base of section 2. The increase in pressure at section 12 toward the top of the tower is likely due to taper of the tower diameter. This taper results in higher surface pressures caused by the disruption of air flow due to smaller panels and closer spacing of tower columns.

When comparing the base overturning moment of the HT2 tower to the equivalent diameter 120 m circular tower, an increase in tower force is observed; however, as mentioned previously, the tower loads caused by wind interaction only account for around 30% of the total Hexcrete tower loads. It was thought that the wind interaction of the Hexcrete tower surface could be improved by designing Hexcrete hybrid towers with circular steel shells accounting for the top third of the tower system. The Hexcrete hybrid towers reduced the load difference between circular and full Hexcrete towers by approximately 50%.

Study results show that ASCE 7-10 shape coefficients adequately predict overturning forces for the Hexcrete tower system. However, in order to further reduce tower loads generated

by wind interaction, relocation of the tower panels to the outside of the tower perimeter was investigated as shown in Figure 6.11. Moving the panels to the outside of the columns may affect the transfer of load between the tower columns, but for the purposes of this study it is assumed that this issue can be adequately addressed with little change in tower design. Two approaches were used to analyze the modified Hexcrete tower geometry with the assumption that the tower gust factor would remain constant. In the first approach, the ASCE 7-10 hexagon shape coefficient (*Cf*) was applied to the modified tower surface area. For the second approach a modified *Cf* value was applied to the tower along with the modified surface area. Two different *Cf* values were applied to the tower with the first being equivalent to the ASCE 7-10 shape factor for a rough, round cross-section and the second equal to ASCE 7-10 very rough, round cross-section. The resulting tower forces by section are shown in Figure 6.12 with resulting base overturning moments in Table 6.4. It can be observed that for the tower forces and base moment to be significantly reduced, a modified *Cf* value must be applied to the system. It is recommended that the modified geometry be analyzed in a CFD program to identify the appropriate shape factor before modifying the tower design.

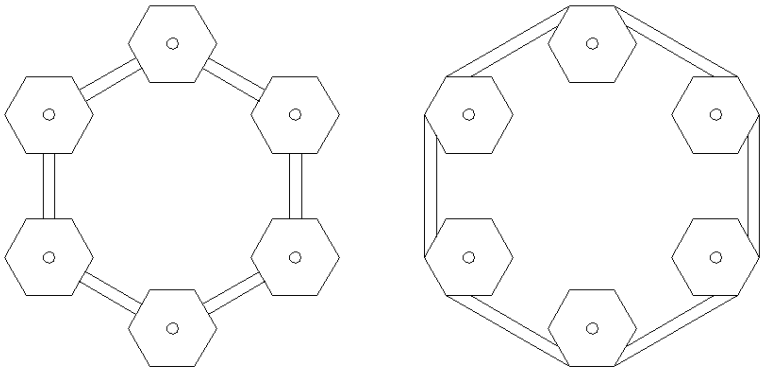

Figure 6.11. Original panel location (left); modified panel location (right)

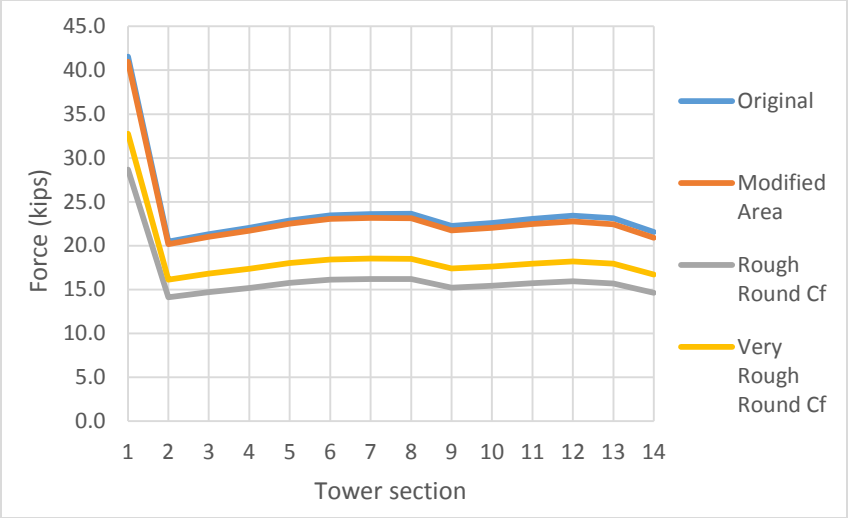

Figure 6.12. Tower section forces for modified Hexcrete tower geometry

Table 6.4. Modified geometry base overturning moments

	Original (k-ft)	Modified Area (k-ft)	Rough Round *Cf* (k-ft)	Very Rough Round *Cf* (k-ft)
Moment	70323	68631	48042	54905
Percent change	0	-2%	-32%	-22%

6.7 Conclusions and recommendations:

The goal of studying the surface pressures and drag coefficients of the Hexcrete tower system was to better characterize the localized tower forces due to wind with the objective of accurate surface pressure characterization leading to increased design efficiency. The characterization of localized surface pressures in accordance with ASCE 7-10 guidelines, in parallel with analysis of static CFD data, provided insight and recommendations for future design of Hexcrete tower systems. With the dynamic CFD study functioning as a comparable baseline, the following conclusions were drawn:

- The numerical analysis provided evidence that the ASCE 7-10 method for evaluating chimneys, tanks, and other structures adequately evaluates the base overturning moment of the 120 m Hexcrete tower system using the hexagon shape coefficient (*Cf*). The calculated ASCE 7-10 base overturning moment was 4% greater than moment measured by the dynamic CFD analysis.

- Of the two loading directions examined for the Hexcrete tower, loading direction 1 produces the largest tower forces, while the calculated average ASCE and static CFD surface pressures are similar along the tower height. With regard to surface pressures, it is recommended that the ASCE average surface pressure be used to calculate tower forces along the tower height with the exception of sections 13 and 14 where consideration should be given to localized pressures. Utilization of the average surface pressure enables a lower surface pressure value to be applied in the design of tower sections 9-12 which may provide opportunity for tower cost reduction.
- Comparison of results from the static CFD data for the two Hexcrete tower loading directions show similar surface pressures until tower section 12. At heights above section 12, direction 1 produces larger surface pressures than direction 2. It is likely that for direction 1, the narrowing panel widths and reduced spacing between the three windward tower columns resulted in increased airflow disturbance when compared to only two windward columns in direction 2.
- The increase in surface pressure of the Hexcrete tower when compared to an equivalent 120 m circular tower results in an increase of the tower base overturning moment due to wind and tower interaction.
- Hybrid Hexcrete towers were designed to reduce the amount of wind interaction and subsequently reduce the total tower load. For the hybrid towers, where the top third is made of steel, the difference in load between the full Hexcrete tower and equivalent circular tower was reduced by 50%.
- Investigation of modifying the panel position to the outside perimeter of the tower was performed in order to identify potential opportunities for reduction in tower forces. It was observed that the resulting change in tower surface area would not significantly decrease tower forces unless the ASCE 7-10 shape coefficient, *Cf*, was also modified. It is recommended that the modified geometry be analyzed in a CFD program to better define the appropriate shape factor value before modifying the tower design.

In order to fully characterize the wind and tower interaction of the Hexcrete tower system, it is recommended that a wind tunnel test be performed. Wind tunnel testing is the

current benchmark for fully characterizing uniquely shaped structures. This study provides predictive data for such a wind tunnel test and also gives numerical and computational data points for comparison. The study was able to add value to the Hexcrete tower design by defining surface pressure according to ASCE 7-10 guideline which will serve as a first step in fully understanding Hexcrete wind interaction behavior. The next step of wind tunnel testing will enable refinement of the tower system and subsequent cost optimization. As the cost of the Hexcrete system continues to be optimized, the technology has the potential to help achieve wind power production in all 50 states and increase the U.S. renewable energy portfolio.

6.8 References

ASCE/AWEA. (2011). *Recommended Practice for Compliance of Large Land-based Wind Turbine Support Structures.* American Wind Energy Association and American Society of Civil Engineers.

Simiu, E., & Scanlan, R. H. (1986). *Wind Effects on Structures.* New York: John Wiley and Sons.

CHAPTER 7 – CONCLUSIONS AND RECOMMENDATIONS

7.1 Introduction:

The Hexcrete wind turbine tower provides a new opportunity to employ precast concrete for hub heights above 328 ft (100 m) and enable economical wind power in all 50 states. It also provides the necessary technology advancement to meet the DOE Wind Vision goal of providing 30% of the U.S. electricity demand with wind power by 2050. Experimental testing, finite element analysis, and numerical models were examined to further validate the Hexcrete tower system. The following sections summarize the findings of the work presented in this dissertation.

7.2 Design and certification:

Three full concrete and three hybrid tower systems were designed according to IEC standards and GL guidelines. The vertical post-tensioning and use of HSC and UHPC materials allow the designer to easily accommodate multiple hub heights and turbine sizes. Dynamic behavior of the tower system was important in the design process with the lower bound 1P blade frequency often influencing the final design of tower dimensions. Input from industry partners resulted in the design of a quick connect bar system to connect the tower segments during construction. The quick connect system provided a method to avoid grouting until after the completion of tower erection.

The design of Hexcrete pedestal systems confirmed that the stiffness of the Hexcrete system allows it to be incorporated as part of the tower foundation up to certain pedestal heights. The pedestal system also provided an opportunity to prototype the Hexcrete tower while taking advantage of current tower practices. Fabrication and installation of a prototype pedestal will allow certification of the tower design and improvement of construction techniques. Certification documents were formulated for submission and verification.

7.3 Full-scale testing:

The full scale test of the Hexcrete tower system validated the tower design for operational and extreme loads and also showed that the tower had significant ductility and reserve capacity under large displacement loads above extreme design criteria. The importance of the vertical tensioning in pre-compression of the Hexcrete panels was also observed due to the absence of pre-compression and subsequent cracking of two test unit panels. It is recommended that the tower system include the use of oversized ducts for the radial post-tensioned tendons to allow easier tendon placement and quicker construction times.

7.4 Finite element modeling and numerical methods:

A finite element model of both the six designed towers and experimental test unit were created using the software program SAP2000. The modeling techniques were successfully verified by comparing the model output with experimental test results. It was found that the initial SAP models overestimated the Hexcrete stiffness and corresponding tower natural frequencies. The frequencies were adjusted according to the verified modeling techniques. Simulations of the test unit model were also run to investigate the spacing of radial post-tensioning tendons and the use of only HSC panels. Based on the model findings, an increase in radial tendon spacing is recommended for simplified construction of the Hexcrete system since this does not result in significant change in panel stresses. HSC panels were found to be a viable construction option, it is recommended that panel pre-compression levels are verified due the larger panel thickness. Numerical methods were also successfully created to quantify the tower force-displacement response, panel stresses, and tower flexural behavior with corresponding tendon and columns strains.

7.5 Surface pressure analysis:

The surface pressure investigation of the Hexcrete tower system found that the ASCE 7-10 method for chimneys, tanks, and other structures was adequate to evaluate the base overturning moment of the Hexcrete tower system by utilizing the ASCE hexagon shape coefficient. Comparison of wind loads between the Hexcrete tower and an equivalent diameter circular tower found that the Hexcrete wind loads were higher for a full concrete tower and that the designed Hexcrete hybrid towers reduced the Hexcrete wind tower loads. It was also found that there may be advantages to relocating the tower panels to the outside of the Hexcrete columns if the resulting surface reduces the ASCE shape coefficient to a factor equivalent to a rough or very rough cylinder.